Scuola Internazionale Superiore di Studi Avanzati - Trieste

LOCALIZATION AND FUNCTIONAL EXPRESSION OF THE CALCIUM-ACTIVATED CHLORIDE CHANNEL TMEM16A IN TASTE BUD CELLS

Thesis submitted for the degree of
"Doctor Philosophiae"

Academic Year 2019/2020

Candidate

Domenico Maria Guarascio

Supervisor: **Prof. Simone Pifferi**

Co-Supervisor: **Prof. Anna Menini**

SCUOLA INTERNAZIONALE SUPERIORE DI STUDI AVANZATI

LOCALIZATION AND FUNCTIONAL EXPRESSION OF THE CALCIUM-ACTIVATED CHLORIDE CHANNEL TMEM16A IN TASTE BUD CELLS

Thesis submitted for the degree of "doctor philosophiae"

the academic year 2020/2021

CANDIDATE

Domenico Maria Guarascio

SUPERVISOR

Prof. Simone Pifferi

CO-SUPERVISOR

Prof. Anna Menini

TABLE OF CONTENTS

ABSTRACT **6**

INTRODUCTION **9**

1 THE SENSE OF TASTE **9**

1.1 Anatomical structure of the taste system *10*

1.1.1 The tongue 10

1.1.2 Anatomical structures of the tongue 11

1.1.3 The taste buds 12

1.1.4 From the tongue to the central nervous system 13

1.2 Three types of taste bud cells *17*

1.2.1 Type I 19

1.2.2 Type II 23

1.2.3 Type III 23

1.3 The transduction mechanisms for the taste qualities *25*

1.3.1 Sweet, Bitter, and Umami 25

1.3.2 Effector pathway for Type II TBCs (sweet, bitter, umami) 26

1.3.2.1 Sweet - responsive TBCs 28

1.3.2.2 Umami (amino acid) - responsive TBCs 29

1.3.3.3 Bitter - responsive TBCs 30

1.3.4 Sour - responsive TBCs 31

1.3.5 Salty - responsive TBCs 32

1.4 The role of saliva in taste sensation *33*

2 CALCIUM-ACTIVATED CHLORIDE CHANNELS **38**

2.1 The TMEM16 family *38*

2.2 TMEM16A *42*

2.2.1 Expression pattern and roles of TMEM16A 42

2.2.2 TMEM16A in cancer 44

2.2.3 TMEM16A structure 44
2.2.4 Biophysical properties of TMEM16A 47
2.2.5 Activation mechanisms of TMEM16A 48
2.2.6 Regulatory mechanisms of TMEM16A 49
2.3 TMEM16B 51
2.3.1 Biophysical properties of TMEM16B 52
2.4 CaCCs in taste cells 54
AIMS 57
RESULTS 58
FUNCTIONAL EXPRESSION OF TMEM16A IN TASTE BUD CELLS 58
SUPPLEMENTARY MATERIALS 94
CONCLUSIONS 97
REFERENCES 100

The universe would probably have been dark if we had not been able to see the light through our eyes. We could not appreciate the perfume of a rose or be excited by a Bach's symphony, if we had not been able to feel the perfume with our nose and the sounds through our ears. What would be the pleasure of munch an apple without our tongue? I would say that "we are, because we percept". Indeed, we can percept the world around us thanks to our five senses. Our senses connect our brain with the external environment, representing our window on the world.

Abstract

Taste is a specialized chemosensory system dedicated to the evaluation and discrimination of different types of chemicals entering the mouth. On the tongue, different types of papillae contain several taste buds, onion-shaped structures composed of up 100 taste bud cells. These cells express specific receptors and ion channels and can be divided into three different types. Type I are the most abundant cells in the taste buds and are considered to have a glial-like function. Type II and III can generate action potentials upon stimulation with different types of tastants.

The Ca^{2+}-activated Cl^- channels TMEM16A and TMEM16B have relevant roles in many physiological processes including neuronal excitability and regulation of Cl^- homeostasis and a recent study reported the expression of both channels in various types of taste cells.

Here, we re-examined the functional expression of Ca^{2+}-activated Cl^- channels in taste cells of mouse vallate papillae by combining immunohistochemical and electrophysiological approaches. By using specific markers and knockout mice, we found that only type I cells expressed TMEM16A, whereas TMEM16B was not expressed in taste cells. Furthermore, TMEM16A was found to largely co-localize with the inwardly rectifying K^+ channel KNCJ1 in the apical part of type I cells.

Whole-cell patch-clamp recordings on dissociated taste cells showed Ca^{2+}-activated Cl^- currents in type I cells have properties similar to those of TMEM16A. Indeed, blockage by Ani9, a specific TMEM16A channel blocker, indicated that Ca^{2+}-activated Cl^- currents are due to TMEM16A channels. On the other hand, we did not detect any Ca^{2+}-activated Cl^- current in type II and type III cells.

ATP is released by type II cells in response to various tastants and reaches type I cells where it is hydrolyzed by ecto-ATPases. Type I cells also express P2Y purinergic receptors and stimulation with ATP can activate a strong Cl^- conductance in these cells. We found that ATP-evoked Cl^- current was blocked by Ani9, indicating a possible role of TMEM16A in ATP-mediated signaling.

Altogether, our results establish that TMEM16A-mediated currents are functional in type I taste cells and provide a foundation for future work investigating the precise physiological role of TMEM16A in the taste system.

List of abbreviation and Acronyms

5-HT	Serotonin
9-AC	Anthracene Carboxylic acid
ACh	Acetylcholine
ATP	Adenosine Triphosphate
CaCCs	Calcium-activated Chloride Channels
CALHM1/3	Calcium Homeostasis Modulator 1/3
CaM	Calmodulin
cAMP	Cyclic Adenosine Monophosphate
CeA	Central Amygdala
CFTR	Cystic Fibrosis Transmembrane Conductance Regulator
CNG	Cyclic Nucleotide-Gated ion channel
CNS	Central Nervous System
CT	Chorda Tympani
CVP	Circumvallate Papillae
DAG	Diacylglycerol
DIDS	4,4'-Diisothiocyanatostilbene-2,2'-Disulphonic acid
DRG	Dorsal Root Ganglia
ENaCs	Epithelial Na^+ Channels
FFA	Flufenamic acid
FoP	Foliate Papillae
FP	Filiform Papillae
FuP	Fungiform
GABA	Gamma-Aminobutyric acid
GC	Gustatory Cortex
GISTs	Gastrointestinal Stromal Tumors
GLAST	Glutamate Aspartate Transporter
GPCRs	G Protein-Coupled Receptors
ICCs	Interstitial Cells of Cajal
IMP	5´ Inosine Monophosphate
IP_3	Inositol Triphosphate
IP_3R_3	Inositol Triphosphate Receptor 3
KCNJ1	Potassium Inwardly Rectifying Channel Subfamily J Member 1
Kir	Inward Rectifier K^+ channel
KO	Knock-Out
LH	Lateral Hypothalamus
mGluR4	metabotropic Glutamate Receptors 4
mPBN	medial region Parabrachial Nucleus
MSG	Monosodium Glutamate
NFA	Niflumic Acid
NMDG	N-methyl-d-Glucamine

NPPB	5-nitro-2-(3-phenylpropyl-amino) benzoic acid
NST	Nucleus of Solitary Tract
NTPDase2	Ectonucleotides Triphosphate Diphosphoydrolase
OE	Olfactory Epithelium
OTOP1	Otopetrin1
PBN	Parabrachial Nucleus
PIP2	Phosphatidylinositol (4,5)-bisphosphate
PKD2L1	Polycystic Kidney Disease 2-like-1
PLCβ2	Phospholipase - C β2
SITS	4-acetamido-4-isothiocyanatostilbene-2,2-disulfonic acid
SNAP25	Synaptosomal Associated Protein,
T16	T16Ainh-A01
T1R1	Taste Receptor 1 member 1
T1R2	Taste Receptor 1 member 2
T1R3	Taste Receptor 1 member 3
T2Rs	Taste Receptors 2
TBCs	Taste Bud Cells
TRPM4	Transient Receptor Potential cation channel subfamily M member 4
TRPM5	Transient Receptor Potential cation channel subfamily M member 5
VFM	Venus Flytrap Module
VPMpc	Ventroposterior Medial thalamic nucleus
WT	Wild Type

1 The sense of taste

The flavor of the food is a complex perceptual experience, and it is mediated by several sensory modalities. It is composed of gustation, olfaction, somatosensation, audition, and vision. The most relevant are the sense of taste and sense of smell. It is common to confuse the flavor with the taste. However, the taste is related only to the perception of signals that originate in organs located in the oral cavity: taste buds. They are triggered by saliva-soluble compounds that contact the apical tips of epithelial cells of the taste buds. In contrast, olfactory signals are generated in the nasal cavity, where volatile compounds contact olfactory sensory neurons. The olfactory system is activated both through the orthonasal pathway and through the retronasal pathway that connects the mouth with the nasal cavity. Although the peripheral organs for taste and smell are distinct, their signals are integrated into the orbitofrontal and other areas of the brain, generating the flavor perception and mediating the recognition of the foods (Roper and Chaudhari, 2017; Shepherd, 2006).

The taste system together with olfaction is involved in chemosensation, the ability for living organisms to perceive chemicals in the environment. The sense of taste allows organisms to identify nutrients while avoiding toxins and inedible foods. Moreover, it is important to guide nutrition by selecting required foods related to specific characteristics, such as caloric intake, protein content, or mineral and salt intake. Humans can distinguish between five taste qualities that are sweet, bitter, umami (savory), sour and salty. However, humans can perceive, probably, more taste qualities such as fatty, metallic, and others (Besnard et al., 2016). In general, sweet and umami (elicited by certain L-amino acids) (Ikeda, 1909) are associated with good tastes and they promote the consumption of nutritive foods or drinks. On the opposite, sour and bitter are related to bad tastes. They alert the organism to toxins and low pH, promoting the rejection of foods containing harmful substances. Salt taste can be repulsive or attractive depending on the concentration of sodium. However, several exceptions do not follow these rules. Indeed, although animals are generally aversive to bitter compounds (for example, coffee) they can modulate and change their preferences. Moreover, our taste perception is strongly modulated by sensations and emotions such as hunger, satiety, or expectation.

1.1 Anatomical structure of the taste system

The taste system, like other sensory modalities, is composed of a peripheral and a central part. The peripheral system includes the sensor organs that molecularly detect chemicals and in which chemical stimuli are being converted into electrical stimuli. The central taste system, located in the brain, receives these electrical stimuli from the periphery and converts them into behavior effects.

1.1.1 The tongue

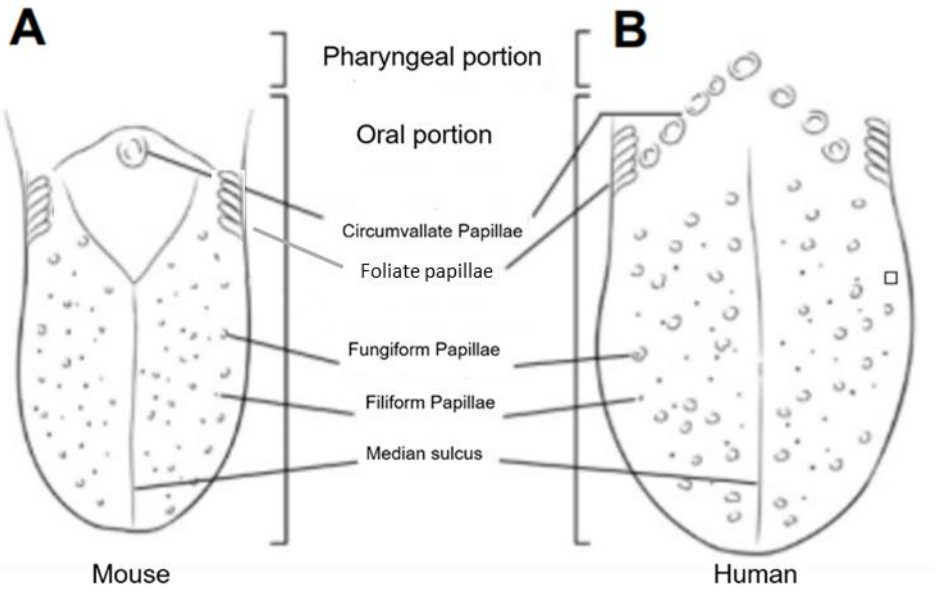

Figure 1. ***Mouse and human tongues****. Comparison between mouse (**A**) and human (**B**) tongues (Jung et al., 2004)*

In mice, as in humans and several mammals, the tongue (Fig. 1) is the main peripheral sensory organ involved in taste perception. On the tongue are located specialized structures called papillae. Papillae are invaginations of the tongue that contain the fundamental units for taste sensation: the taste buds. We distinguish four different types of papillae: Filiform, Fungiform, Foliate, and Circumvallate (Fig 2). The classification is based on their position on the tongue, their shape, and the number of taste buds that they contain.

1.1.2 Anatomical structures of the tongue

i) **Filiform papillae** (FP) appear small with an elongated shape. They are numerous, cover almost the whole dorsal surface of the tongue, and are important for mechanical perception. Indeed, FP do not have taste buds and they are not considered taste papillae (Kawasaki et al., 2012).

ii) **Fungiform papillae (FuP)** are tissue projections located on the anterior two-thirds of the tongue and they are distributed among filiform papillae (Gardner and Carpenter, 2019). Each fungiform papilla contains a single taste bud (Barlow, 2015).

iii) **Foliate papillae (FoP)** are in edges of the posterior portion of the tongue. They appear as linear projections of lingual mucosa perpendicular to the longitudinal axis of the tongue. These projections are parallel to one another and several taste buds are embedded in them (Liu and Lee, 1982).

iv) **Circumvallate papillae (CVP)** are more complex. They have a circular shape and are the biggest papillae on the tongue. Rodents possess only one CVP in the posterior portion of the tongue, while the number of CVP can vary in other mammals (Barlow, 2015). Moreover, CVP also contains the biggest number of taste buds.

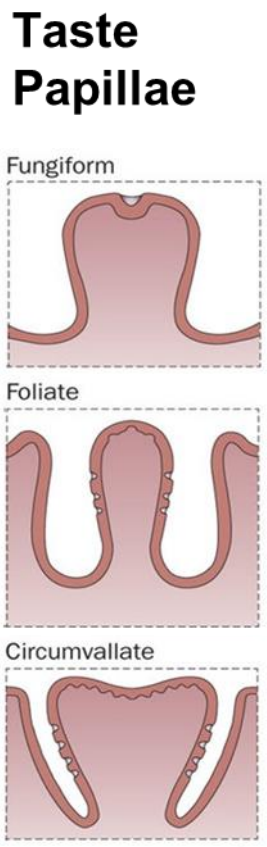

*Figure 2. **The taste papillae.** Representation of taste papillae. Image modified from Calvo and Egan, (2015).*

Although most taste buds are distributed in the different papillae on the tongue, single taste buds can be found also in other districts such as soft palate and epiglottis (Roper and Chaudhari, 2017). Taste buds of soft palate have been shown to be functional in mammals and they contribute conspicuously to taste sensation (Noguchi et al., 2003).

1.1.3 The taste buds

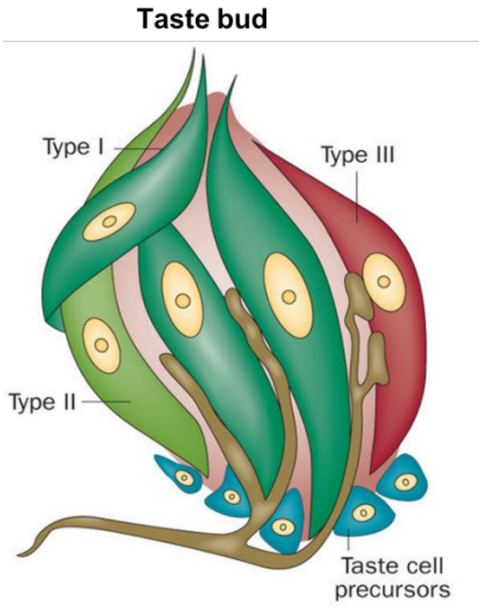

Figure 3. ***Structure of taste bud****. The picture is the schematic representation of a taste bud and intragemmal nerve fibers. In the picture are represented the conventional taste bud cells: Type I-III and taste cell precursors. Note that only Type III TBCs form conventional synapses with afferent nerve fibers. Image modified from Calvo and Egan (2015).*

The taste buds are the fundamental units responsible for taste sensation. They are onion-shaped structures composed of 50-100 epithelial sensory cells called taste bud cells (TBCs) (Fig 3). Some of these cells are the primary receptor cells responsible for taste sensation. These cells are closely packed in taste buds with a precise orientation. In particular, they extend from the base of the bud to the apical surface of the epithelium, where a taste pore allows direct contact with mouth lumen, thus chemicals in the environment can interact with TBCs (Roper and Chaudhari, 2017; Liman et al., 2014; Barlow, 2015; Yarmolinsky et al., 2009; Kinnamon and Finger, 2019). The apical parts of TBCs are connected by tight junctions, therefore the taste pore is the only connection between TBCs and the mouth environment. Indeed, typical tight junction components such as claudins and ZO-1 are detected at the apical tips of taste buds (Michlig et al., 2007) (Fig. 4). In this way, in the taste buds, like other epithelial

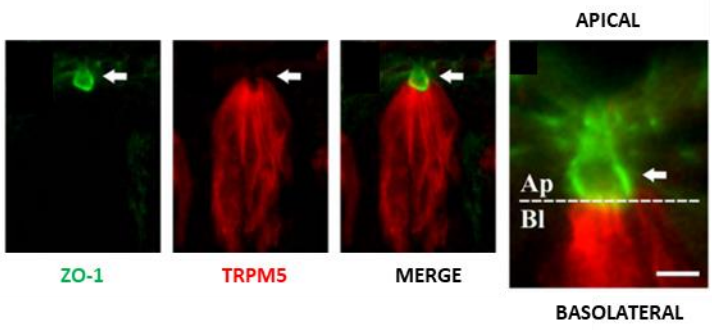

Figure 4. ***ZO-1 a tight junction component****. Representation of a tight junction protein ZO-1 in green and TRPM5 marker of Type II TBCs in red. Note the defined separation between apical (Ap) and basolateral (Bl) portion of the taste bud due to tight junctions. Image modified from Gao et al., (2009).*

tissues, the permeation of water and many solutes between the two sides of the epithelium is avoided. However, paracellular pathways through taste buds have been demonstrated for some ionic and non-polar compounds (Ye et al., 1991). In humans ≈5.000 taste buds are distributed in the oral cavity, most of them are situated on the tongue, others are in the soft palate and epiglottis (Chaudhari and Roper, 2010).

1.1.4 From the tongue to the central nervous system

Taste information processed in the taste buds is relayed to afferent fibers from three cranial nerves (CN): the facial (CN VII), the glossopharyngeal (CN IX), and the vagus (CN X) (Fig 5). The nuclei of these fibers are located in the cranial nerve ganglia (Geniculate ganglia and Petrosal ganglia), whose central branches enter the central nervous system (CNS) in the brainstem. The terminal fields of these cranial nerves project to the Nucleus of Solitary Tract (NST) in a course rostrocaudal topographic organization (Contreras et al., 1982; Hamilton and Norgren, 1984; Corson et al., 2012). Two branches of the facial nerve, namely the chorda tympani (CT) and the greater superficial petrosal, send their axons to the rostral portion of the NST. They carry gustatory information from the anterior portion of the tongue and soft palate, respectively (Whitehead and Frank, 1983). The glossopharyngeal nerve carries taste information from taste buds of the caudal portion of the tongue to the rostral and caudal NST. The vagus nerve transmits gustatory information from the epiglottis and projects mainly to the caudal portion of the NST (Hamilton and Norgren, 1984).

The NST also receives somatosensory inputs from the oral cavity through lingual branches of the trigeminal nerve (Hamilton and Norgren, 1984). For this reason, NST integrates thermal and tactile

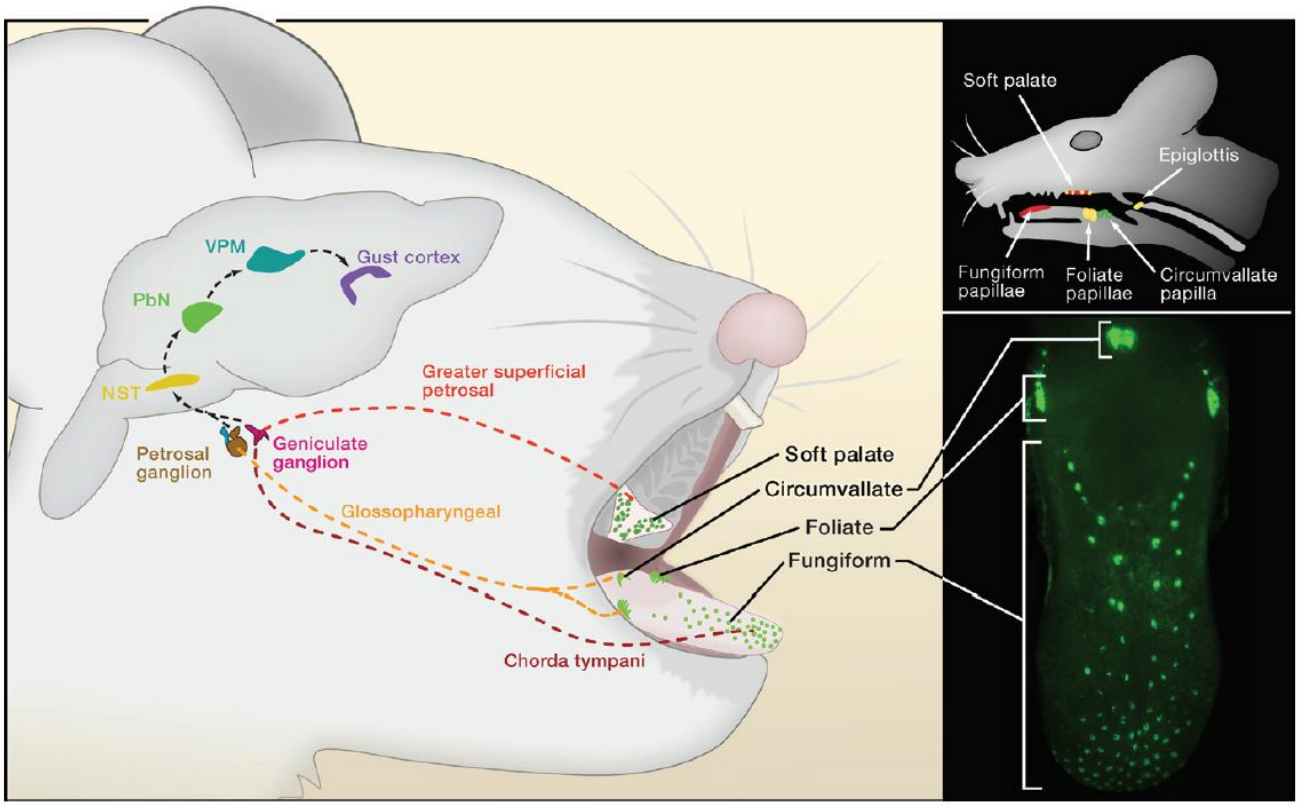

Figure 5. ***Taste networking, from the periphery to CNS****. On the left scheme is shown the mouse taste networking from the periphery to CNS. Chorda tympani, greater superficial petrosal and glossopharyngeal nerves carry taste information to nucleus of solitary tract (NST) in the brain stem. From NST taste inputs are transmitted and processed through the parabrachial nucleus (PbN) and the thalamus (VPM) to the primary gustatory cortex (GC) in the insula. Taste buds are distributed in taste papillae on the tongue. In the right panel is represented mouse taste papillae location in the whole taste system (top panel) and TBCs expressing the green fluorescent protein GFP on the tongue (bottom panel). Image modified from Yarmolinsky et al., (2009).*

somatosensory information, and it receives information also from other brain regions, for example, from the parabrachial nucleus (PBN), central amygdala (CeA), lateral hypothalamus (LH) and gustatory cortex (GC) (Kinnamon and Finger, 2019). Information from brain regions, especially involved in sensory processing, cognition, reward processing, and energy homeostasis are thought to modulate gustatory inputs. For example, GC, sending feedback projections to NST, modulates the gustatory inputs and outputs in the nucleus, while in LH there are neurons that respond to taste stimuli inducing feeding

behaviors (Shipley, 1982; Gselifstim, 1962). In any case, it has been estimated that in the rat up to 80% of rostral NST taste responsive neurons project to PBN (Di Lorenzo and Mornroe, 1995).

The PBN is composed of different nuclei in the brainstem (Bianchi et al., 1998). It can be divided into three main regions: the ventral region (Kolliker-Fuse nucleus), the medial region (mPBN), and the dorsolateral PBN region (dlPBN) (Bianchi et al., 1998).

After a relay in PBN, in rodents the gustatory information reaches the parvicellular portion of the ventroposterior medial thalamic nucleus (VPMpc). In primates, NST gustatory efferent bypass the PBN relaying and projecting directly to the VPMpc (Beckstead et al., 1980; Rolls,1989). This nucleus receives inhibitory inputs from the reticular thalamus (gustatory portion) and excitatory fibers from the GC (Allen et al., 1991; Holtz et al., 2015).

The efferent fibers from the VPMpc target mostly the GC and the amygdala (Turner and Herkenham, 1991).

In rodents, it has been shown that these two fundamental networks contribute to transmitting to higher brain areas different features of taste: the first, the parabrachial-thalamic (PBN- VPMpc) carries pure sensory information via thalamic pathway to GC, the second, the parabrachial-amygdalar (PBN-CeA), transmits hedonic information via the amygdalar pathway (Lundy and Norgren, 2004). Other efferent projections from PBN reach the LH or directly to the GC (Saper, 1982; Zhang et al., 2011).

The GC is located in a portion of the insular cortex and, in primates, also in a part of the operculum (Benjamin and Burton, 1968; Yamamoto et al., 1980; Mufson and Mesulam, 1982; Kosar et al., 1986). The insular cortex can be divided into three parts based on the presence and the cytomorphology of layer 4: (i) the first is defined as a granular layer with a typical neocortical architecture; (ii) the second is called dysgranular because it contains a dysmorphic and progressively fading of layer 4, (iii); the last is defined as agranular layer characterized by the absence of an identifiable layer 4 (Fig. 6) (Allen et al., 1991; Maffei et al., 2012).

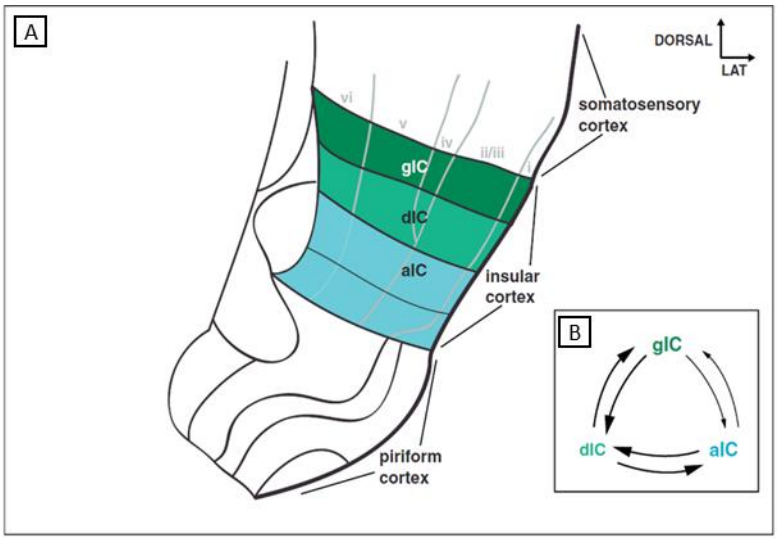

Figure 6. ***The three layers of gustatory cortex.*** *(**A**) Coronal view of the region of a rat brain which includes the somatosensory cortex, the insular cortex, and the pyriform cortex. Insular cortex has been divided in its three layers with a color code; dark green corresponds to the granular insula cortex (gIC), light green to the dysgranular insular cortex (dIC), and light blue to the agranular insular cortex (aIC). (**B**) Communication between the three layers. (Maffei et al., 2012)*

GC receives afferent fibers from many brain areas, such as, VPMpc that target the dysgranular portion (Allen et al., 1991), PBN, CeA, LH, and prefrontal cortices that target both the dysgranular and the agranular portion (Mufson and Mesulam, 1982; Allen et al., 1991). These are not the only inputs driven to the GC, afferent fibers arrive from neuromodulatory nuclei (locus coeruleus and nucleus of basalis of Meynert) (Linster and Fontanini, 2014), olfactory areas (Shipley and Geinisman, 1984), and other portions of the insular cortex (Shi and Cassell, 1998; Fujita et al., 2010; Adachi et al., 2013). Moreover, it has been shown that GC reveals a high degree of internal interconnectivity (Shi and Cassell, 1998; Fujita et al., 2010; Adachi et al., 2013).

Regarding the efferent projections, it has been shown that GC targets many brain areas, such as subcortical regions belonging to the limbic network (LH, CeA) (Allen et al., 1991; Shi and Cassell, 1998), mediodorsal thalamus, nucleus accubens, anterior cingulate cortex (ACC) and the orbitofrontal cortex (OFC) (Wright and Groenewegen, 1996; Gabbott et al., 2003; Baylis et al., 1995; Cavada, 2000). One of the most important sensory recipients of GC, beyond gustatory regions, is the endopiriform nucleus which integrates gustatory and olfactory information (Fu et al., 2004).

From GC outputs are sent to multiple sensory and reward-related regions, producing several feedback loops. All these aspects remain to be explored.

1.2 Three types of taste bud cells

Taste buds are considered as the fundamental units involved in taste sensation; indeed, they contain the taste receptor cells responsible for detecting chemical compounds in the mouth generating the input signals sent to the CNS (Fig. 7). Although they develop from epithelial tissue, these cells are considered neuron-like or modified epithelial cells, because they have the characteristic of excitatory cells as neurons (Roper and Chaudhari, 2017; Liman et al., 2014; Bigiani et al., 2002).

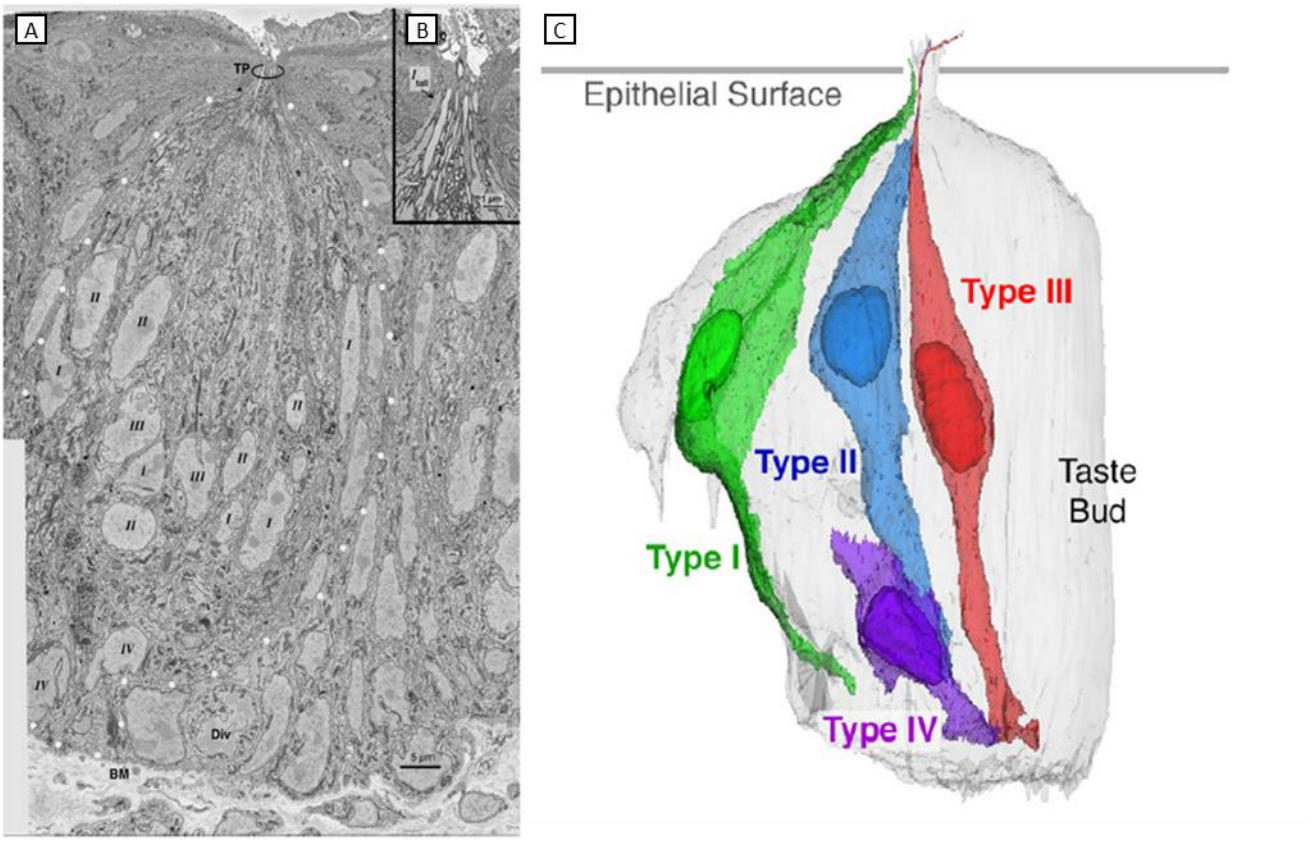

Figure 7. ***Cell types in a taste bud****. Electron microscope micrograph longitudinal section from sbfSEM (Serial blockface scanning electron microscopy) acquisition of a taste bud (****A****). In the inset (****B****) is represented the taste pore at high magnification.*
*(****C****) 3-D reconstruction of the taste bud represented in A. Four different morphologically and molecularly distinct cell types populate the taste buds. Type II and Type III transduce several classes of tastes, while Type I are considered to have glial-like functions. Type IV are immature cells, which develop into the other cell types. Image modified from Kinnamon and Finger, (2019).*

Indeed, some of them can generate action potentials (Chen et al., 1996). In the opposite of typical neurons TBCs conserved characteristics of epithelial cells, for example, they can regenerate during adult life. Indeed, TBCs usually live an average of only 2 weeks before dying and being replaced by newly born cells (Barlow, 2015; Lindemann, 2001). Based on morphological and functional characteristics we can distinguish three types of TBCs that are called Type I, Type II, and Type III (Fig. 8) (Murray, 1993; Pumplin et al., 1997; Liman et al., 2014; Roper and Chaudhari, 2017). In addition to these three subclasses of TBCs, some authors report also a fourth group that represents the immature TBCs. These latter cells are basal cells and are called Type IV by some authors (Kinnamon and Finger, 2019).

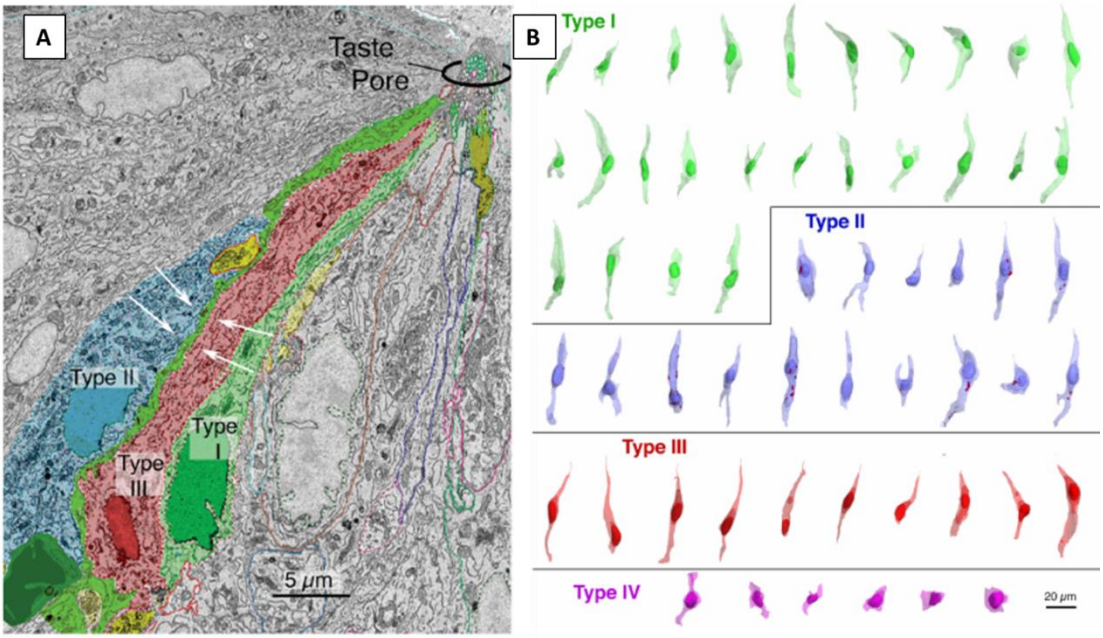

Figure 8. ***Shapes of cells in a taste bud****. (**A**) Electron micrograph from sbfSEM (Serial blockface scanning electron microscopy) acquisition showing a longitudinal section of a taste bud. Type I TBCs (green) can have an elongated shape and their membrane can separate Type II (blue) and Type III (red) TBCs. (**B**) Representation of 3-D reconstruction of fully segmented cells from a single taste bud, showing the diversity of cellular morphologies of the different cell types (Yang et al., 2020).*

1.2.1 Type I

The Type I TBCs are the most abundant cells in taste buds. They appear morphologically narrow, electrodense at electron microscopy micrographs. They present microvilli connected with the mouth lumen through the taste pore and cytoplasmic membrane extensions that wrap up the other TBCs (Murray, 1993). Although several scientists identified and described this sub-population of TBCs, some of their properties and functions are still unknown (Roper and Chaudhari, 2017).

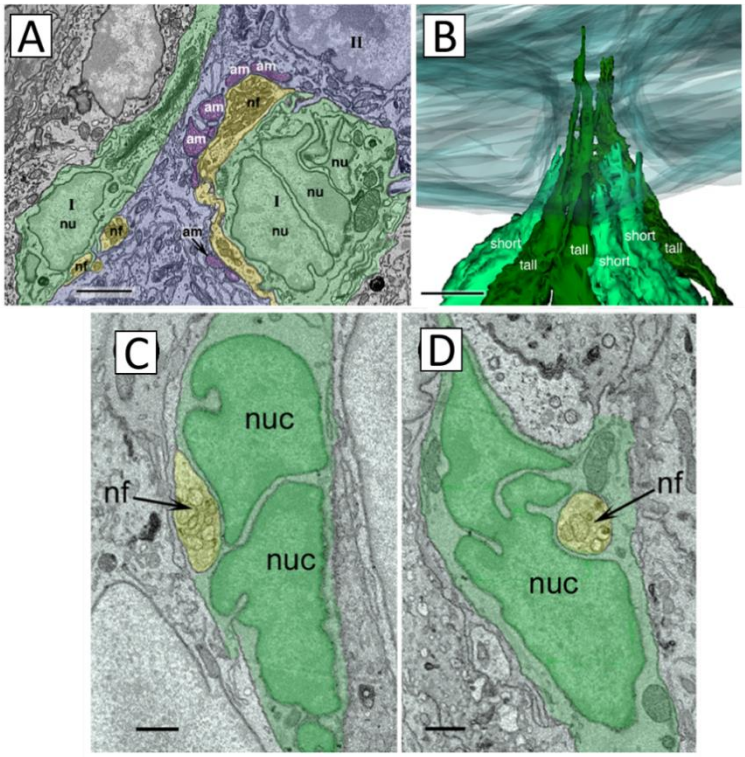

Figure 9. ***Type I TBCs morphology acquired using sbfSEM (Serial blockface scanning electron microscopy)****. (**A**) Type I TBCs electron micrographs showing fragmented nuclei and converge together with Type II TBCs juxtaposed to the synapse on afferent nerve fibers. (**B**) 3-D reconstruction of taste pore in which Type I TBCs show different morphological microvilli: tall microvilli (dark green) and short microvilli (light green). (**C**-**D**) Electron micrographs exhibiting Type I TBCs juxtaposed to the afferent nerve fibers. Abbreviations:* ***am****-atypical mitochondria,* ***nf****-nerve fibers,* ***nu*** *or* ***nuc****-nucleo. Image from Yang et al., (2020).*

A recent work using serial block-face scanning electron microscopy, conducted by Yang et al., (2020), clarifies some details about Type I TBCs. They found two distinct morphological features associated with Type I TBCs: one that presents tall-microvilli, and a second one with short microvilli. It has been proposed that these different morphologies could be related to different functions of these cells

(Fig. 9). In response to taste stimuli different neurotransmitters are released in taste buds, and they are fundamental in generating responses in afferent nerve fibers. In particular, recent studies revealed that ATP (Adenosine triphosphate) is an important neurotransmitter in the taste bud. ATP released by type II TBCs promotes responses to sweet, bitter, umami, and salt (Roper and Chaudhari, 2017; Nomura et al., 2020). Also, glutamate appears to be a possible candidate involved in a feedback mechanism between Type III cells and nerve fibers (Roper and Chaudhari, 2017). Type I TBCs expressing GLAST (Glutamate Aspartate Transporter) and NTPDase2 (Ectonucleotides Triphosphate Diphosphoydrolase) are thought to be involved in terminating synaptic activity (Chaudhari and Roper, 2010). Indeed, GLAST is involved in glutamate reuptake in the brain (Storck et al., 1992) and in particular it is found in glial processes, associated with glutamatergic synapses (Chaudhry et al., 1995; Lehre et al., 1997). It is also expressed in the peripheral nervous system such as in the supporting cells that surround the sensory receptors of both inner ear and retina (Furness and Lehre, 1997; Takumi et al., 1997; Lehre et al., 1997).

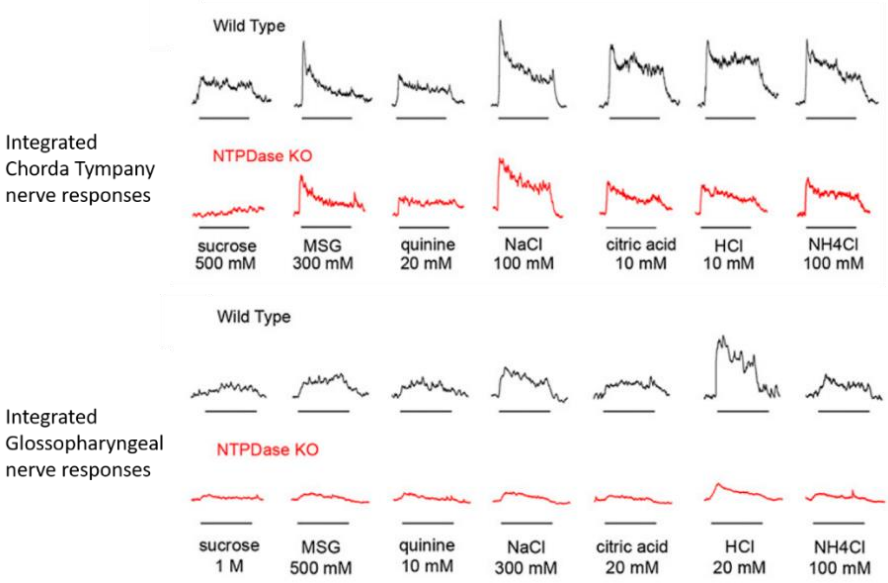

Figure 10. ***Gustatory nerve responses****. Integrated Chorda Tympani and Glossopharyngeal nerve responses are reduced in Entpd2-Knockout mice compare with WT. Image modified from Vandenbeuch et al., (2013).*

NTPDase-2, encoded by *Entpd*2, belongs to the ecto-nucleosidase triphosphate diphosphohydrolase family (Zimmerman 2001). NTPDase-2 is localized in the plasma membrane of type I TBCs and its main role is the degradation of ATP from interstitial space (Bartel et al., 2008). Electrophysiological recordings from glossopharyngeal and chorda tympani nerve fibers in Entpd2-Knockout mice showed reduced responses to all taste qualities (Fig. 10) (Vandenbeuch et al., 2013).

They suggest that excessive levels of extracellular ATP, due to eliminating NTDPase2, could desensitize purinergic receptors P2X expressed in nerve fibers, causing a decrease in taste responses (Vandenbeuch et al., 2013).

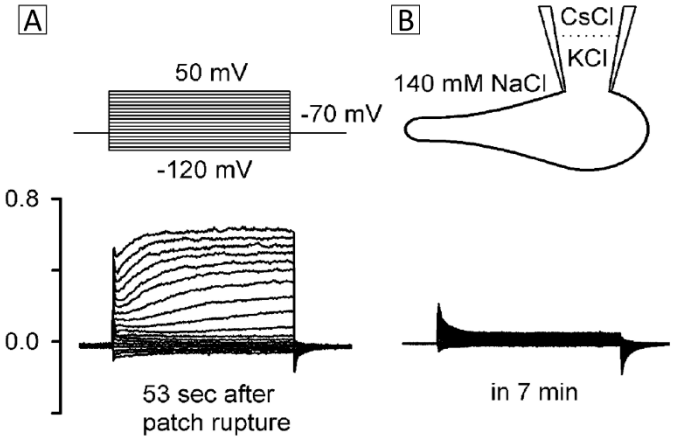

Figure 11. ***Type I electrophysiological profile****. Type I TBC recorded with KCl in* ***A*** *and the same cell recorded with CsCl in* ***B****. Image modified from Romanov and Kolesnikov, (2006).*

Several studies show that each subclass of TBCs is characterized by a specific electrophysiological profile. Type I TBCs show a robust outward K^+ current (see Fig. 11, A) (Bigiani, 2001; Romanov and Kolesnikov, 2006; Noguchi et al., 2003; Medler et al., 2003; Vandenbeuch et al., 2008). The substitution of KCl with CsCl in the intracellular solution abolishes outward K^+ current (Fig. 11, B). Romanov and Kolesnikov, increasing the [K^+] in the extracellular solution, revealed that Type I TBCs also show an inward rectifier K^+ current (Fig. 12).

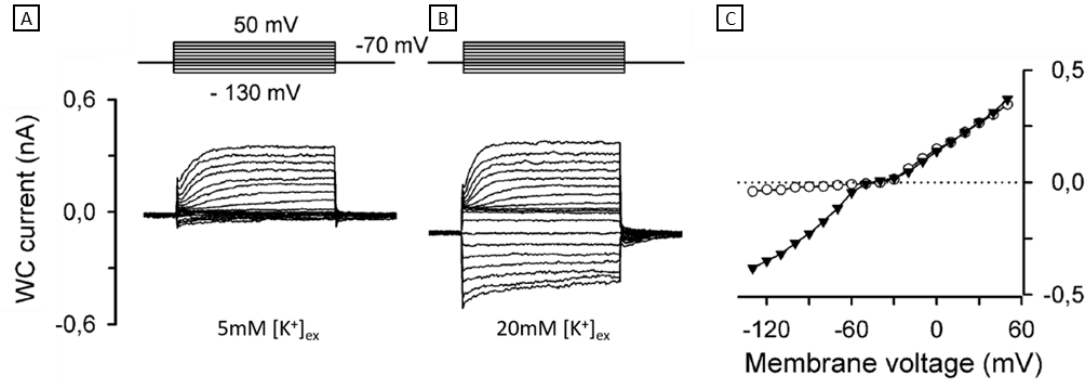

Figure 12. ***Type I electrophysiological characterization****. Whole-Cell currents recorded from Type I TBCs stepped from -130 mV to 50 mV from a holding potential of -70mV. The image compares the cell kept in 5 mM (****A****) and 20 mM (****B****) external K^+. (****C****) IV relationship from the cells recorded in A and B. Image modified from Romanov and Kolesnikov, (2006).*

In accordance with previous results, Dvoryanchikov et al. (2009) revealed the expression in type I TBCs of KCNJ1 (Potassium Inwardly Rectifying Channel Subfamily J Member 1), an inward rectifier K^+ channel also known as ROMK or Kir1.1. This channel seems to be selectively localized in the apical portion of these cells (Fig. 13) (Dvoryanchikov et al., 2009).

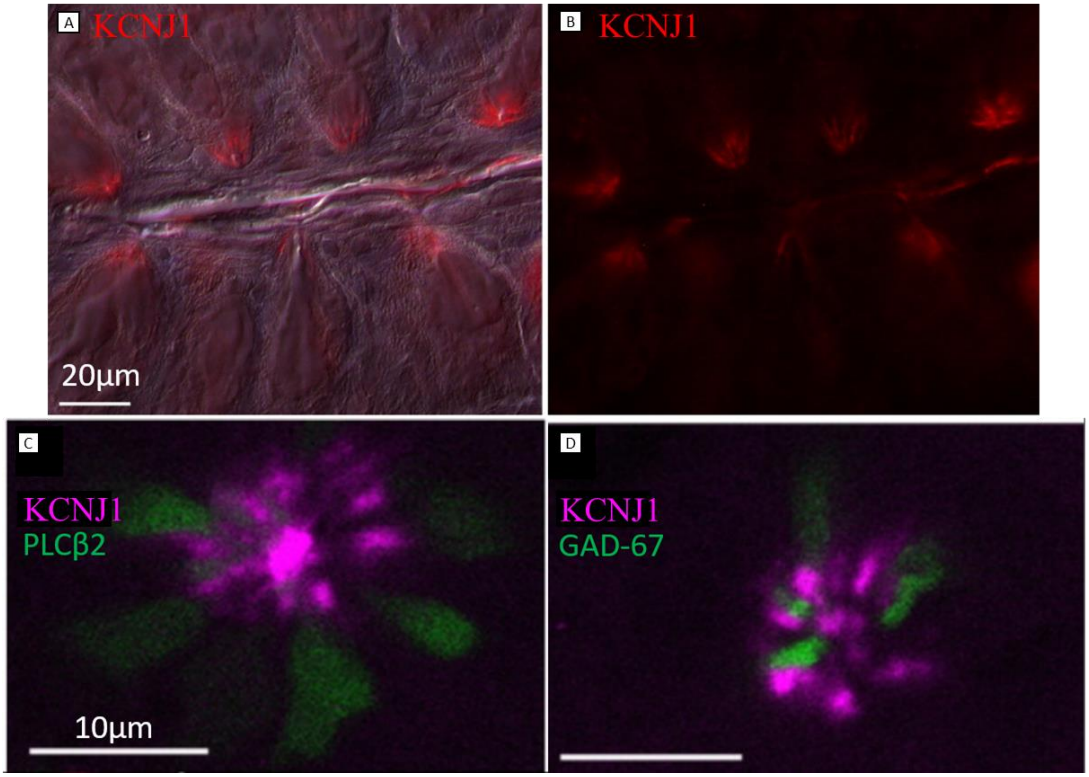

Figure 13. ***Localization of K^+ channel KCNJ1 in TBCs****. Type I TBCs labelled for KCNJ1. (**A**-**B**) TBCs stained for KCNJ1 (red) in mouse Circumvallate papilla. TBCs stained for KCNJ1 (magenta) and PLCβ2 (green), marker of Type II TBCs (**C**), and GAD-67(green), marker of Type III TBCs (**D**). Image modified from Dvoryanchikov et al., (2009).*

Type I TBCs characteristics support the hypothesis that this subclass of TBCs is involved mainly in maintaining the taste bud structure and buffering the ion composition in the extracellular solution, that surrounds the other TBCs. Indeed, the accumulation of K^+ in the interstitial space could affect the passive membrane properties of the other TBCs reflecting a possible disruption of membrane excitability (Bigiani, 2001).

1.2.2 Type II

The type II TBCs are responsible for detecting sweet, bitter, and umami tastes. Moreover, according to recent studies, these cells mediate also salty sensation (Roebber et al., 2019; Nomura et al., 2020). Indeed, salt perception seems to be mediated by two distinct modalities: one, that is considered amiloride-sensitive, by only type II TBCs, and a second one that is insensitive to amiloride mediated by type II and III TBCs (see paragraph 1.3.5) (Nomura et al., 2020; Oka et al., 2013; Kinnamon and Finger, 2019). Type II cells appear morphologically narrow with an elongated shape and they present short microvilli in the apical portion. The nuclei of these cells are big and the cytosol is electron-lucent (Roper and Chaudhari, 2017; Pumplin et al., 1997). Approximately, one-third of the cells in a taste bud are type II TBCs (Roper and Chaudhari, 2017).

Type II cells are the most important cells in generating taste inputs into afferent nerve fibers. This is possible by releasing neurotransmitters in a depolarization-mediated manner (Finger, et al., 2005). Type II TBCs secrete at least two different neurotransmitters: ATP and Acetylcholine (ACh). The role of ATP in taste buds is largely understood (Chaudhari and Roper, 2010; Liman et al., 2014; Kinnamon and Finger, 2019; Roper and Chaudhari, 2017). It is responsible to activate afferent nerve fibers sending taste information to the CNS (Finger, et al., 2005). It has also an autocrine and paracrine effect. ATP release is potentiated by autocrine feedback via P2X and P2Y receptors expressed by Type II TBCs (Huang et al., 2011b). Moreover, it can induce Serotonin (5-HT) release by Type III TBCs that express P2X receptors (Huang et al., 2009b). Secretion of ACh by Type II TBCs is suggested by the fact that taste buds are rich in acetylcholinesterase (Paran and Mattern, 1975; Dando and Roper, 2012), however, the role of ACh is not completely understood. It seems to be involved in an autocrine mechanism to increase the release of ATP (Roper and Chaudhari, 2017).

Type II TBCs are excitable cells and can generate action potentials. Indeed, they show a specific set of voltage-gated ion channels. Although tastants bind to these cells using different receptors and mediating different taste qualities, they share the same transduction pathway cascade. Indeed, all of them converge in a common intracellular signaling pathway that will be described in paragraph 1.3.2.

1.2.3 Type III

Type III TBCs mediate sour sensation and appear to be involved in the “amiloride insensitive” modality for salt sensation (see paragraph 1.3.5)(Lewandowski et al., 2016; Larson et al., 2020). They

are also known as “presynaptic cells” because they are the only TBCs that present conventional synapses with the afferent nerve fibers (Roper and Chaudhari, 2017; Kinnamon and Finger, 2019). Indeed, type III TBCs show ultrastructurally recognizable synapses (Murray, 1993) and express numerous synapses-associated proteins such as SNARE (soluble N-ethylmaleimide-sensitive factor attachment protein receptor), SNAP25 (synaptosomal associated protein), NCAM (Neural Cell Adhesion Molecule) a cell surface adhesion molecules, and voltage-gated Ca^{2+} channels typically associated with neurotransmitter release (DeFazio, 2006; Chaudhari and Roper, 2010). Moreover, it has been shown that type III TBCs express the TRP channels PKD2L1/3 (Polycystic kidney disease 2-like-1/3), and they were thought to play a key role in detecting sour substances (Ishimaru Y and Matsunami, 2009; Kataoka et al., 2008). However, knockout of the PKD2L1/3 genes has a little effect on cellular and gustatory nerve responses to acids (Horio et al., 2011).

This subpopulation of TBCs is the least represented in the taste buds (2-20% of the cells in a taste bud). Moreover, taste buds from the posterior tongue (CVP and FoP) contain more type III cells in comparison with taste buds of FuP (Roper and Chaudhari, 2017). These cells display slender profiles and oblong nuclei (Roper and Chaudhari, 2017).

Type III TBCs express several voltage-gated ion channels, including Na^+ channels, voltage-gated rectifying K^+ channels, Cl^- channels, and Ca^{2+} channels, and can generate action potentials (Medler et al., 2003; Romanov and Kolesnikov, 2006; Noguchi et al., 2003; Bigiani and Cuoghi, 2007). Moreover, Ca^{2+} channels are fundamental in these cells to release neurotransmitters by conventional-synaptic mechanisms and trigger afferent nerve fibers (Liman et al., 2014; Vandenbeuch et al., 2010). Some evidence suggests that type III TBCs release numerous neurotransmitters in the taste buds. One of the first neurotransmitters found was 5-HT (Huang, 2005). Indeed, several sour stimuli, including KCl-induced depolarization, elicit 5-HT release from type III TBCs (Huang et al., 2011). Two distinct mechanisms can induce 5-HT release from Type III: one triggered by sour stimuli (Huang et al., 2011) and a second one activated by ATP released by Type II TBCs (Huang et al., 2009b). The role of 5-HT is still unclear but it has been suggested that it could inhibit ATP release by Type II TBCs, and it could have a direct effect on afferent nerve fibers (Larson et al. 2015). Type III TBCs can also release GABA (gamma-Aminobutyric acid), which is thought to have an inhibitory effect on ATP release by Type II TBCs (Huang et al., 2011; Dvoryanchikov et al., 2011). Moreover, type III TBCs can uptake and accumulate noradrenalin (Huang et al., 2008). Likely, noradrenalin secreted by afferent nerve fibers can be re-uptaken by Type III TBCs from the extracellular space, although its role is still unclear (Roper and Chaudhari, 2017).

1.3 The transduction mechanisms for the taste qualities

The three types of TBCs described in the previous paragraphs are responsible to mediate the five basic taste qualities: sweet, bitter, umami (savory), sour, and salty. Different TBCs respond to one of the basic tastes, however, there is some evidence suggesting that, in particular conditions, TBCs can mediate also different taste modalities (Roper and Chaudhari, 2017).

How can taste cells discriminate between the five taste qualities? On one side, some scientists support the "labelled-line coding model", while others prefer "the combinatorial model of taste coding". The labelled-line mode assumes that individual taste cells respond to only one taste quality and this information travel to the CNS through specialized/dedicated nerve fibers. Moreover, afferent nerve fibers projects to neurons that are labelled with the same taste quality. In this way, from the periphery to the CNS, taste qualities information travel on a dedicated labelled line (Roper and Chaudhari, 2017; Yarmolinsky et al., 2009). On the other hand, according to the combinatorial mode, the perception of taste qualities is due to a combination of signals. Some taste cells, which are called "narrowly tuned" (or specialist) respond specifically to single taste quality while other cells can respond to different taste qualities and are called "broadly tuned" (or generalist) (Roper and Chaudhari, 2017; Frank, 1973). For example, type II cells respond mainly to single taste quality, while type III can respond directly to sour stimuli but indirectly (via cell-cell communication) to multiple taste stimuli; electrophysiological recordings from ganglion neurons showed that some of these cells are highly tuned (specialist neurons) to single taste quality, while other neurons respond to different taste qualities (generalist neurons) (Yoshida et al., 2009, 2006; Tomchik et al., 2007).

1.3.1 Sweet, Bitter, and Umami

Sweet, Bitter, and Umami (savory) stimuli activate the same class of TBCs: Type II. However, Type II TBCs differ from each other because they express and use different types of GPCRs (G protein-coupled receptors) to detect classes of tastants. Although type II TBCs express distinct receptors and bind different molecules, all type II cells share the same transduction cascade mechanism.

1.3.2 Effector pathway for Type II TBCs (sweet, bitter, umami)

Type II taste cells express taste receptors T1R or T2R, as explained in detail in the following sections. T1R and T2R are GPCRs coupled to heterotrimeric G proteins that include $G\beta_3$, $G\gamma 1_3$, $G\alpha_{gus}$ (also known as Gustducin) (Wong et al, 1996), $G\alpha_{14}$ and $G\alpha_i$. In the current view, the primary function of Gα subunits is to regulate Gβγ subunits, while Gβγ subunits activate PLCβ2 (Phospholipase C β2) (Roper and Chaudhari, 2017; (Rössler et al., 1998).

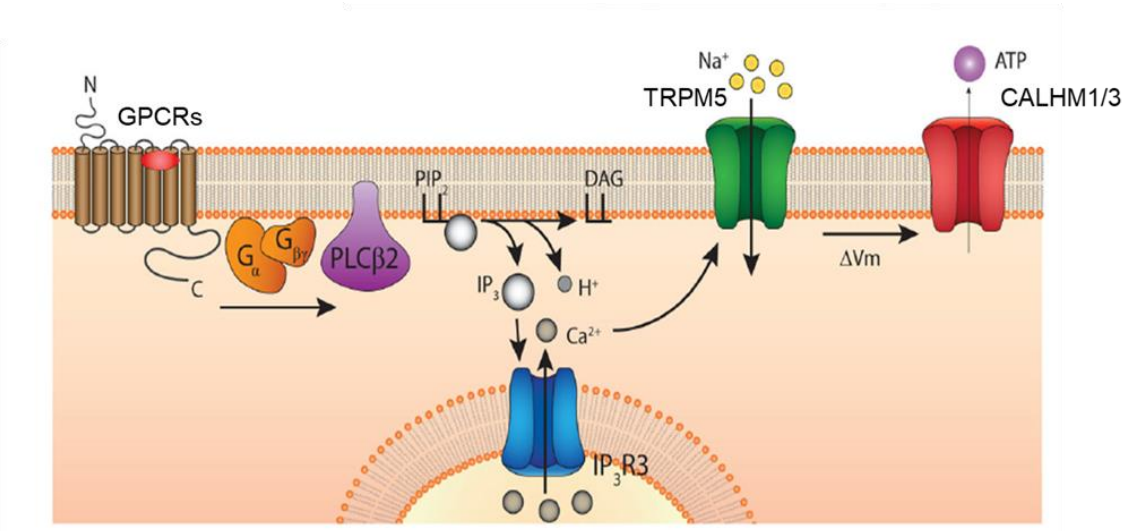

Figure 14. ***Transduction cascade in Type II TBCs****. Transduction of bitter, sweet and umami mediated by a PLC-signaling cascade, that culminates in the opening of the TRPM5 ion channel. This produces a depolarization that may allow CALMH1/3 channels to open and secrete ATP, which serves as neurotransmitter. Image modified from Liman et al., (2014).*

The phospholipase C generates the second messengers IP_3 (Inositol Triphosphate), DAG (diacylglycerol), and H^+. IP_3 acting on IP_3 receptor (IP_3R_3) promotes releasing of Ca^{2+} in the cytosol from stores and the Ca^{2+} gates the TRPM5 (Transient receptor potential cation channel subfamily M member 5) and TRPM4 channels (Transient receptor potential cation channel subfamily M member 4) (Liman et al., 2014; Roper and Chaudhari, 2017; Roper, 2007; Zhang et al., 2007; Liu and Liman, 2003; Banik et al., 2018). Activation of TRPM5 and TRPM4 allows the depolarization of Type II TBCs (Liman et al., 2014; Roper and Chaudhari, 2017). TRPM5 is a member of the TRP family ion channels and from previous experiments conducted in heterologous systems, it results activated by intracellular Ca^{2+} and it is permeable to monovalent but not divalent cations (Liman et al., 2014). Together with TRPM5, also

three Na^+ channels allow transient inward current for depolarization: SCN2A, SCN3A, and SCN9A (Sodium Voltage-Gated Channel Alpha Subunit 2-3-9) (Gao et al., 2009). Moreover, K^+ and Cl^- channels have been found in Type II TBCs. They are involved in membrane repolarization or in maintaining the resting membrane potential (Gao et al., 2009; Wang et al., 2009; Bigiani et al., 2002; Ghiaroni, et al., 2003). Type II cells use a non-conventional mechanism of releasing neurotransmitters. Indeed, ATP is released by the large non-selective channel CALHM1/3 (Calcium Homeostasis Modulator 1/3) (Taruno et al., 2013; Ma et al., 2018; Romanov et al., 2018). The production of ATP is ensured by a large number of atypical mitochondria juxtaposed to the nerve fibers (Fig. 15 C) (Yang et al., 2020). ATP acts as the primary neurotransmitter to stimulate P2X2/3 receptors on afferent gustatory neurons (Kinnamon and Finger, 2019; Liman et al., 2014; Romanov et al., 2018; Finger, et al., 2005). Indeed, double-knockout [$P2X2/P2X3^{Dbl-/-}$] lost completely nerve responses when stimulated by several tastants compared with WT (Wilde Type) animals (Fig. 15) (Finger, et al., 2005). Moreover, knockout for CALHM1/3 strongly reduced ATP released from Type II TBCs (Ma et al., 2018), demonstrating that this non-conventional releasing mechanism is fundamental in taste sensation.

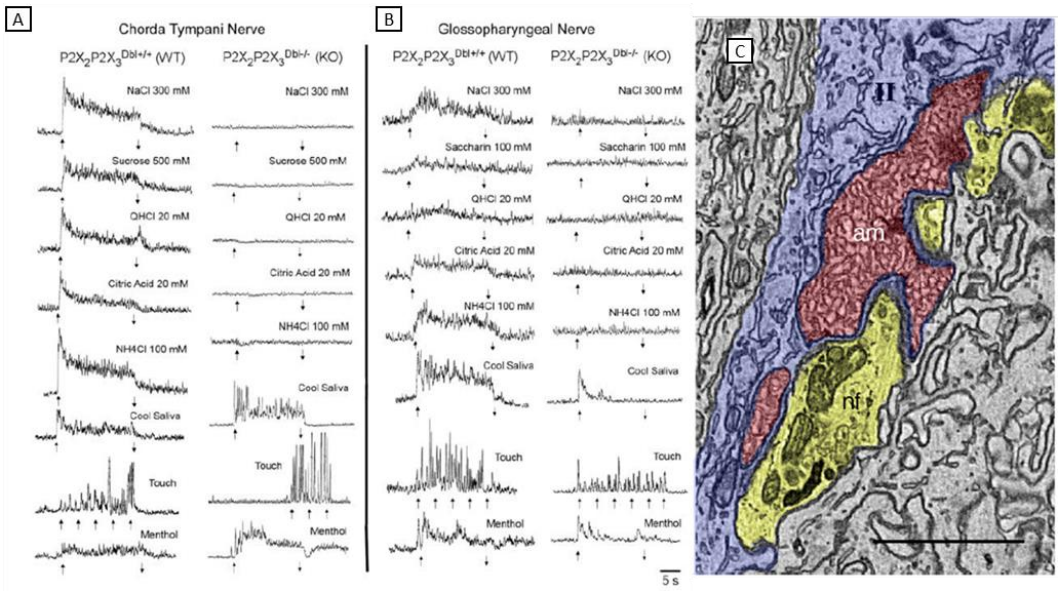

Figure 15. ***ATP is crucial for communication from taste cells to gustatory nerves****. (**A**-**B**) Nerve recordings from $P2X_2P2X_3^{Dl+/+}$ (WT) and $P2X_2P2X_3^{Dl-/-}$ (KO) mice. Comparison of responses magnitude to a variety of taste, tactile and thermal stimuli. KO animals lost responsiveness only to taste stimuli. (**C**) Electron microscope micrograph shows how Type II TBCs possess non-conventional synapses. They also show atypical mitochondria (am) juxtaposed to afferent fibers. (Finger, et al., 2005; Yang et al., 2020)*

1.3.2.1 Sweet - responsive TBCs

Sweet tastants are associated with appetible foods and correspond to different classes of molecules such as glucose, fructose, artificial sweeteners, some amino acids, starch (especially in mice), and other types of carbohydrates. All these molecules are rich in energy and their palatability is important to stimulate our appetite. Sugars are detected from TBCs with different strategies. The best-studied is associated with the expression of two GPCRs namely taste receptor type 1 member 2 (T1R2) and taste receptor type 1 member 3 (T1R3) (Pin et al., 2003). They work as heterodimers and present multiple ligand-binding sites (Fig. 16). They expose a long extracellular amino terminus that forms a venus flytrap module (VFM). Sugars and dipeptide sweeteners, usually, bind in the cleft of VFM (Cui et al., 2006). It has been reported that mice that lack T1R2 or T1R3 lose all behavioral sensitivity and neuronal responses to sugars and artificial sweeteners (Zhao et al., 2003), while deletion of only T1R3 seems associated with the loss of artificial sweeteners-mediated responses (Damak et al., 2003). Moreover, when the two receptors are co-transfected in a heterologous system, cells acquire the ability to respond to a large variety of sweet tastants (Nelson et al., 2001, 2002). Another proposed mechanism for glucose sensing involves the transporters GLUT2, GLUT4, GLUT5, and SGLT1 (Margolskee et al., 2007; Merigo et al., 2011; Roper and Chaudhari, 2017). They have been shown to transport glucose in the cells, increasing cytosolic ATP. ATP generated in this pathway blocks ATP-inhibited K^+ channels causing depolarization of the membrane (Yee et al., 2011). This modality, that includes glucose transporters, could explain why Na^+ salt can potentiate sweet taste (Kumazawa and Kurihara, 1990).

Figure 16. ***Receptors for sweets****. Receptors for sweets are GPCRs and may function as monomers or dimers (Yarmolinsky et al., 2009)*

1.3.2.2 Umami (amino acid) - responsive TBCs

Umami or savory is the sensation elicited by glutamate (in humans) and other amino acids (in rodents). The name is derived from a Japanese word that means delicious. We have experience of umami sensation when we eat foods rich in glutamates such as meat, fishes, and some vegetables. The classic stimulus that can elicit umami responses is monosodium glutamate (MSG) and it is largely used in the alimentary industry to amplify the palatability of the foods. It has been reported that when 5´ nucleotides, such as 5´ inosine monophosphate (IMP) is present together with glutamate occur a synergistic increase of umami taste (Yamaguchi, 1991; Roper and Chaudhari, 2017). Many authors documented that two GPCRs T1R1 (Taste receptor 1 member 1) -T1R3 heterodimers are responsible for transducing umami taste (Fig. 17) (Roper and Chaudhari, 2017; Liman et al., 2014), however recent works using Tas1r1 and Tas1r3 (which encode respectively T1R1, T1R3) knockout mice line showed neuronal and behavioral responses to umami similar to wild type phenotypes (Damak et al., 2003; Delay et al., 2006; Kusuhara et al., 2013). These findings indicate that there are, likely, other receptors for glutamate. Other receptors that have been found in taste buds are the metabotropic glutamate receptors mGluR4 (metabotropic Glutamate Receptors 4) (Chaudhari et al., 2000, 2009) and mGluR1(San Gabriel et al., 2009). Indeed, experiments using mGluR4 knockout mice revealed reduce responses to MSG and IMP, confirming its possible role in umami taste sensation (Yasumatsu et al., 2015).

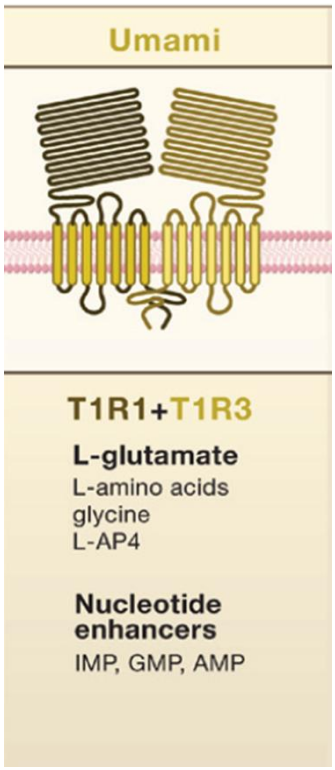

Figure 17. ***Receptors for umami****. Umami receptors are GPCRs and may function as modimers or dimers (Yarmolinsky et al., 2009)*

1.3.3.3 Bitter - responsive TBCs

A large variety of compounds can stimulate a bitter sensation. Bitter is one of the tastes that mediates repulsive behavior in humans and many other species. Generally, the bitter sensation is associated with harmful foods and substances, and it results necessary to avoid potentially toxic aliments. One characteristic of bitter tastants is that they are detected at much smaller concentrations compare with sweet and umami compounds. This underlines the importance of this perception to avoid lethal dietary mistakes (Yarmolinsky et al., 2009). Bitter tastants can be detected by receptors called T2Rs that belong to a class of A GPCRs. They have short N- termini and ligand-binding sites in the transmembrane segments (Fig. 18) (Behrens and Meyerhof, 2013). T2Rs have a highly variable structure with only a small portion conserved. This diversity of the sequence reflects the need to recognize a large variety of chemicals (Yarmolinsky et al., 2009). In general, each bitter-responsive TBCs express several types of bitter receptors (Adler et al., 2000). Moreover, T2Rs never colocalize in the same cell with sweet and umami receptors (Adler et al., 2000). Likely, the taste system differentiates between cells that detect appetitive or aversive stimuli (Roper and Chaudhari, 2017). There are pieces of evidence that bitter compounds can activate different T2Rs (Meyerhof et al., 2010; Sainz et al., 2007), or in some cases only a few of them. In this last case, we are talking about "narrowly tuned" or "specialist": cells that detect only one or a few bitter compounds (Meyerhof et al., 2010). On the opposite, T2Rs that can detect many chemicals, are called "generalist" (Behrens and Meyerhof, 2009).

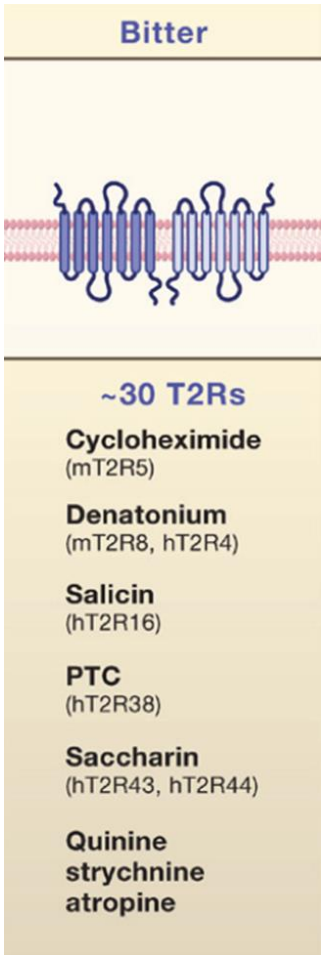

Fig. 18. ***Receptors for bitter****. Bitter receptors are GPCRs and they have a highly variable structure that allow them to bind several compounds (Yarmolinsky et al., 2009)*

1.3.4 Sour - responsive TBCs

Sour is detected by Type III TBCs (Huang et al., 2008; Richter et al., 2003; Chang et al., 2010). The proximate stimulus for sour taste is cytosol acidification. It has been shown that low intracellular pH blocks the K^+ channel Kir 2.1 (Inward Rectifier K^+-channel 1.2) leading to membrane depolarization, action potential firing, and consequent releasing of neurotransmitters (Fig. 19) (Chang et al., 2010; Bushman et al., 2015; Saotome et al., 2019; Teng et al., 2019). Acidification can occur by two different pathways: one associated with weak acids and a second one with strong acids (or mineral acids). Weak acids in the protonated form (undissociated) can easily cross the membrane acidifying the cytosol. Instead, strong acids that generally are in a dissociated form have more difficulty to cross the membrane. Recent studies revealed that protons (H^+) can be directly carried into the cell cytoplasm through a proton-selective channel expressed in the apical membrane of Type III TBCs. Liman and collaborators identified the channel as Otopetrin1 (OTOP1), a selective proton channel. Moreover, they demonstrated, using OTOP1 knockout mice, that this channel is necessary to detect strong acids in mice (Teng et al., 2019; Zhang et al., 2019).

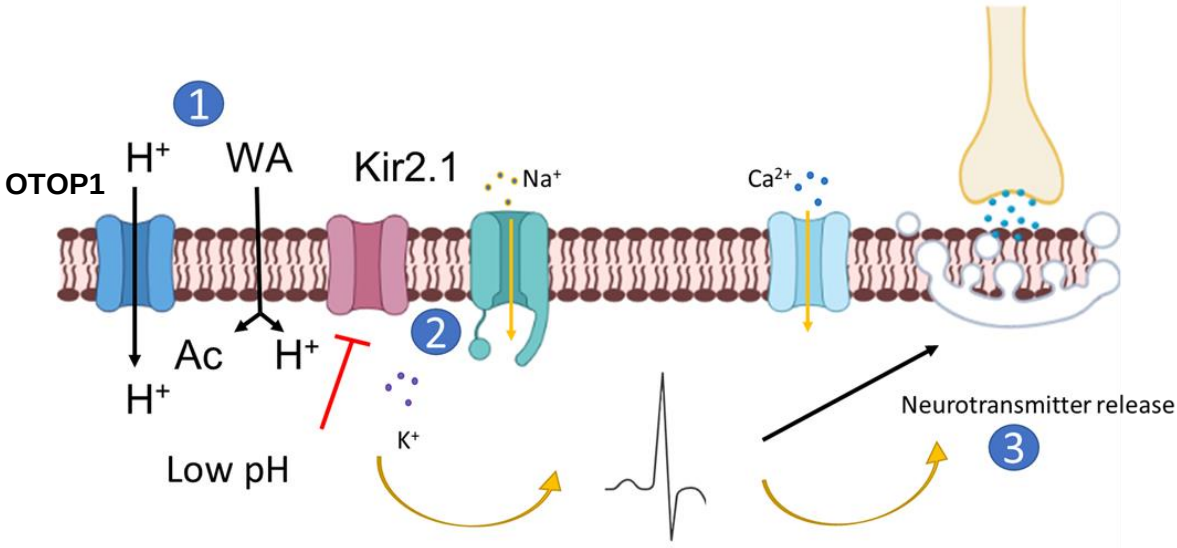

Figure 19. ***Sour transduction cascade****. (1) Strong acids generally are dissociated in R^- and H^+. H^+ from strong acids go into the cells through OTOP1 channel, while weak acids (WA), that cross the membrane, can release H^+ in the cell cytosol. (2) Low pH can block Kir 2.1, a resting K^+ channel, leading to cell membrane depolarization. This occurs by activation of Na^+ and Ca^{2+} channels. (3) Increasing in cytosolic Ca^{2+} leads the cell to release neurotransmitter from the basal portion of the cell membrane. Image based on Teng et al., (2019).*

1.3.5 Salty - responsive TBCs

Among the five basic tastes, the taste of salt (NaCl) is the least understood. Consumption of NaCl by animals is essential for life. It is an important mineral that regulates the osmolarity of biological fluids such as blood, plasma, and extracellular matrix. NaCl is necessary for the functioning of neurons and muscles and for the other cells that compose our organism. The perception of NaCl is the way to ensure the adequate ingestion of this essential mineral. However, the palatability of NaCl occurs only for low concentration of this salt, while animals tend to avoid high concentration of NaCl that results noxious and can induce hypernatremia and dehydration (Roper and Chaudhari, 2017). Indeed, the perception of NaCl could be divided into two separate modalities: low concentration of salt (approximately below 150 mM) that induces attractive behaviors, and high concentrations (beyond 150 mM) that are generally associated with aversive behaviors (Roper and Chaudhari, 2017). We still do not know exactly what kind of TBCs transduce NaCl (Roper and Chaudhari, 2017). In rodents, many data show that amiloride, a known diuretic, can decrease the nerve responses to NaCl and it can also decrease the attractive behaviors to NaCl in mice (Heck et al., 1984; Halpern, 1998). However, amiloride does not affect the perception of other salts (Halpern, 1998), and it does not change the perception of NaCl in humans (Ossebaard, 1996; Halpern, 1998). For these reasons, some authors refer to this specific pathway as "Amiloride sensitive" (AS) (Roper and Chaudhari, 2017; Liman et al., 2014; Vandenbeuch et al., 2008; Kinnamon and Finger, 2019). Given that amiloride is a blocker of epithelial Na^+ channels (ENaCs), ENaCs were considered candidate low salt receptors. ENaCs are composed of three subunits α, β, and γ, of which α is the pore-forming subunit of the channel (Canessa et al., 1994). It has been shown that ENaC α subunit knockout animals lost the sensitivity and the behavioral attraction to a low concentration of salt (Chandrashekar et al., 2010). Moreover, whole-cell patch-clamp experiments showed that amiloride inhibits a resting Na^+ conductance in isolated taste cells from the anterior tongue in rats (Bigiani and Cuoghi, 2007; Doolin and Gilbertson, 1996) and mice (Vandenbeuch et al., 2008). This result indicates the essential role of ENaCs to transduce a low concentration of NaCl. However, which kind of TBCs express these subunits? A recent paper from Lossow et al. (2020), using engineered mice that express fluorescent reporter proteins in cells expressing αENaC and βENaC, showed that not a single taste cell express both subunits (α, β). Moreover, they found that αENaC is mostly expressed in Type III TBCs, βENaC was found mainly in type I and type II TBCs, while γENaC subunit was found primarily in Type II cells, with small amounts in Type I and Type III cells. The subunits were found in TBCs from all tongues (anterior and posterior). This result is in contrast with previous findings showing that the

amiloride-sensitive component occurs only in the anterior portion of the tongue (Ninomiya, 1998). Confocal Ca^{2+} imaging experiments in TBCs from FuP via GCaMP3 expressed in Type II and Type III taste cells, showed that these cells respond to NaCl increasing cytosolic Ca^{2+}. Post hoc immunostaining experiments revealed that >80% of NaCl- responsive TBCs were Type II (Roebber et al., 2019). A recent work, however, revealed that Type II TBCs respond to NaCl generating action potentials and releasing ATP also without increasing cytosolic Ca^{2+} (Nomura et al., 2020). Although many papers suggest that Type II TBCs mediate the salty perception, Vandenbeuch et al. (2008), showed that also Type I TBCs, exhibiting only outward current, responded to amiloride. This finding is in accordance with the expression of ENaC subunits in the same cells (Lossow et al., 2020).

Responses to high concentrations of NaCl seem to follow an independent pathway, related to aversive behavior. Indeed, responses to high concentrations of NaCl are not affected by amiloride. The pathway is also called amiloride-insensitive (AI) (Roper and Chaudhari, 2017; Liman et al., 2014; Vandenbeuch et al., 2008; Kinnamon and Finger, 2019). Understanding this pathway is important because several experiments revealed that humans, unlike mice, use an amiloride-insensitive salt transduction pathway (Roper and Chaudhari, 2017; Roebber et al., 2019). However, we still do not know the receptors that mediate the behavioral responses to high NaCl (Liman et al., 2014). At least two subpopulations of TBCs are involved in the perception of high NaCl: bitter-responsive TBCs (type II) and sour TBCs (type III) (Oka et al., 2013). One characteristic shared by these two subpopulations is that both mediate aversive behaviors. Indeed, experiments in which TRPM5 or PLCβ2- expressing cells were inactivated showed a decrease in the high salt response. Moreover, a further silencing of PKD2L1-expressing sour cells (type III) eliminated the response to high salt concentrations (Oka et al., 2013). It is interesting to note that mice in which TRPM5-expressing cells were knocked out and PKD2L1 cells were deleted found a high concentration of NaCl attractive (Oka et al., 2013), which may be due to the ENaCs-mediated pathway.

1.4 The role of saliva in taste sensation

Saliva is a mucoserous fluid secreted in the mouth, where it performs several roles. Saliva is produced and secreted by several gland that are usually named major or minor glands, depending on their dimensions. The major glands are the biggest involved in saliva secretion and are parotid, submandibular, and sublingual glands (Matsuo, 2000). Of the major salivary glands, parotid is the biggest and alone contributes to 60 % of the whole salivary flow when stimulated by taste or chewing (Matsuo, 2000). The

minors glands are labial, lingual, buccal, and palatal glands, but hundreds of other small salivary glands are localized in the submucosa throughout the oral cavity. These glands secrete a small volume of saliva (<1 µl min^{-1} per gland) (Carpenter, 2013). A small subpopulation of minor glands is the Von Ebner's glands that are directly related to the taste buds contained in vallate and foliate papillae (Carpenter, 2013). Indeed, Von Ebner's glands are located in the crypts of vallate and foliate papillae, but not in fungiform papillae. These glands, as the parotid ones, appear more serous than mucous and they produce also proteins involved in food processing, such as lipocalin and lingual lipase (Carpenter, 2013). Saliva is a very diluted fluid composed of more than 99% of water, and it includes electrolytes such as Na^+, K^+, Cl^-, Ca^{2+}, Mg^{2+}, HCO_3^-. Saliva contains also hormones, immunoglobulins, proteins, enzymes, mucins, and nitrogenous products, like urea and ammonia (Humphrey and Williamson, 2001). All these components are necessary for several functions (Fig. 20): water and mucins are important in lubrication and cleaning of oral mucosa from exogenous microorganisms; bicarbonates, phosphates, and urea act to modulate pH; calcium, phosphate, and proteins work as an insolubility factor to maintain dental mineralization; immunoglobulins, proteins, and enzymes are fundamental in food processing and microbial homeostasis (Carpenter, 2013; Humphrey and Williamson, 2001).

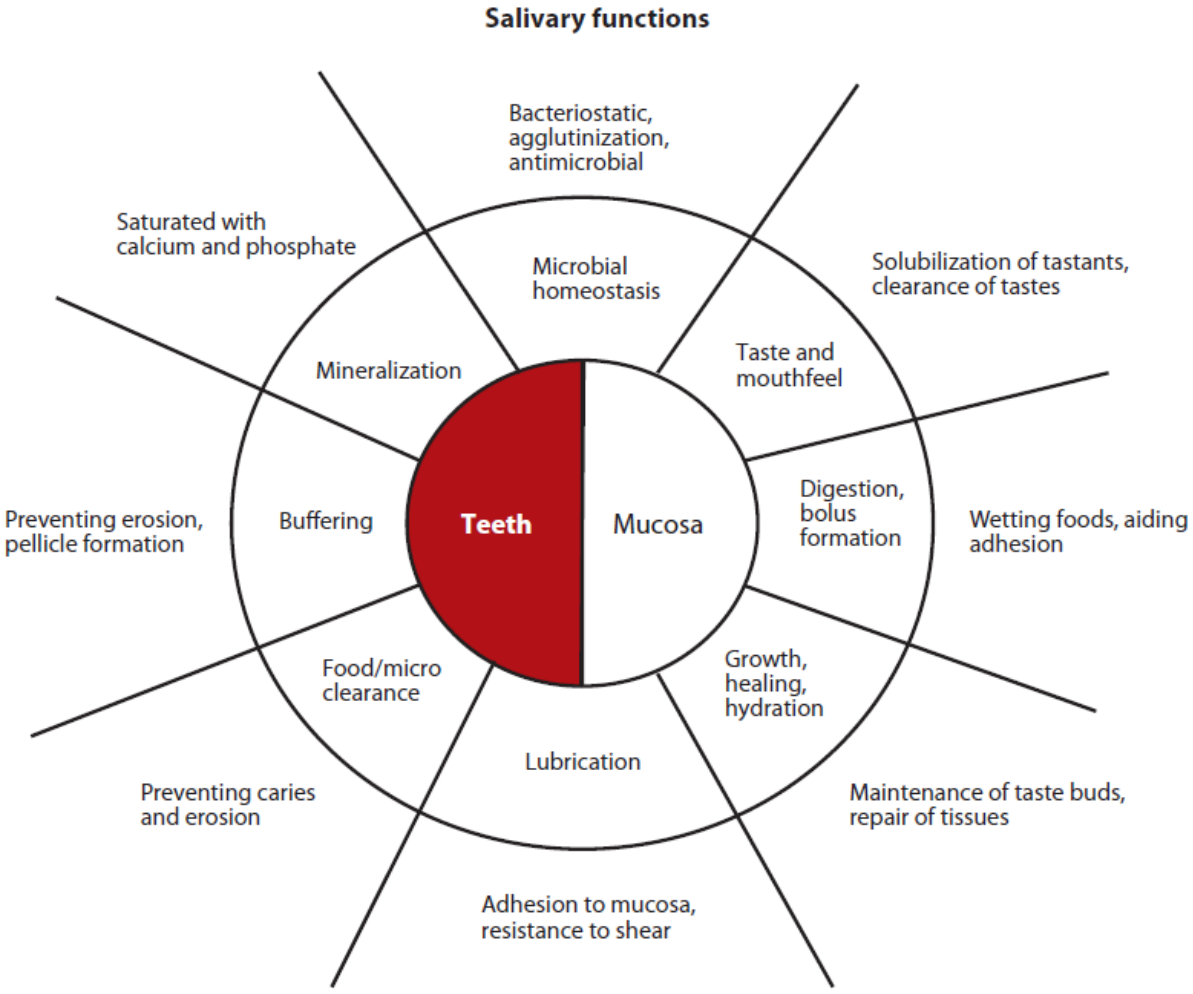

Figure 20. ***Summary of main saliva functions****. Functions of saliva can be divided according to the surfaces: teeth and mucosa. Several functions, like mineralization, are unique to one surface, while others are common to both surfaces, like lubrication and microbial homeostasis. Figure from (Carpenter, 2013)*

One of the more studied and controversial functions of saliva is its role in taste perception. Many pieces of evidence suggest that saliva is necessary for the solubilization of tastants before they reach the taste receptors, expressed on the microvilli surface of the TBCs. Indeed, electrophysiological recordings from chorda timpani nerve show different responses when rats receive tastants diluted in liquids (e. g. 0.1 – 0.3 M NaCl and 0.5 sucrose dissolved in distilled water) compared with dry food pellets. Responses to solutions are characterized by initial fast transient (phasic) chorda timpani discharges followed by a prolonged steady-state phase, while dry food pellets produce gradually increasing chorda timpani discharges that then reach a stable (tonic) level (Fig. 21).

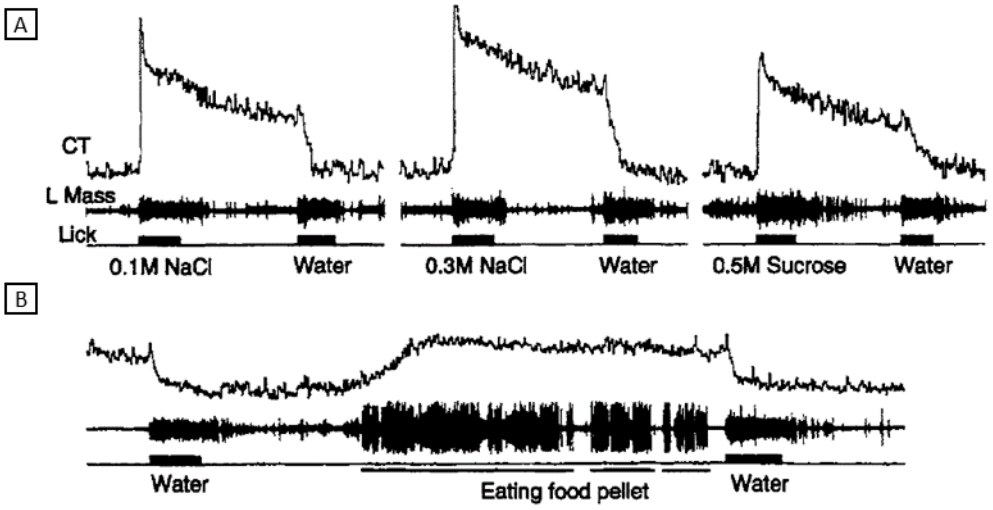

Figure 21. ***Chorda tympani responses during licking or eating pellet****. Each recording is composed by digitally summated chorda tympani discharges (CT), electromyographic activity of left messenter muscle (L Mass), and the lick signal (Lick). (**A**) responses to solutions and (**B**) responses to a dry food pellet. Modified from Matsuo, (2000).*

Moreover, some data suggest that changes in quantity and quality of saliva can influence taste perception (Matsuo, 2000). It is well known that sour taste is modulated by saliva. Acid stimuli are directly associated with increasing H^+ concentrations dissociated in saliva (Beidler and Smallman, 1965; Norris et al., 1984), but the production of bicarbonate secreted by glands can reduce the sour intensity, buffering the low pH (Helm et al., 1982). Saliva contains also organic substances, as proline-rich proteins (PRPs), that bind and precipitate plant polyphenols reducing their aversive (bitterness and astringency) taste (Mehansho et al. 1987; Murray et al., 1994). It is important to know that, although TBCs are continuously stimulated by salivary elements we cannot recognize the taste of saliva. This is because TBCs are adapted to the salivary environment (Matsuo, 2000). For example, the concentrations of electrolytes as Na^+, K^+, Cl^- and HCO_3^- vary in saliva, depending on the salivary production rate. Normally Na^+ concentration is between 5-100 mM, K^+ 10-25 mM, Cl^- 15-40 mM and HCO_3^- 5-60 mM. It is well known that Na^+ in saliva can affect the salty taste of NaCl. In particular, it has been shown that increasing Na^+ in saliva can elevate taste thresholds and decrease supra-thresholds intensities of NaCl (McBurney and Pfaffmann, 1963). In addition, the anion Cl^- seems involved in NaCl perception, and while Na^+ increases membrane potential of TBCs flowing through amiloride-sensitive channels, Cl^- penetrating through the tight junctions between taste cells (paracellular pathway), can directly modify the membrane potential evoked

by Na^+ (Elliott and Simon, 1990). Altogether these results underline the importance of saliva in taste perception, especially in FoP and CVP papillae where taste buds, located in the tissue invaginations, are strictly coupled with von Ebner's glands. Moreover, probably also TBCs themselves could produce saliva (Matsuo, 2000).

2 Calcium-activated chloride channels

Calcium-activated chloride channels (CaCCs) are Cl^- channels activated by intracellular Ca^+. They are expressed in different species, ranging from fungi to mammals, and are present in various tissues (Oh and Jung, 2016). The first evidence of functional CaCCs was from studies on *Xenopus laevis* oocytes, where CaCCs are involved in the block the polyspermy (Jaffe and Cross, 1984). CaCCs are expressed in several cells such as neurons; epithelial cells; olfactory and photo-receptors; cardiac, smooth, and skeletal muscles; Sertoli cells; mast cells; neutrophils, lymphocytes; uterine muscle; brown fat adipocytes; hepatocytes; insulin-secreting beta cells; mammary glands; sweat glands (Hartzell et al., 2005) and airway epithelial cells (Wagner et al., 1991; Gray et al., 1995). CaCCs play several physiological roles such as modulation of the cardiac action potential (Zygmunt and Gibbons, 1991; Wang et al., 1995; Collier et al., 1996; Kawano et al., 1995), vascular tone regulation (Nilius et al., 1997; Nelson et al., 1997), control of neuronal excitability (De Castro et al., 1997) modulation of epithelial secretion (Romanenko et al., 2010).

CaCCs show outward rectification at low concentrations of intracellular Ca^{2+}, and voltage dependence. Ca^{2+}-activated Cl^- currents deactivate at negative potentials and activate slowly at positive potentials. Outward tail currents slowly decay, while inward tail currents decay faster. Ca^{2+}-activated Cl^- currents are inhibited by 4,4'-Diisothiocyanatostilbene-2,2'-disulphonic acid (DIDS), by niflumic acid (NFA) (Nilius et al., 1997; Kuruma and Hartzell, 1999). Furthermore, their ion permeability follows the selectivity sequence $I^->Br^->Cl^->F^-$ (Hartzell et al., 2005; Nilius et al., 1997). Although CaCCs were deep studied in several tissues, and their biophysical properties were well described, their molecular identity was clarified only in 2008 independently by three different groups using different approaches (Caputo et al.2008, Yang et al. 2008, Schroeder et al. 2008).

2.1 The TMEM16 family

The TMEM16 (also named anoctamin) protein family includes ten members, from TMEM16A to TMEM16H (TMEM16I is excluded). The same members are also called Ano followed by a number, producing a parallel taxonomy (from Ano1 to Ano10) (Fig. 22).

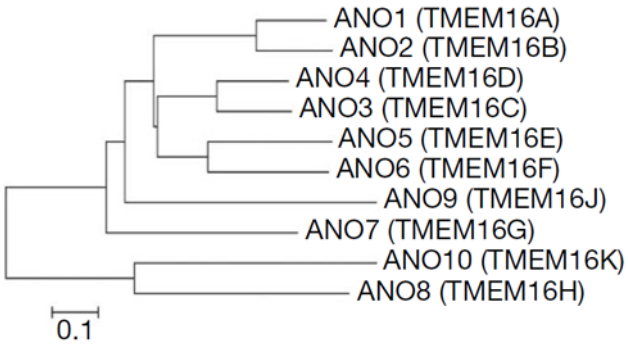

Figure 22. ***Phylogenetic tree representing the TMEM16 family in human****. Scale bar 0.1 nucleotide substitutions per site. (Yang et al., 2008)*

As recent studies revealed that these proteins are composed of ten transmembrane domains rather than eight, the name anoctamin, that was referred to proteins containing eight transmembrane domains, is currently being disputed (Paulino et al., 2017; Brunner et al., 2014; Salzer and Boehm, 2019). Although the high level of sequence identity among TMEM16 subfamilies suggests evolutionarily conserved functions, the biological roles of TMEM16 members have been elucidated for only a few of them. TMEM16A (Ano1) and TMEM16B (Ano2) are the most studied, and their functions are well explored (see next paragraph). Both of them function as CaCCs and are involved in several physiological processes (Milenkovic et al., 2010; Pedemonte and Galietta, 2014; Schroeder et al., 2008). mRNA encoding the TMEM16 proteins has been detected in a broad range of murine tissues. In particular, TMEM16B, TMEM16C, and TMEM16D are predominantly expressed in neuronal tissues, TMEM16F, TMEM16H, and TMEM16K are equally expressed in all tissues, while other TMEM16 are tissue-specific: TMEM16A has been found in all electrolyte transporting tissues, TMEM16E is associated with the skeletal muscle, and TMEM16G is found predominantly in the stomach (Schreiber et al., 2010) (Fig. 23).

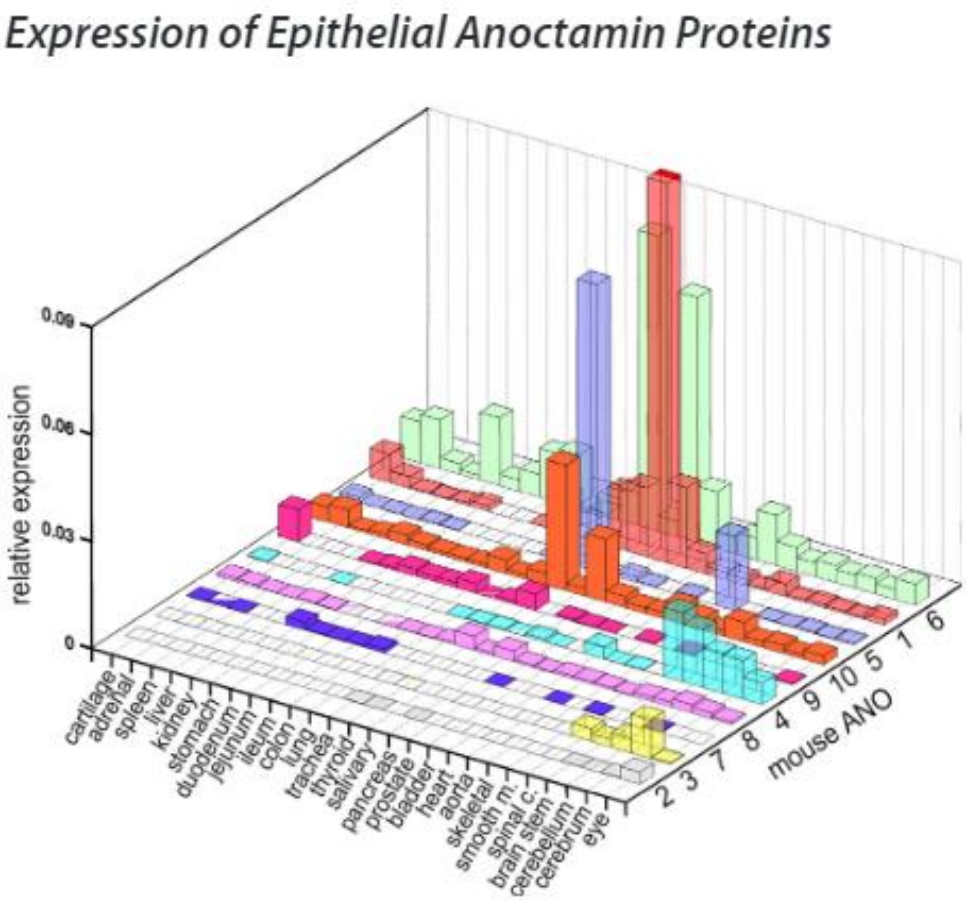

Figure 23. ***Expression pattern of TMEM16 proteins in murine tissues****. RT-PCR was performed from total mRNA of different mouse tissues (Schreiber et al., 2010).*

Recent findings revealed the relation between TMEM16F (Ano6) and Scott Syndrome. Scott syndrome is a rare bleeding disorder with a defect in Ca^{2+}-activated phospholipid scrambling in the platelets. Externalization of phosphatidylserine (PS) in platelets triggers the coagulation cascade, however, a mutation of TMEM16F seems to inhibit this mechanism. Experiments on TMEM16F knockout mice showed that these mice exhibit bleeding defects, resembling the pathophysiological defects of Scott syndrome (Yang et al., 2012). TMEM16F, indeed, is considered to function as a Ca^{2+}-activated scramblase. However, several studies suggest that TMEM16F can also generate Ca^{2+}-activated non-selective and Cl^- currents, working as an ion channel (Pedemonte and Galietta, 2014). Little is known about the other members of the TMEM16 family. TMEM16C is expressed in the central and peripheral nervous system of mice and rats, especially in a subset of nociceptive neurons in dorsal root ganglia. In these cells, TMEM16C does not form an ion channel by itself but enhances the Na^+ sensitivity and single-channel conductance of Slack. Slack is a Na^+-activated K^+ channel involved in the hyperpolarization of

the cell membrane (Huang et al., 2013). There is evidence that TMEM16C, as well as TMEM16F, TMEM16D, TMEM16G, and TMEM16J, are also involved in Ca^{2+}-mediated scrambling of phospholipids. TMEM16H and TMEM16K show neither scramblase nor channel activity (Schreiber et al., 2010). Suzuki et al. proposed that this lack of function may be due to a prevalent intracellular expression (Suzuki et al., 2013). Finally, TMEM16E/Ano5 seems to work both as an ion channel and a scramblase (Di Zanni et al., 2020), however, it has also been suggested to be a protein prevalently expressed intracellularly (Duran et al., 2012). Mutations in TMEM16E gene can cause Gnathodiaphyseal dysplasia (GDD), a rare bone malformation and fragility disorder (Mizuta et al., 2007).

2.2 TMEM16A

TMEM16A, also known as Ano1 or Dog1, is the first member of the TMEM16 family to be discovered and is the most studied and best characterized. TMEM16A functions as a CaCC and has fundamental roles in several physiological processes. Its lack is incompatible with life, as demonstrated by *Tmem16A* KO mice. Indeed, 90% of *Tmem16A* null mice die within the first 9 days after birth and never survive longer than 30 days postpartum. These mice do not gain weight at the same rate as their littermates and they present anomalies during organs development, especially defects in respiratory and/or digestive tracts (Rock et al., 2008). Histological examinations of craniofacial development showed defects in palate, tongue, and larynx in *Tmem16A* KO pups mice (Rock et al., 2008).

2.2.1 Expression pattern and roles of TMEM16A

Acinar cells and exocrine glands. TMEM16A plays an important function in transepithelial ion transport. In particular, Cl^- ions represent the primary driving force for fluid secretion in most acinar cells. TMEM16A has been revealed in salivary glands, especially in the submandibular salivary glands (Yang et al., 2008; Romanenko et al., 2010).

Airway epithelial cells. Caputo et al. in (2008) identified the presence of TMEM16A for the first time in airway epithelial cells. Results from Rock et al. (2009) established that TMEM16A contribution in Cl^- secretion was negligible at basal state (unstimulated), but its activity increased when stimulated by UTP (Rock et al., 2009) or when activated by cytokines (Caputo et al., 2008). Airway epithelial cells also express an important cAMP-regulated Cl^- channel called cystic fibrosis transmembrane conductance regulator (CFTR). This channel is fundamental in maintaining electrolyte and fluid secretion, especially for mucous hydration (Huang et al., 2012a). Indeed, its mutation causes cystic fibrosis syndrome (Cuthbert, 2011). It has been shown that CFTRs, under basal condition, contribute significantly to airway surface liquid (ASL) (Tarran et al., 2002). For this strict correlation between TMEM16A and CFTR, some scientists propose to use TMEM16A as a potential therapeutic target against cystic fibrosis (Cuthbert, 2011).

Smooth muscle cells. TMEM16A appears to be expressed in the smooth muscle of the airway and reproductive tract (Huang et al., 2009a), but also in smooth muscle cells isolated from mouse portal vein, thoracic aorta, and carotid artery (Davis et al., 2010). TMEM16A and other CaCCs contribute to membrane depolarization and sustain contraction. Indeed, NFA, a blocker of CaCCs reduces the

amplitude and the frequency of spontaneous contractions of smooth muscles of the portal vein (Saleh and Greenwood, 2005).

Interstitial Cells of Cajal. The interstitial cells of Cajal (ICCs) are pacemaker cells that control smooth muscle cells contraction in the gastrointestinal tract, and the lack of TMEM16A in these cells perturb the proper rhythmicity of the smooth muscle contractions in the stomach, especially due to the loss of the intestinal slow waves (Gomez-Pinilla et al., 2009; Hwang et al., 2011; Huang et al., 2009a). In gastrointestinal stromal tumors (GISTs) an ICCs high expression of TMEM16A has been found (Hwang et al., 2011).

TMEM16A in other tissues. TMEM16A was also found in subpopulations of rat dorsal root ganglia (DRG) sensory neurons, where it contributes to membrane depolarization (Yang et al., 2008). It is involved in nociception, and it is considered a potential target for analgesic therapies (Huang et al., 2009a; Pedemonte and Galietta, 2014). Moreover, recent data showed that TMEM16A is expressed also in the olfactory and vomeronasal systems: high expression of TMEM16A was found in supporting cells of the olfactory epithelium (OE), but its function is still unclear (Maurya et al., 2015; Henriques et al., 2019). Functional TMEM16A is also present in vomeronasal sensory neurons, where it modulates the membrane excitability of the cells (Amjad et al., 2015).

2.2.2 TMEM16A in cancer

Even before the discovery of their molecular identity, it was clear that CaCCs were highly expressed in numerous human cancer cells. For example, DOG1, which was well known as an upregulated protein and a marker in GISTs, was later identified as TMEM16A (Berglund et al., 2014; Katoh et al., 2003). It was amplified and overexpressed also in the neck and head squamous cell carcinomas (HNCCs) (Huang et al., 2006b), in breast cancer, and prostate carcinoma (Britschgi et al., 2013).

The expression of TMEM16A is thought to be strictly associated with cell cancer growth and cell proliferation. Both characteristics are associated with increased metastatic potential. For example, downregulation of TMEM16A in GIST cells results in upregulation of insulin-like growth factor-binding protein (IGFBP5) a potent anti-angiogenic factor (Simon et al., 2013). In breast cancer cells, TMEM16A was shown to increase the EGF (Epidermal Growth Factor) receptor, a known growth factor (Britschgi et al., 2013). Furthermore, TMEM16A in these cells can also increase phosphorylation of ERK1/2 and cyclin D1, indicating up-regulation of the cell cycle (Duvvuri et al., 2012).

In summary, many studies suggest an important role of TMEM16A in cell cancer proliferation, and it is becoming a prognostic marker of aggressive tumors. TMEM16A results also in a potential target for cancer therapy.

2.2.3 TMEM16A structure

TMEM16A was first proposed to be formed by 8 transmembrane domains (Yang et al., 2008) but only recent studies revealed the structure of TMEM16A (Paulino et al., 2017). By using cryo-EM technology Paulino et al. (2017) discovered that the protein is composed of 10 transmembrane domains rather than eight and confirmed that the protein is formed by homodimers. Moreover, each monomer is independently gated by Ca^{2+} and forms a physically distinct Cl^- permeation pathway (Fig. 24).

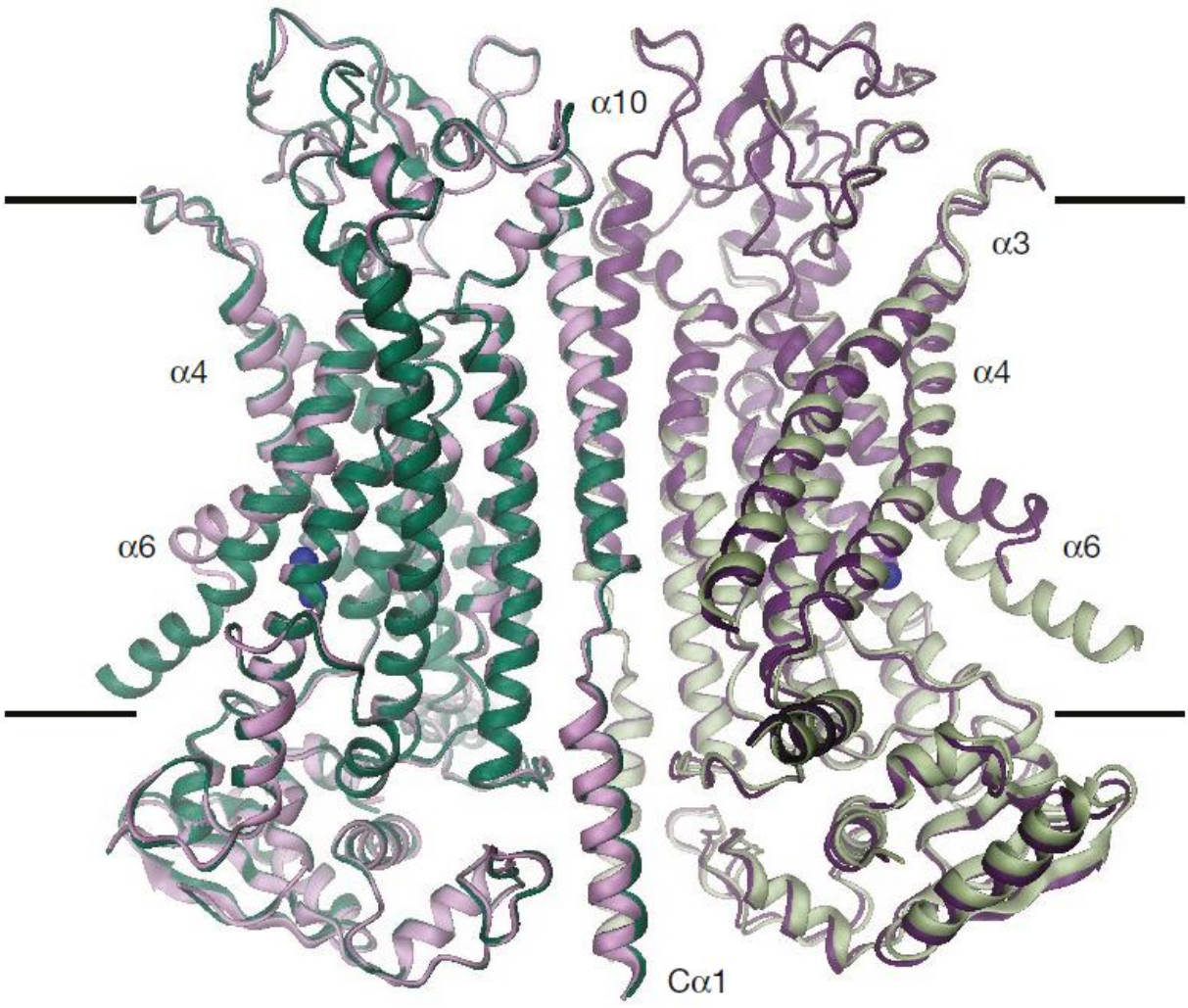

Figure 24. ***The TMEM16A structure****. Ribbon representation of TMEM16A protein obtained superimposing the Ca^{2+}-bound state (green) and the Ca^{2+}-free bound state (violet) (Paulino et al., 2017).*

Each subunit of the homodimer is formed of 10-membrane-spanning α-helices (α1- α10), cytosolic N- and C- terminal domains, followed by an extracellular component, and contains a conduction pore, which is formed by α2 - α7 helices. The shape of the permeation pore resembles an hourglass with a narrow neck region about 20 Å long. The protein was isolated in two different states: bonded with Ca^{2+}, when the protein should be in an open state, or without Ca^{2+}. Indeed, in the conformation with Ca^{2+}-bound it was possible to visualize a conducting pore of 2.5 Å diameter at its constriction point. Although this diameter is much smaller compared with the diameters of the permeating anions Cl^- (3.6 Å) or I^- (4.1 Å), the pore could expand thanks to the flexibility of α-3 and local changes in the side-chains conformations. Moreover, some conformations of the helices and the

excess of basic amino acids confer to the structure a positive electrostatic environment that allows Cl^- to pass throughout the pore (Paulino et al., 2017). In the Ca^{2+}-bound state, conserved residues of α-6 and α-8 form a Ca^{2+}-binding site at the cytosolic side. On the opposite, the protein structure isolated without Ca^{2+} shows substantial differences, especially in the pore region. The α-6 helix detaches from α-7 closing the gap between both the helices, producing a change in the conformation of the pore, that now results covered by negative electrostatic charges increasing the barrier for anion conduction. At the same time, α-6 uncovers the Ca^{2+} binding site (Paulino et al., 2017) (Fig. 25).

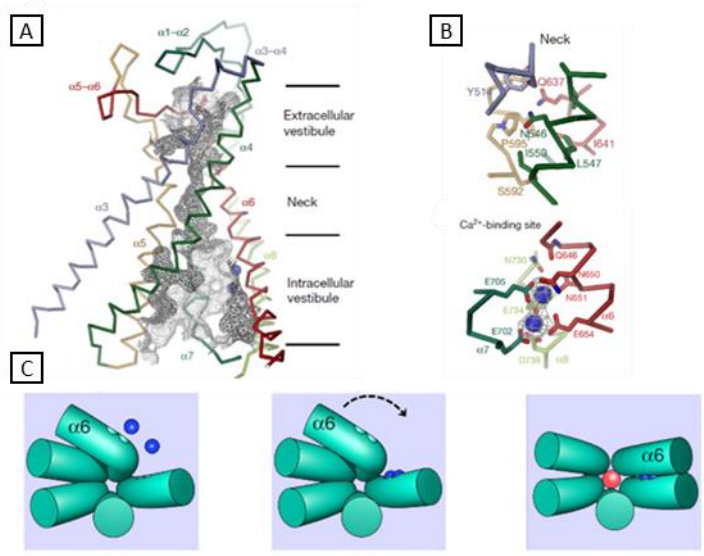

Figure 25. ***Conformational changes of TMEM16A during Ca^{2+} binding****. (**A**) Ion conduction pore with a classic hourglass shape. (**B**) Sections of the ion conduction pore at the level of the neck (top) and at the level of the Ca^{2+} binding site (bottom). (**C**) Schematic drawings of the conformational changes that allow Cl^- to flow throughout the channel. Blue circles, Ca^{2+}; red circle, Cl^-. Left, closed state without Ca^{2+}; center, closed state Ca^{2+}-bound; right, open state Ca^{2+}-bound. Modified from (Paulino et al., 2017).*

2.2.4 Biophysical properties of TMEM16A

TMEM16A faithfully mimics the biophysical properties of endogenous CaCCs (Yang et al., 2008; Caputo et al., 2008; Pedemonte and Galietta, 2014; Schroeder et al., 2008). Several electrophysiological studies were conducted on TMEM16A and all of them converge to similar results.

Expression of TMEM16A in heterologous systems, such as HEK-293 cells or FRT cells, generates robust outwardly rectifying currents in the presence of cytosolic Ca^{2+}, followed by deactivating tail currents upon repolarization (Yang et al., 2008; Caputo et al., 2008; Hartzell et al., 2009). Moreover, TMEM16A is also voltage-dependent and can generate currents in the absence of Ca^{2+} with depolarization steps >100 mV (Xiao et al., 2011). Yang et al. (2008) reported that EC_{50} of Ca^{2+}-dependent activation for TMEM16A in HEK-293 cells was about 2.6 µM at -60 mV and 0.3 µM at +60 mV (Yang et al., 2008). Xiao et al. (2011) reported that the IV relationship was outward rectifying at low intracellular Ca^{2+} concentrations, while it became almost linear in high Ca^{2+}, as represented in Fig. 26. Single-channel conductance experiments revealed a conductance of 3.5 pS in HEK-293 cells, in accordance with that reported for endogenous CaCCs (Adomaviciene et al., 2013).

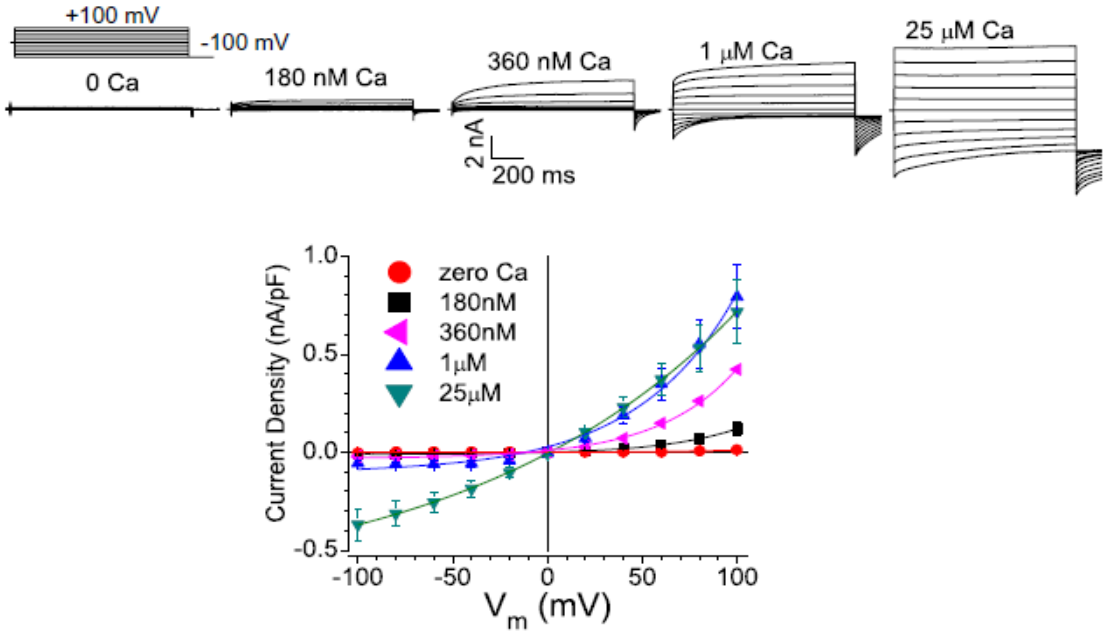

Figure 26. ***TMEM16A Ca^{2+} dependence****. Representative recordings from HEK-293 cells transfected with TMEM16A and dialyzed with free Ca^{2+} concentrations as indicated upper the traces. In the panel below, IV relationship from the cells represented in the upper panel (Xiao et al., 2011).*

Permeability ratios (P_x/P_{Cl}) were obtained using a Goldman-Hodgkin-Katz equation from reversal potential changes induced by substitution of extracellular Cl^- with different anions. The relative permeabilities for the monovalent anions were NO_3^- (2.20) > I^- (1.85) > Br^- (1.74) > Cl^- (1) > F^- (0.43) (Yang et al., 2008), indicating that TMEM16A is permeable to most anions.

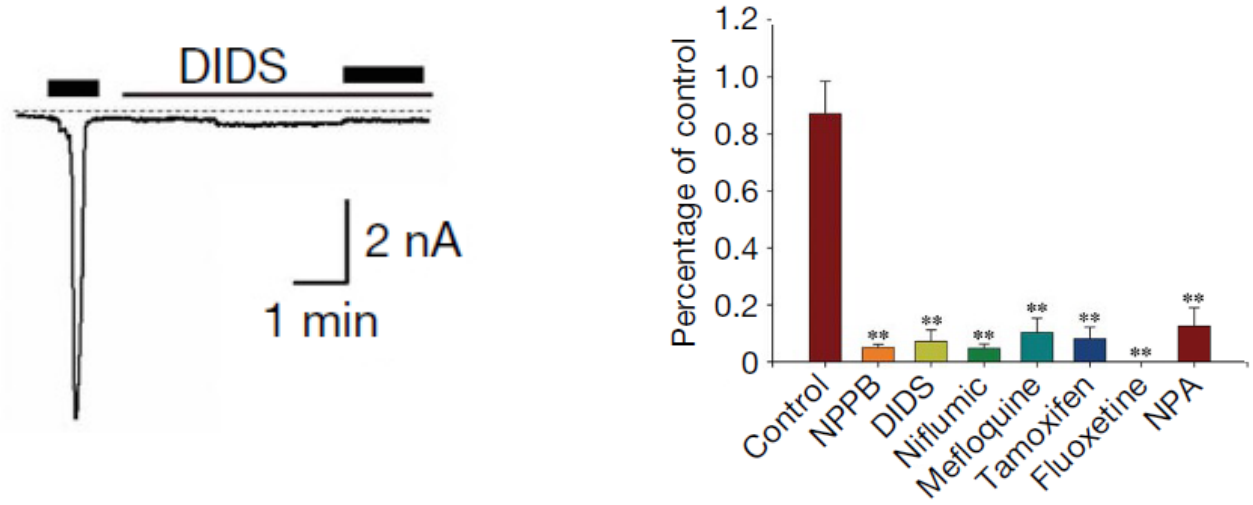

*Figure 27. **TMEM16A blockers**. On the left of the panel, it is represented a typical current evoked by endothelin 1 (black bars) in HEK-293 cells transfected with TMEM16A and the Endothelin receptor type A. Application of DIDS blocked the evoked-current. On the right of the panel are reported the blocking effects of several Cl^- channel blockers. The blockers were used at 10 μM except for mefloquine that was used at 5 μM. Picture modified from (Yang et al., 2008)*

It was shown that TMEM16A, as the most of CaCCs, was inhibited by several Cl^- channel blockers such as DIDS, NPPB (5-nitro-2-(3-phenylpropyl-amino) benzoic acid, and NFA (Yang et al., 2008; Caputo et al., 2008) (Fig. 27).

2.2.5 Activation mechanisms of TMEM16A

TMEM16A requires a rise in intracellular Ca^{2+} to open and generate the current. However, Ca^{2+} that activates CaCCs can be originated from different pathways such as the influx of Ca^{2+} from the extracellular space or mobilization of Ca^{2+} from intracellular stores. For example in DRG neurons, intracellular Ca^{2+} could increase in three different ways (Fig. 28): 1) activation of GPCRs that release Ca^{2+} from intracellular stores via PLC activity and the formation of IP_3, 2) activation of voltage-gated of Ca^{2+} channels, or 3) opening of TRPV1, a non-selective cation channels (Salzer and Boehm, 2019).

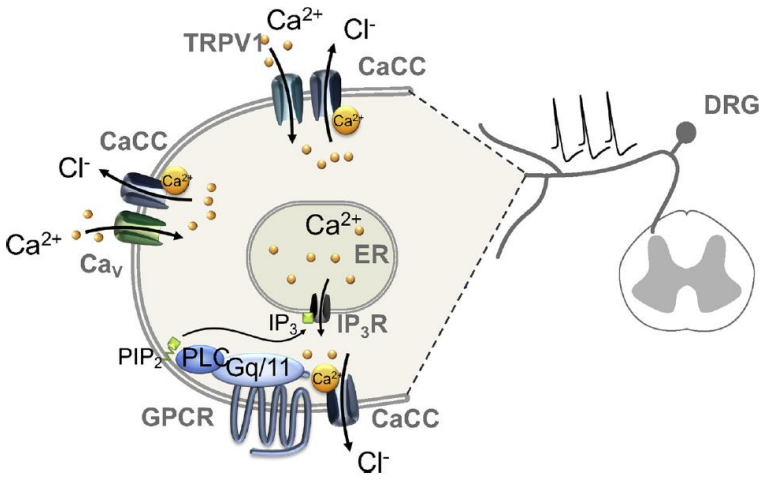

Figure 28. ***The three Ca^{2+} sources for CaCCs activation in DRG neurons****. Activation via PLC - IP_3 and intracellular stores, activation by voltage-gated calcium channels, or by TRPV1 channel, a known non-selective cation channel expressed in DRG neurons (Salzer and Boehm, 2019).*

2.2.6 Regulatory mechanisms of TMEM16A

Although intracellular Ca^{2+} is the main activator of TMEM16A, many studies suggest that various mechanisms are involved in the regulation of this channel. For example, TMEM16A is influenced by membrane potential that modifies the EC_{50} for Ca^{2+} from 0.3 µM at +60 mV to 2.6 µM at -60 mV (Yang et al., 2008).

It has been reported that TMEM16A and other native CaCCs can be directly activated by calcium increase in the cytosolic side of isolated membrane patches (inside-out configuration) (Yang et al., 2008; Xiao et al., 2011). However, in many studies, the current evoked by Ca^{2+} was not persistent but deactivated with time. This phenomenon was called "rundown" or "desensitization" (Tian et al., 2011). An explanation of this phenomenon is the regulation of the channel by other compounds probably lost in the excised patches. Indeed, a recent work from Le et al. (2019) revealed the importance of phosphatidylinositol (4,5)-bisphosphate (PIP_2) as a TMEM16A modulator. In this work, they showed that PIP_2 strongly reduces the rundown of TMEM16A in excised patches (Fig. 29). Furthermore, they proposed that PIP_2 binding to a putative binding module of the amino acids sequence of TMEM16A can stabilize the open state of the conduction pore (Le et al., 2019).

To summarize, several studies showed that TMEM16A is activated by Ca^{2+} and voltage allowing the permeation of anions and that additional compounds could modulate the channel activity in a native system.

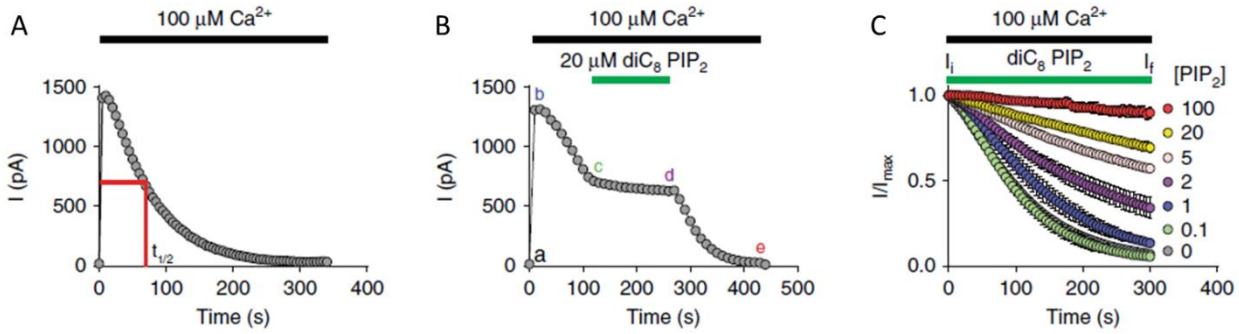

Figure 29. ***PIP_2 reduces rundown in excised patches expressing TMEM16A in high concentration of cytosolic Ca^{2+}****. (**A**) Control condition showing TMEM16A current rundown. (**B**) Application of PIP_2 (green bar) reduces rundown. (**C**) Dose-response for PIP_2 application (green bar) at different concentrations represented by different colors. Modified from (Le et al., 2019)*

2.3 TMEM16B

TMEM16B, also known as Ano2, is the homologous of the TMEM16A. The two proteins share 62% of the amino acid sequence and are phylogenetically classified in the same subfamily of the TMEM16 proteins (Pedemonte and Galietta, 2014; Milenkovic et al., 2010). TMEM16B was identified as a CaCC for the first time by Schroeder et al. in 2008 and later confirmed by three other teams (Pifferi et al., 2009; Stohr et al., 2009; Stephan et al., 2009). TMEM16B, as TMEM16A, exists in different isoforms depending on the tissue (Stephan et al., 2009) and each isoform can have different biophysical properties (Pedemonte and Galietta, 2014).

TMEM16B is involved in physiological processes in several cells, including olfactory sensory neurons, photoreceptors, and hippocampal neurons (Huang et al., 2012b; Thoreson et al., 2000; Dibattista et al., 2017). In the olfactory sensory neurons, TMEM16B takes part in the transduction pathway cascade. When odorant molecules bind to odorant receptors on the surface of the cilia of olfactory neurons they activate an enzymatic cascade that causes the increase of cAMP and the opening of the CNG channel, a non-selective cation channel. The CNG channel allows Na^+ and Ca^{2+} to flow inside the cell cytoplasm. Rising Ca^{2+} in the cytoplasm gates the TMEM16B causing a consecutive efflux of Cl^-. Na^+ and Ca^{2+} in the cytoplasm depolarize the cell, and this effect is amplified by Cl^- efflux throughout the TMEM16B channel (Boccaccio and Menini, 2007; Kurahashi and Yau, 1994; Dibattista et al., 2017). From a physiological point of view, TMEM16B plays a key role in the regulation of firing in olfactory sensory neurons, and it is important in perceive odors. Indeed, Pietra et al., (2016) showed that the firing rate in TMEM16B KO mice increased compared to WT, and that KO mice had a reduced ability to finding food, showing a deficit in perceiving odors (Pietra et al., 2016).

In photoreceptors, TMEM16B was found both in cones and rods and it seems to have a feedback regulatory role on voltage-dependent Ca^{2+} channels through an anion-binding site (Thoreson et al., 2000; Pedemonte and Galietta, 2014).

An important role of TMEM16B is played in the somatodendritic region of hippocampal neurons. The role of TMEM16B is to avoid the summation of excitatory postsynaptic potentials raising their action potential threshold (Huang et al., 2012b).

All these data suggest that TMEM16B is expressed in several tissues and it functions as a CaCCs. However, it was also found in cells in which its role is controversial. For example, TMEM16B is highly expressed together with TMEM16A in vomeronasal sensory neurons but its role is not clear. Indeed, the

lack of TMEM16A is sufficient to abolish the Ca^{2+}-activated Cl^- current in these cells (Amjad et al., 2015).

2.3.1 Biophysical properties of TMEM16B

TMEM16B, as TMEM16A, functions as a CaCC but has some different biophysical characteristics from those of TMEM16A (Pedemonte and Galietta, 2014).

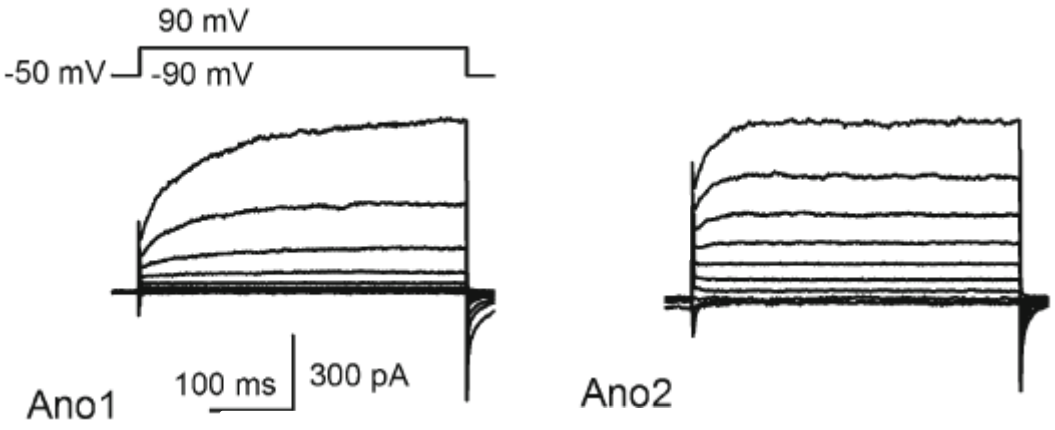

Figure 30. ***Comparison between TMEM16A and TMEM16B****. Representative whole-cell recordings obtained in CHO cells transfected with TMEM16A (Ano1) (left panel) or TMEM16B (Ano2) (right panel). Voltage pulses between -90 and 90 mV. Recordings were obtained using 140 CsCl and nominally 700 nM free-Ca^{2+} in the patch pipette. The bath solution contained 140 mM NaCl, 5 mM KCl, 1 mM MgCl2, 1 mM CaCl2, 10 mM HEPES-NaOH (pH 7.4), and 5 mM glucose. Modified from Cherkashin et al., (2016).*

TMEM16B is less sensitive to Ca^{2+} than TMEM16A and its EC_{50} is about 1-3 µM at positive membrane potentials (Pifferi et al., 2009; Pedemonte and Galietta, 2014; Stephan et al., 2009). TMEM16B shows also faster activation and deactivation kinetics compared to TMEM16A when activated by Ca^{2+} (Fig. 30) (Pedemonte and Galietta, 2014; Stephan et al., 2009). Stephan et al. (2009) suggested that the faster kinetics of TMEM16B could be involved in the rapid signaling of neurons, while slow kinetics of TMEM16A better suit for cellular secretion mechanisms (Stephan et al., 2009). Furthermore, TMEM16B shows less single-channel conductance compared with TMEM16A. Indeed, single-channel conductance was estimated to be 1.2 pS for TMEM16B, whereas for TMEM16A was 3.5 pS (Pifferi et al., 2009; Pedemonte and Galietta, 2014; Adomaviciene et al., 2013).

TMEM16B, as TMEM16A, is permeable to anions with the following relative permeability: I^- (3.85) > Br^- (1.78) > Cl^- (1) > F^- (0.12) (Stephan et al., 2009).

In excised patches, the phenomenon called rundown, a time-dependent current decay in prolonged stimulation by saturating Ca^{2+} concentrations, occurs also in TMEM16B (Pifferi et al., 2009; Stephan et al., 2009).

Moreover, despite TMEM16B isoform from the olfactory epithelium and hippocampal neurons show current inactivation, the isoform from rods does not inactivate (Vocke et al., 2013). Vocke et al. revealed also that TMEM16B in the retina contained four additional amino acids in the sequence and that those were responsible for the inactivation of TMEM16B.

TMEM16B and TMEM16A have some common pharmacological inhibitors such as NFA, NPPB, SITS (4-acetamido-4-isothiocyanatostilbene-2,2-disulfonic acid), and DIDS (Pifferi et al., 2009; Yang et al., 2008).

However, Ani9, a novel blocker discovered by Seo et al. (2016), has been shown to selectively inhibit TMEM16A rather than TMEM16B (Fig. 31), especially using concentrations below 1 µM (Seo et al., 2016).

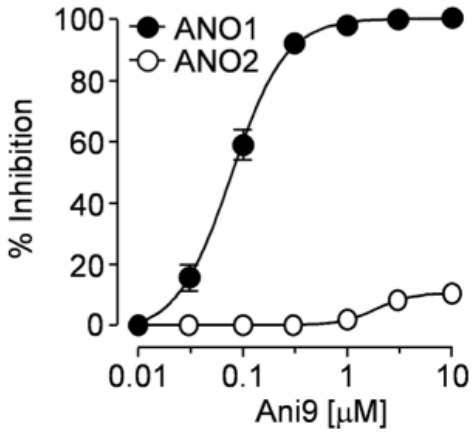

Figure 31. ***Ani9, a selective TMEM16A blocker****. Dose-response obtained by the percentage of inhibition of TMEM16A and TMEM16B activity at different concentrations of Ani9. Measurements were obtained using YFP quenching assay in FRT cells expressing TMEM16A or TMEM16B and the halide-sensing YFP. Modified from Seo et al. (2016).*

Although TMEM16A and TMEM16B are similar in structure and function, their biophysical differences and their different expression patterns suggest that the two channels are involved differently in specific physiological processes.

2.4 CaCCs in taste cells

Functional CaCCs were first found in *Necturus* taste cells by McBride and Roper in 1991. *Necturus* taste cells produce action potentials in response to taste stimuli. Action potentials are followed by an outward current mediated by CaCCs, which open in response to the gating of voltage-gated Ca^{2+} channels with the consecutive influx of Ca^{2+} (Fig. 32) (McBride and Roper, 1991; Taylor and Roper, 1994). Moreover, Taylor and Roper in 1994, proposed that CaCCs were involved in the repolarization of the cell membrane and that they could be involved in taste adaptation, limiting the repetitive firing of action potentials (Taylor and Roper, 1994; Wladkowski et al., 1998).

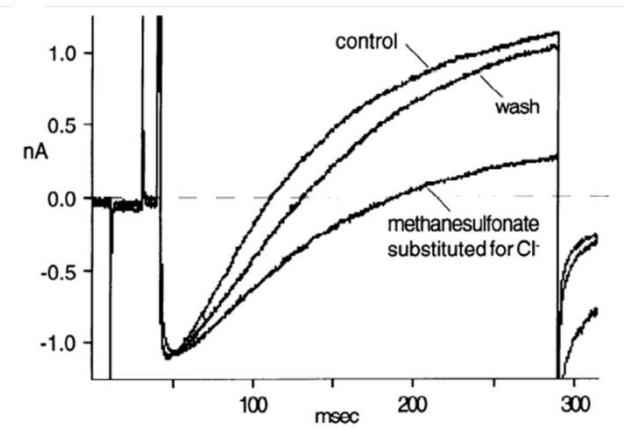

Figure 32. ***CaCCs in Necturus taste cells****. Representative recordings showing outward currents generated by Ca^{2+} influx in Necturus taste cells. Substitution of Cl^- with methanesulfonate caused a reduction of the outward current, indicating that the current was mediated by Cl^- ions (Taylor and Roper, 1994)*

Afterward, CaCCs were found also in mammalian taste cells. In particular, CaCCs have been described in rat TBCs from Wladkowiski et al. (1998) and Herness and Sun (1999) using different approaches. Wladkowiski et al. (1998) revealed the presence of CaCCs using voltage-clamp experiments with the Ussing Chamber and with whole-cell recordings in single TBCs. In both cases, Cl^- conductances were inhibited by the Cl^- channels blockers flufenamic acid (FFA) and NFA (Wladkowski et al., 1998). Herness and Sun (1999) obtained similar results showing that most of the Cl^- conductances in rat TBCs were outward rectifying and a portion of this current was due to CaCCs because it was inhibited by the Cl^- channel blocker DIDS and by blocking the influx of Ca^{2+}.

All these results suggest that CaCCs cloud be involved in taste transduction cascade in response to taste stimuli.

In 2000, Kim et al. discovered that a subpopulation of TBCs in mice, with no voltage-gated Na^+ and Ca^{2+} channels, responded to ATP stimulation with an inward current. While the replacement of Na^+ with N-methyl-d-glucamine (NMDG), an impermeant cation, in the bath solution did not influence the ATP-evoked current, the substitution of Cl^- with methanesulfonate, a big anion impermeant in most Cl^- channels, shifted the reversal potential to positive values. The shift of the reversal potential to the

equilibrium potential calculated for Cl^- indicated that the ATP-evoked current was mainly mediated by Cl^- ions. Moreover, they showed that the current was inhibited by anthracene carboxylic acid (9-AC) a common blocker of CaCCs, and by U73122, a blocker of the phospholipase C (PLC). Generally, PLC is considered an important intermediate to mobilize Ca^{2+} from the intracellular stores. For this reason, the inhibition of ATP-evoked current by U73122 implicates that cytosolic Ca^{2+} increase derives from intracellular Ca^{2+} stores and not from Ca^{2+} influx, indicating that P_2Y (metabotropic) rather than P_2X (ionotropic) receptors are activated in this subpopulation of TBCs. These data strongly suggest the expression of CaCCs in mice TBCs.

In 2016, Cherkashin et al. extended the previous results looking for the identity of the CaCCs involved in TBCs. Using immunohistochemistry, RT-PCR analysis, and electrophysiology they found the presence of both TMEM16A and TMEM16B CaCCs. Electrophysiological experiments, using the perforated patch configuration, showed that a subpopulation of TBCs, identified as type I, produced a strong inward Cl^- current when stimulated with ionomycin. To reveal the identity of the CaCCs involved in this type of taste cells they investigated the effects of specific blockers, e. g. the T16 (T16Ainh-A01), which was considered a specific blocker for TMEM16A (Liu et al., 2015). T16 was not able to block the Ca^{2+}-activated currents in type I cells indicating that these cells do not express TMEM16A. Furthermore, they showed that the Cl^- current was inhibited by anthracene-9-carboxylic acid (9-AC),a general Cl^- blocker, suggesting the involvement of other CaCCs.

Cherkashin et al. (2016) investigated the presence of TMEM16A and TMEM16B also in type II and type III cells. They were able to elicit an inward current in type II cells with two different approaches: using ionomycin or releasing intracellular Ca^{2+} from NP-EGTA by UV flashes. Before increasing Ca^{2+} concentration, they blocked the contribution of TRMP5, a non-selective cation channel known to be specifically expressed in these cells, by using its specific blocker TPPO. 5µM ionomycin was enough to elicit an inward current subsequentially inhibited by 1 mM 9-AC, a non-selective blocker of CaCCs, in the presence of TPPO in the bath. This result indicated that the ionomycin-activated current was mediated by CaCCs. Moreover, in four out of seven cells, T16 was sufficient to inhibit the ionomycin-activated current in presence of TPPO, suggesting that TMEM16A could be the main contributor in generating this current.

Experiments in type III cells did not show any Ca^{2+} -activated Cl^- current.

To summarize, Cherkashin et al. (2016) concluded that CaCCs are functional in TBCs and they identified these channels as TMEM16A and TMEM16B. Moreover, electrophysiological results

combined with RT-PCR analysis on single taste cells suggested that TMEM16A is mainly expressed in type II TBCs, while TMEM16B is expressed in both type I and type II taste cells.

Aims

The aims of this work were:

- To test if Ca^{2+}-activated Cl^- currents could be activated in taste bud cells in mouse vallate papillae by using voltage-clamp experiments in the whole-cell configuration.

- To investigate by immunohistochemistry the expression patterns of TMEM16A and TMEM16B in different taste cell types by using KO mice as control.

- To test with patch-clamp experiments if TMEM16A and/or TMEM16B are necessary for mediating the Ca^{2+}-activated Cl^- currents in taste cells by using KO mice and pharmacological blockers.

- To investigate the physiological roles of CaCCs in taste physiology.

RESULTS

Functional expression of TMEM16A in taste bud cells

Domenico M. Guarascio[1], Kevin Y. Gonzalez-Velandia[1], Andres Hernandez-Clavijo[1]*, Anna Menini[1]*, Simone Pifferi[1,2]*

1 Neurobiology Group, SISSA, Scuola Internazionale Superiore di Studi Avanzati, 34136 Trieste, Italy.
2 Department of Experimental and Clinical Medicine, Università Politecnica delle Marche, 60126 Ancona, Italy. 9

*Corresponding Authors

Submitted manuscript.

Key Points

- Taste transduction occurs in taste buds in the tongue epithelium

- The Ca2+-activated Cl- channels TMEM16A and TMEM16B play relevant physiological roles in several sensory systems

- Here, we report that TMEM16A, but not TMEM16B, is expressed in the apical part of taste buds

- Large Ca2+-activated Cl−currents blocked by Ani-9, a selective inhibitor of TMEM16A, are measured in type I, but not in type II or III taste cells

- ATP indirectly activates Ca2+-activated Cl- currents in type I cells through TMEM16A channels

- These results indicate that TMEM16A is functional in type I taste cells and contribute to understand the largely unknown physiological roles of these cells

Abstract

The Ca^{2+}-activated Cl^- channels TMEM16A and TMEM16B have relevant roles in many physiological processes including neuronal excitability and regulation of Cl^- homeostasis. Here, we examined the presence of Ca^{2+}-activated Cl^- channels in taste cells of mouse vallate papillae by using immunohistochemistry and electrophysiological recordings. By immunohistochemistry we showed that only TMEM16A, and not TMEM16B, was expressed in taste bud cells where it largely co-localized with the inwardly rectifying K^+ channel KNCJ1 in the apical part of type I cells. By using whole-cell patch-clamp recordings in isolated cells from taste buds, we measured an average current of -1083 pA at -100 mV in 1.5 μM Ca^{2+} and symmetrical Cl^- in type I cells. Ion substitution experiments and blockage by Ani-9, a specific TMEM16A channel blocker, indicated that Ca^{2+} activated anionic currents through TMEM16A channels. We did not detect any Ca^{2+}-activated Cl^- currents in type II or III taste cells. ATP is released by type II cells in response to various tastants and reaches type I cells where it is hydrolyzed by ecto-ATPases. Type I cells also express P2Y purinergic receptors and stimulation of type I cells with extracellular ATP produced large Ca^{2+}-activated Cl^- currents blocked by Ani-9, indicating a possible role of TMEM16A in ATP-mediated signaling. These results provide a definitive demonstration that TMEM16A-mediated currents are functional in type I taste cells and provide a foundation for future studies investigating physiological roles for these often-neglected taste cells.

INTRODUCTION

In vertebrates, the process of taste transduction occurs in cells of taste buds, that are mainly located in the tongue epithelium. Taste buds are onion-shaped clusters of about 50-100 elongated epithelial cells that extend from the basal lamina to the surface of the tongue, where a pore allows the apical part of taste cells to directly contact chemicals dissolved in the mouth saliva. Taste buds also contain basal cells that will form new taste cells. In several species, at least three main types of elongated taste cells have been identified and named type I, II or III. These cell types can be distinguished based on their ultrastructural morphology, expression of specific proteins, and functional properties. Type II and type III cells express taste receptors and respond to tastants, while type I cells mainly have glial-like functions. Type I cells have also been suggested to be involved in salt transduction because they express amiloride-sensitive Na^+ channels (Baumer-Harrison *et al.*, 2020; Roper & Chaudhari, 2017; Vandenbeuch *et al.*, 2008; Yang *et al.*, 2020) but a recent study demonstrated that amiloride-sensitive salt taste is transmitted to the nervous system by a unique cell type that expresses the ATP release channel CALHM1/3 and voltage-gated Na^+ channels, neither of which are found in Type I taste cells (Nomura *et al*., 2020).

Type II cells express G protein-coupled receptors for sweet (TAS1R2-TAS1R3), umami (TAS1R1-TAS1R3) or bitter (TAS2Rs) detection and use at least one common transduction cascade that involves the G-protein alpha subunit gustducin (GNAT3), phospholipase-C-beta-2 (PLCβ2), inositol-3-phosphate (IP3), and Ca^{2+} release from intracellular stores (Hisatsune *et al.*, 2007; Zhang *et al.*, 2003). The increased intracellular Ca^{2+} concentration activates TRPM5 and TRPM4, causing membrane depolarization by Na^+ entry and release of ATP through voltage-gated CALHM1/CALHM3 channels (Dutta Banik *et al.*, 2018; Ma *et al.*, 2018).

Type III cells mediate sour detection through the apical ion channel OTOP1, that allows entry of H^+ and cell membrane depolarization, which is further amplified by the block of the inwardly rectifier K^+ channel KCNJ2 by low pH (Tu *et al.*, 2018; Teng *et al.*, 2019; Ye *et al.*, 2016). Type III are the only taste cells that form canonical synapses with afferent nerve fibers. They express the presynaptic synaptosomal-associated protein 25 (SNAP25), the glutamic acid decarboxylase 67 (GAD67), and voltage-gated Ca^{2+} channels, which trigger the release of neurotransmitters (DeFazio *et al.*, 2006; Huang *et al.*, 2008; Tomchik *et al.*, 2007; Vandenbeuch *et al.*, 2010; Yang *et al.*, 2000).

Type I cells are called “glial-like” cells and are mainly considered to have a supporting role in the taste buds. These cells have projections that wrap around other cells and express proteins involved in removing neurotransmitters, such as the ectonucleotidase NTPDase2 (encoded by *Entpd2*) and the

glutamate transporter GLAST (Bartel *et al.*, 2006; Lawton *et al.*, 2000). Moreover, the inwardly rectifier K^+ channel KCNJ1 (also named $K_{ir}1.1$ or renal outer medullary K, ROMK) is expressed at the apical tips of type I cells and may be involved in K^+ homeostasis (Dvoryanchikov *et al.*, 2009).

The three cell types can also be identified by their electrophysiological fingerprint. Indeed, by using voltage-clamp whole-cell recordings in pseudo-physiological solutions, type I cells are characterized by the presence of voltage-gated outward K^+ currents and no inward currents, type II cells by voltage-gated inward Na^+ currents and voltage-gated outward non-selective currents, and type III cells by voltage-gated inward Na^+ and Ca^{2+} currents and by voltage gated-outward K^+ currents (Clapp *et al.*, 2006; Medler *et al.*, 2003; Romanov & Kolesnikov, 2006; Romanov *et al.*, 2007; Taruno *et al.*, 2013).

Multiple chloride conductances, including Ca^{2+}-dependent Cl^- currents, have been recorded in some taste cells (Cherkashin *et al.*, 2016; Herness & Sun, 1999; Kim *et al.*, 2000; McBride & Roper, 1991; Taylor & Roper, 1994; Wladkowski *et al.*, 1998). Kim et al. (2000) clearly demonstrated that a subpopulation of unidentified taste cells had Ca^{2+}-activated Cl^- currents and that extracellular ATP could indirectly activate these channels by intracellular Ca^{2+} increase through activation of P2Y receptors. Ca^{2+}-activated Cl^- channels are encoded by two proteins of the TMEM16 family, TMEM16A and TMEM16B (also named Ano1 and Ano2, respectively). They share several electrophysiological properties such as ionic permeability and voltage dependence but can be functionally distinguished by different Ca^{2+}-sensitivity and pharmacological profile (Caputo *et al.*, 2008; Pedemonte & Galietta, 2014; Pifferi *et al.*, 2009*a*; Schroeder *et al.*, 2008; Scudieri *et al.*, 2012; Stephan *et al.*, 2009; Stöhr *et al.*, 2009; Yang *et al.*, 2008). Cherkashin *et al.* (2016) confirmed and extended previous results from Kim *et al.* (2000) showing that the population of taste cells generating Ca^{2+}-activated Cl^- currents in response to P2Y agonists largely consisted of type I cells, but that also some type II cells exhibited small Ca^{2+}-activated Cl^- currents. They indicated that TMEM16B was functional in type I cells, TMEM16A and TMEM16B produced small currents in type II cells, while type III cells did not exhibit any Ca^{2+}-activated Cl^- current.

Here, by taking advantage of *Tmem16a* and *Tmem16b* KO mice models (Rock *et al.*, 2008; Zhang *et al.*, 2017) and of a recently discovered specific blocker of TMEM16A, Ani-9 (Seo *et al.*, 2016), we re-examined the functional expression of the two Ca^{2+}-dependent Cl^- channels of the TMEM16 family in taste cells of vallate papillae by using electrophysiological recordings and immunohistochemistry. Surprisingly, we found that only TMEM16A, and not TMEM16B, is expressed in taste buds. In particular, TMEM16A is largely colocalized with the inwardly rectifier K^+ channel KCNJ1 at the apical portion of type I cells. Moreover, by using patch-clamp whole-cell recordings we functionally measured

TMEM16A-mediated currents only in type I and not in type II cells. We then asked whether TMEM16A-mediated currents in type I cells could be activated by extracellular ATP, a well-known transmitter released by type II cells in taste buds and found that ATP induced Ca^{2+}-activated Cl^- currents that were blocked by Ani-9, further confirming that they were due to TMEM16A channels. We conclude that TMEM16A, but not TMEM16B, plays a role in taste buds.

Although type I cells make up more than 50% of the cells in each taste bud and are known to have glial-like functions, they have often been overlooked in favor of studies on type II and III cells. A complete knowledge of the functional ion channels of type I cells will help to understand additional roles that these cells may play in taste buds. Although further studies are required to determine the physiological role of TMEM16A in taste buds, we discuss some possible scenarios.

METHODS

Animals and ethical approval

Mice were handled according to the guidelines of the Italian Animal Welfare Act (Decreto legislativo 26/2014/) and European Union guidelines on animal research (2010/63) under a protocol approved by the Italian Ministry of Health. Mice had free access to water and food. Every effort was made to minimize animal suffering and to reduce the number of animals used. Adult (> 8 weeks) mice were anesthetized with CO_2 and decapitated before tongue and nose removal. Young postnatal days 8-10 (P8-P10) mice were decapitated before tongue removal. Experiments were performed on tissues from both male and female C57BL/6, GAD67-GFP (Oliva *et al.*, 2000), *Tmem16a* KO (Rock *et al.*, 2008), or mCherry *Tmem16b* KO mice (Zhang *et al.*, 2017). *Tmem16a* KO and WT littermates were obtained by breeding heterozygous mice. mCherry *Tmem16b* KO mice were kindly provided by Dr. Lily Jan (University of California, San Francisco, USA, Zhang et al., 2017). The generated *Tmem16b* -deficient mice were engineered by inserting *mCherry* sequence with a farnesylation signal at the C-terminus (mCherry-F) in frame with the alternative start ATG codon in the 3rd exon of *Tmem16b*, therefore membrane associated mCherry marks cells that normally express *Tmem16b* (see Fig. S2C of Zhang *et al*., 2017).

Tissue preparation

The epithelium containing the taste papillae was peeled using an enzymatic-mechanical dissociation protocol slightly modified from those previously reported (Béhé *et al.*, 1990; Bigiani, 2001; Cherkashin *et al.*, 2016). Once removed, the tongue was placed in a Sylgard Petri dish filled with a standard mammalian Ringer's solution containing (in mM): 140 NaCl, 5 KCl, 2 $CaCl_2$, 1 $MgCl_2$, 10 HEPES, 10 glucose, pH 7.4, with NaOH. Using an insulin syringe, 0.5 ml Ringer's solution containing 2 mg/ml dispase II (D4693, Sigma), 0.2 mg/ml elastase (E0127, Sigma) and 0.7 mg/ml collagenase B (C9891, Sigma) was injected under the epithelium. The syringe needle was carefully inserted from the posterior to the most anterior part of the tongue. Injection of the enzymatic solution was performed while the needle was gently withdrawn to allow the solution to reach the entire epithelium. After 30 min of incubation, the epithelium was peeled off from the underlying muscle and the vallate papilla and taste cells were isolated as described in the following sections.

RT-PCR

The vallate papilla was cut from the peeled tongue epithelium and directly placed in the lysis buffer of the mRNA isolation kit (S1550S, New England Biolabs). The olfactory epithelium was isolated as previously described (Pifferi *et al.*, 2006; Sagheddu *et al.*, 2010). The olfactory turbinates were exposed by bisecting the head along the midline, the epithelium was carefully removed from turbinates, septum and the roof of the nasal cavity and placed directly in the lysis buffer of the mRNA isolation kit. Vallate papillae mRNA was extracted from 4 adult C57BL/6 and olfactory epithelium mRNA was extracted from 2 adult C57BL/6 mice. mRNA isolation kit was used with Oligo $d(T)_{25}$ magnetic beads for mRNA isolation. After extraction, mRNA was further incubated with DNAase I (M0303S, New England Biolabs) to remove any residual genomic DNA. cDNA was synthesized using the SMARTER cDNA synthesis kit from 25 ng of mRNA (634860, Takara).

PCR was performed in a thermocycler (ThermaCycler2720, Life Technologies) using Phusion HS II High-Fidelity DNA Polymerase (F549S, ThermoFisher Scientific), 0.2 mM for each dNTPs (N0447S, New England Biolabs) and 200 pmol forward/reverse target-specific primers. Cycling parameters were: an initial denaturation step (98 °C, 2 minutes) followed by 38 cycles, each of these cycles included a denaturation step (98 °C, 10 seconds), a primer annealing step (62-64°C, 30 seconds), and an extension step (72 °C, 30 seconds) step. The reaction was completed by a final extension step at 72 °C for 5 minutes.

The following primer sequences were used to amplify target DNAs: *Gapdh* fwd 5'-TGCTGAGTATGTCGTGGAGTCT-3' rev 5'-TGCTGTAGCCGTATTCATTGTC-3' (Tm = 64 °C; 691 bp; GenBank. accession no. NM_008084.3); *Olfr73* fwd 5'-GCTGGTATTGGGATCCTATGCTT-3' rev 5'- CGTCCACTTGCTGACTTCATCTT-3' (Tm = 62 °C; 272 bp; GenBank. accession no. NM_054090.1); *Tmem16a* fwd 5'- ATGAAGCCAGAGTCTTAGAGAAGT-3' rev 5'-AAACTTCATCCAGCAGAATGAT-3' (Tm = 62 °C; 296 bp; GenBank. accession no. NM_178642.6); *Tmem16b* fwd 5'- ATGCACTTTCACGACAACCA -3' rev 5'-GCCCAGCAGCCATCAGGTTG-3' (Tm = 62 °C; 243 bp; GenBank. accession no. NM_001364563.1); *Entpd2* fwd 5'-CTCAAGTATGGCATCGTTCTGG -3' rev 5'- CAGAGACGAGGTCACGACAGAG -3' (Tm = 62 °C; 834 bp; GenBank. accession no. NM_009849.2); *Plcβ2* fwd 5'-TGGAGGTGACAGCTTATGAGGA -3' rev 5'-GGTTGGCAAGGGCTACTGTAAG -3' (Tm = 62 °C; 842 bp; GenBank. accession no. NM_001290790.1); *Snap25* fwd 5'-TGGCATCAGGACTTTGGTTATG-3' rev 5'-GCATCTTTGTTGCACGTTGGT-3' (Tm = 62 °C; 481 bp; GenBank. accession no. NM_001355254.1).

The products were visualized following agarose gel electrophoresis (1.5%) and DNA was stained with Midori Green Advance (MG04, Nippon Genetics).

Immunohistochemistry

Immunohistochemistry was performed on tongue sections containing the vallate papilla and on olfactory epithelium sections. The dissected tongues were directly fixed in 4% paraformaldehyde in PBS, pH 7.4, for 3-4 h at 4°C. For nose isolation, the lower jaw, the posterior part of the brain and the skinhead were removed. The remaining head, containing the nasal cavity, was fixed in 4% paraformaldehyde in PBS, pH 7.4, for 4-5 h at 4 °C and then decalcified in 0.5 M EDTA, pH 8, for 2 days, as previously described (Henriques *et al.*, 2019; Maurya & Menini, 2014; Maurya *et al.*, 2015; Pifferi *et al.*, 2006, 2009*b*). For cryoprotection, tongue and olfactory tissues were equilibrated overnight in 30% (wt/vol) sucrose in PBS at 4 °C. Tissues were frozen in optimal cutting temperature compound (Bio-Optica, Milano, Italy) and stored at -80 °C before sectioning with a cryostat. Coronal sections (14–16 µm thick) were cut with a cryostat and mounted on Superfrost Plus Adhesion Microscope Slides (ThermoFisher Scientific). Sections were air-dried for 3 h and stored at -80 °C for further use. For antigen retrieval, sections were kept in SDS 0.5% (wt/vol) in PBS for 15 min at room temperature. After pretreatment, sections were incubated in blocking solution (5% (vol/vol) FBS or donkey serum and 0.3% (vol/vol) Triton X-100 in PBS) for 2 h, and then with the primary antibody (diluted in the blocking solution) overnight at 4°C. Slices were then rinsed with PBS and incubated with the chosen fluorophore-conjugated secondary antibody diluted in PBS-T (0.1% Tween 20 in PBS) for 2 h at room temperature. After washing with PBS-T, sections were treated with DAPI (0.2 µg/ml) for 30 min, washed with PBS-T, and mounted with Vectashield (Vector Laboratories) or Fluoromount-G (TermoFisher).

The following primary antibodies (dilution; catalog number, company) were used: polyclonal rabbit anti-TMEM16A (1:100; ab53212, Abcam), polyclonal goat anti-TMEM16A (1:50; sc-69343, Santa Cruz Biotechnology), polyclonal rabbit anti-TMEM16B (1:200; 20647-1-P; Proteintech), polyclonal rabbit anti-NTPDase2 (1:500; mN2-36LI6, from J. Sévigny at Centre de Recherche du CHU de Québec, Université Laval, Quebec http://ectonucleotidases-ab.com), polyclonal rabbit anti-KCNJ (1:500; APC-001, Alomone Labs), polyclonal goat anti-GNAT3 (1:1000; OAEB00418, Aviva Systems Biology), polyclonal rabbit anti-PLCβ2 (1:200; sc-206, Santa Cruz Biotechnology), polyclonal chicken anti-GFP (1:200; GTX13970, GeneTex), polyclonal rabbit anti-RFP antibody (1:500, Rockland, 600-401-379). The following secondary antibodies were used: donkey anti-rabbit Alexa Fluor Plus 594 (1:500; A32754, Life Technologies), donkey anti-goat Alexa Fluor 488 (1:500; A11055, Life

Technologies), donkey anti-rabbit Alexa Fluor 488 (1:500; A21206, Life Technologies), donkey anti-goat Alexa Fluor Plus 647 (1:500; A32849, Life Technologies), goat anti-chicken Alexa Fluor 488 (1:500, A-11039, Invitrogen).

Immunofluorescence was visualized with a confocal laser scanning microscope (A1R or C1, Nikon, Japan). Images were acquired using NIS-Elements Nikon software at 1024 x 1024 pixels resolution and analyzed with ImageJ software (National Institute of Health). Control experiments, excluding primary antibodies, were performed for each immunolocalization experiment and gave no signal. In addition, negative control experiments for the polyclonal rabbit anti-TMEM16A (Fig. 2*D*) and polyclonal goat anti-TMEM16A (not shown) were made in vallate papillae from *Tmem16a* KO mice.

Electrophysiological recordings

The peeled tongue epithelium was placed upside-down in a Sylgard Petri dish, in Ca^{2+}-free Ringer's solution containing (in mM): 140 NaCl, 5 KCl, 1 $MgCl_2$, 0.5 EDTA, 10 HEPES, 10 glucose, pH 7.4, with NaOH. After 30 min of incubation, cells were removed from taste buds of the vallate papilla by gentle suction with a flame-polished glass capillary tube with an opening diameter of 40-50 µm and plated in Petri dishes, precoated with 5 mM Concanavalin-A (Type V, Sigma, Milan, Italy), for at least 1 hour to favor cell adhesion.

Isolated taste cells were continuously perfused with Ringer's solution. Cells were viewed with an inverted microscope (IMT-2 or IX70, Olympus), equipped with 10X and 40X objectives and an additional 1.5X auxiliary lens, and identified by their elongated shape. Whole-cell membrane currents were recorded at room temperature (21-24 °C) in the voltage-clamp mode, using an Axopatch 200B or a Multiclamp 700B amplifier controlled by Clampex 9 or 10 via a Digidata 1332A (Molecular Devices). Patch pipettes were made using borosilicate capillaries (WPI) and pulled with a Narishige PP83 puller (Narishige, Tokyo, Japan). Patch pipettes filled with intracellular solutions had resistances of 2–7 MΩ. Currents were low-pass filtered at 1 or 5 kHz and sampled at 10 kHz. We used two main intracellular solutions: (i) a KCl based intracellular solution containing (in mM): 140 KCl, 10 HEDTA, 10 HEPES, pH 7.2, with KOH, and (ii) a N-methyl-D-glucamine-Cl (NMDG-Cl) based solution containing (in mM): 140 NMDG-Cl, 10 HEDTA, 10 HEPES, adjusted to pH 7.2 with NMDG. To measure Ca^{2+}-activated currents, 3.209 mM $CaCl_2$ was added to the NMDG-Cl solution to obtain the final concentration of 1.5 µM free Ca^{2+}, as calculated with the program WinMAXC (C. Patton, Stanford University, Stanford, CA) and previously described in detail (Patton *et al.*, 2004; Pifferi *et al.*, 2006, 2009*b*, 2009*a*). The extracellular mammalian Ringer's solution contained (in mM): 140 NaCl, 5 KCl, 2 $CaCl_2$, 1 $MgCl_2$, 10

HEPES, and 10 glucose, adjusted to pH 7.4 with NaOH. N-methyl-D-glucamine-Cl (NMDG-Cl) extracellular solution contained (in mM): 140 NMDG-Cl, 1 $MgCl_2$, 10 HEPES, adjusted to pH 7.4 with NMDG. For ion selectivity experiments, extracellular NMDG-Cl was replaced by NMDG-Methanesulfonate (NMDG-MeS). Ani-9 was prepared in DMSO at 10 mM as a stock solution and diluted in the extracellular solution to the final concentration of 1 µM. $GdCl_3$ was prepared as a 1 M stock solution and daily diluted in the extracellular solution to the final concentration of 200 µM.

For recordings of ATP-activated currents, the patch pipette solution contained (in mM): 140 NMDG-Cl, 2 HEDTA, 10 HEPES, adjusted to pH 7.2 with NMDG and no added Ca^{2+}. 50 µM ATP was added to the extracellular Ringer's solution on the day of the experiment. For ion selectivity experiments, NaCl in the extracellular Ringer's solution was replaced by equimolar Na-Gluconate. I-V relations were measured using a ramp protocol from -70 mV to +100 mV at 0.85 mV/ms.

Extracellular solutions were exchanged through a 3-barrel square glass (3SG700-5, Warner Instruments) using the gravity-driven perfusion system Fast-Step SF-77B (Warner Instruments). Different solutions were flowing side by side in each glass pipe and a stepper motor moved different pipes, and therefore different solution, in front of the cell. The time course of solution exchange was about 50 ms (Fig. S1).

The bath was grounded through a 3 M KCl agar bridge connected to an Ag/AgCl reference electrode. Membrane potentials were not corrected for liquid junction potentials whose values were less than 7 mV as calculated using the Clampex's Junction Potential Calculator (based on (Barry, 1994)). Chemicals, unless otherwise stated, were purchased from Sigma.

Analysis of electrophysiological data

IGOR Pro software (WaveMetrics) was used for data analysis and to produce the figures. All averaged data from individual experiments in different cells are presented as mean ± standard deviation and number of cells (n). Statistical analyses of normally distributed data (Shapiro-Wilk test) were performed using unpaired t-test. For not normally distributed data, the Mann–Whitney U-test was used. The homogeneity of the variance was tested using Levene's test. P values of <0.05 were considered statistically significant.

RESULTS

RT-PCR

To evaluate the expression of *Tmem16a* and *Tmem16b* transcripts in taste buds, we performed RT-PCR analysis on whole mRNA extract from vallate papillae (Fig. 1). To check the integrity and specificity of the mRNA extracts, we amplified markers for the three types of taste bud cells: *Entpd2* for type I, *Plcβ_2* for type II, *Snap25* for type III, and for the housekeeping gene *Gapdh* (Fig. 1*B*). By using primers that span specific and conserved regions from *Tmem16a* and *Tmem16b* sequences, to recognize all isoforms described for both proteins (O'Driscoll *et al.*, 2011; Ponissery Saidu *et al.*, 2013), we amplified *Tmem16a*, but not *Tmem16b* mRNA (Fig. 1*A*). As lack of *Tmem16b* transcript amplification could be due to problems in the primers themselves, we validated them by performing RT-PCR on whole mRNA extracts from the olfactory epithelium, where expression of *Tmem16a* and *Tmem16b* is well established (Dauner *et al.*, 2012; Maurya & Menini, 2014). RT-PCR from the olfactory epithelium showed the expression of both *Tmem16a* and *Tmem16b* transcripts (Fig. 1*C*), confirming primers' integrity. These results indicate that *Tmem16a*, but not *Tmem16b*, transcripts are expressed in mouse vallate papillae.

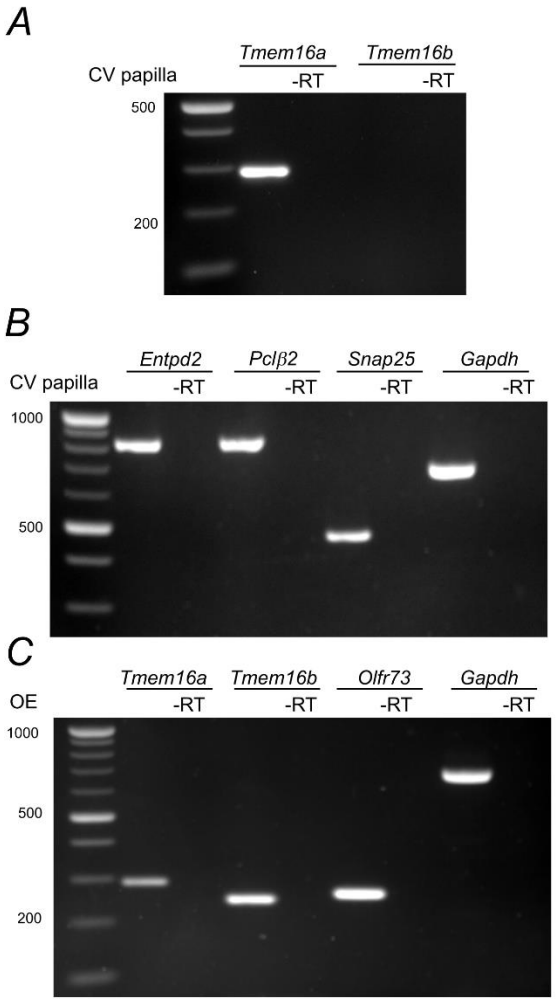

Figure 1. TMEM16A mRNA is expressed in vallate taste buds.

*Total mRNA extracted from vallate papillae (VP) was amplified by RT-PCR using specific primers for: (**A**) Tmem16a and Tmem16b, (**B**) Entpd2, Plcβ2, Snap25, and Gapdh. **C**, to test primer efficiency, total mRNA extracted from the whole olfactory epithelium (OE) was amplified for Tmem16a, Tmem16b, Olf73, and Gapdh. Control experiments were made using the same sample template without retro-transcriptase.*

Expression of TMEM16A in taste buds of vallate papillae

To examine the expression and localization of the TMEM16A and TMEM16B proteins in mouse taste buds from vallate papillae we performed immunohistochemistry and used KO mice as controls (Figs. 2, 3). Figure 2*B* shows that TMEM16A was expressed in taste buds from adult mice, with a more intense staining near the apical tip. To verify the specificity of the TMEM16A antibody, we performed control experiments using *Tmem16a* KO mice (Fig. *2C, D*). As these mice die a few days after birth

(Rock *et al.*, 2008), we could not test adult animals, but we compared results from WT and KO mice of about the same age (P8-P10). We found no signal for *Tmem16a* in KO mice (Fig. 2*D*), confirming the specificity of the immunostaining for TMEM16A obtained in WT mice.

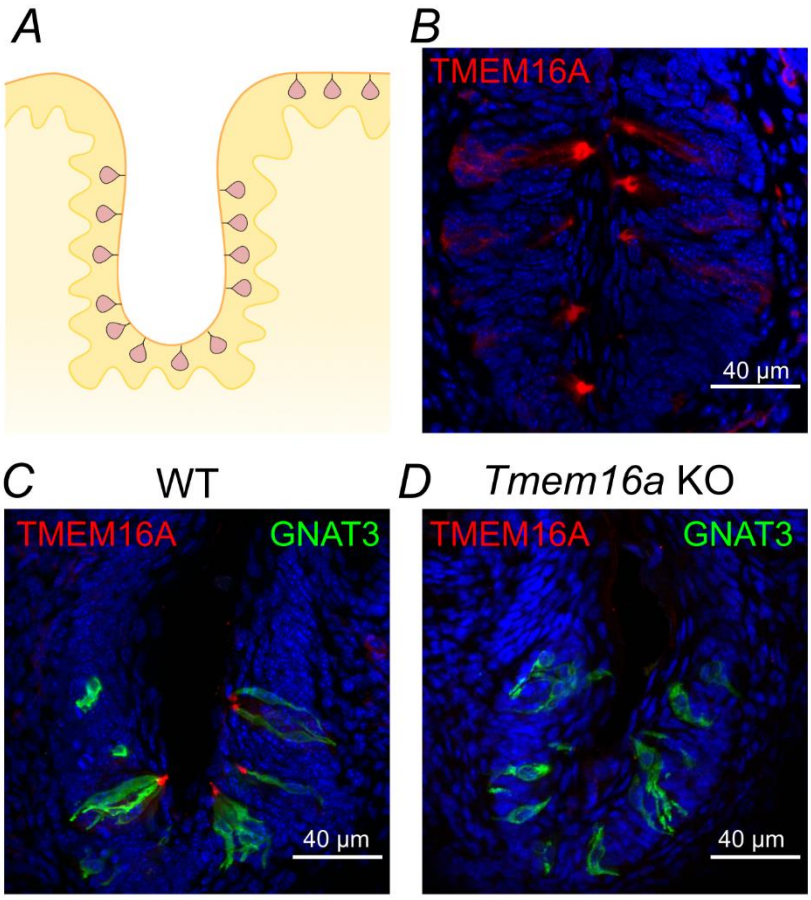

Figure 2. TMEM16A is expressed in vallate taste buds.

***A**, schematic drawing of a coronal section of a portion of a vallate papilla (VP) showing the distribution of taste buds. **B**, confocal micrograph of a coronal section of a vallate papilla immunostained for TMEM16A. TMEM16A was mainly expressed at the apical part of taste buds. **C** and **D**, confocal micrographs of sections of vallate papillae from WT (P10) or Tmem16a KO (P8) mice immunostained for TMEM16A (red) and GNAT3 (green). No immunoreactivity to TMEM16A was detected from KO tissue. Cell nuclei were stained by DAPI (blue).*

On the contrary, we did not detect immunoreactivity to TMEM16B in taste buds. Figure 3 shows a comparison between confocal micrographs from sections of mouse vallate papilla (top row) and olfactory epithelium (bottom row). TMEM16B immunoreactivity was absent in taste buds (Fig. 3*B*), although the same antibody revealed the expression of TMEM16B at the apical surface of the olfactory epithelium (Fig. 3*E*), as previously shown (Dibattista *et al.*, 2017; Maurya *et al.*, 2015). We further investigated the expression of TMEM16B in taste buds by taking advantage of a *Tmem16b* KO mice line that was engineered to express mCherry in cells that normally express TMEM16B (Zhang *et al.*, 2017). It is important to note that the use of mCherry *Tmem16b* KO mice allows the visualization of the entire cells including all membranes that allow farnesylated mCherry to associate with. As a positive control, we used the olfactory epithelium, where TMEM16B is expressed at the apical side of olfactory sensory neurons (Fig. 3*E*). Figure 3*F* shows that mCherry was expressed, as expected, in the entire olfactory neurons of KO mice, including cilia, dendrites, somas and axons. On the contrary, mCherry was not expressed in taste buds (Fig. 3*C*) further indicating that TMEM16B is not expressed in mouse vallate papillae.

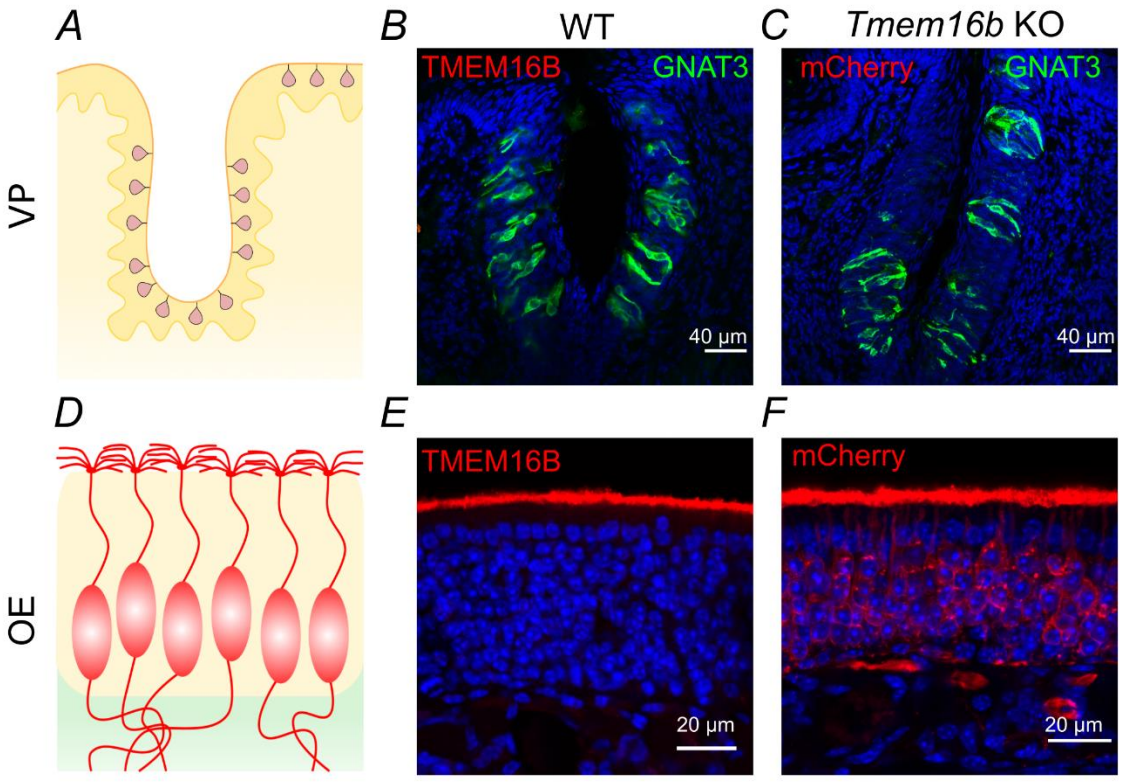

Figure 3. TMEM16B is not expressed in vallate taste buds.

***A**, schematic drawing of a coronal section of a vallate papilla (VP) showing the distribution of taste buds. **B**, confocal micrographs of a vallate papilla from a WT mice immunostained with antibody against TMEM16B (red) and GNAT3 (green). No immunoreactivity to TMEM16B was detected in taste buds. **C**, confocal micrograph of a section of a vallate papilla from Tmem16b KO mouse expressing mCherry on the membrane of cells that normally express TMEM16B (see Methods section for details on the generation of the KO mice by Zhang et al., 2017), immunostained with antibody against red fluorescent proteins (red) and GNAT3 (green). No immunoreactivity to mCherry was detected in taste buds from KO indicating that TMEM16B was not expressed in WT taste buds. **D**, schematic drawing of a coronal section of the olfactory epithelium (OE) showing olfactory sensory neurons with cilia in the apical layer. **E**, TMEM16B was normally detected in the apical layer of the WT olfactory epithelium using the same TMEM16B antibody used in B. **F**, mCherry (red) was detected in olfactory sensory neurons from Tmem16b KO mice. In these KO mice, mCherry was expressed, as expected, in the membrane of entire olfactory neurons that normally express TMEM16B at the apical side. Cell nuclei were stained by DAPI (blue).*

To identify which cell types express TMEM16A in the taste buds, we performed immunohistochemistry using specific markers for each cell type. Indeed, taste buds are composed of three major cell types, characterized by their morphology and expression of specific proteins (Kinnamon

& Finger, 2019; Liman *et al.*, 2014; Roper & Chaudhari, 2017). Type I cells are often identified by NTPDase2 expression (Bartel *et al.*, 2006) and also strongly express at their apical tip the inwardly rectifying potassium channel KCNJ1 (Dvoryanchikov *et al.*, 2009). Type II cells specifically express PLCβ2 (Zhang *et al.*, 2003), while GAD-67 can be used to stain a subset of type III cells (DeFazio *et al.*, 2006; Tomchik *et al.*, 2007). Figure 4*A-C* shows that TMEM16A was mainly expressed at the apical part of the taste buds and it was difficult to assess co-expression with NTPDase2, PLCβ2 or GAD-67. Lack of co-localization of TMEM16A with these cell markers, can be explained because of the different sub-cellular expression. We took advantage of the specific expression of KCNJ1 at the apical tips of type I cells, and we evaluated the co-localization of this marker with TMEM16A. Figure 4*D-F* shows that TMEM16A co-localized with KCNJ1 at the apical tip of taste buds, indicating the expression of TMEM16A in type I cells.

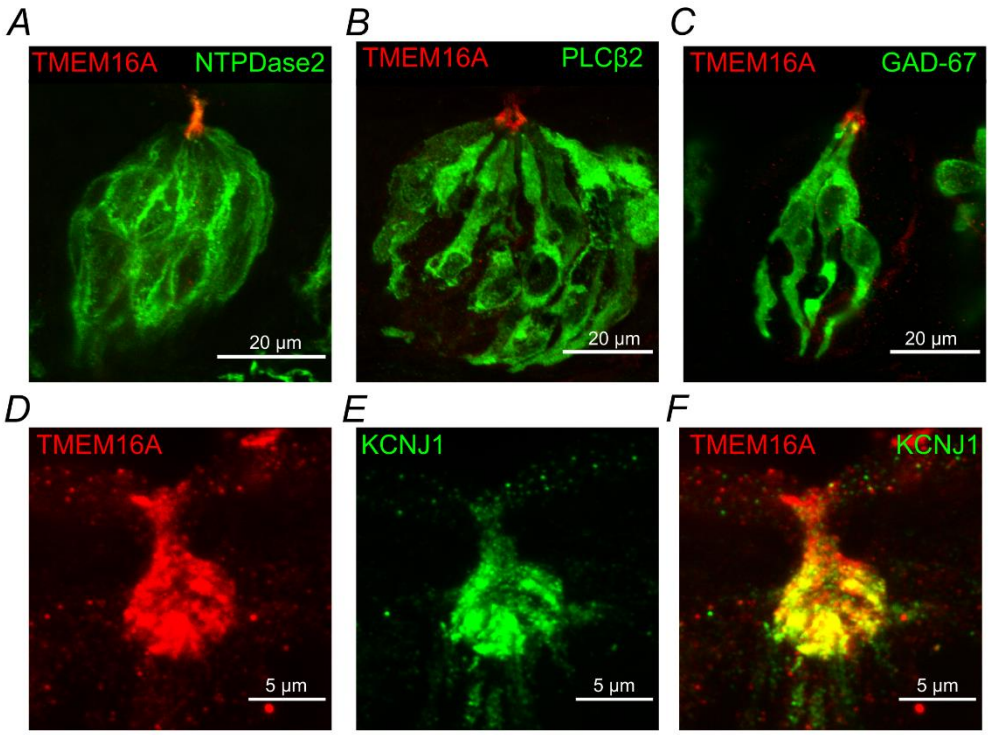

Figure 4. TMEM16A colocalizes with KCNJ1 in type I taste bud cells.

Confocal micrographs of coronal sections of vallate papillae. ***A-C****, immunostaining for TMEM16A and NTPDase2, PLCβ2, and GFP (GAD67-GFP mouse).* ***D-F****, immunostaining for TMEM16A (red) and KCNJ1 (green). Merging of the signals shows co-localization of TMEM16A and KCNJ1 at the apical part of taste buds.*

Altogether, these results show that TMEM16A, but not TMEM16B, is expressed in taste buds of vallate papillae, and that TMEM16A is mainly localized at the apical part of type I cells.

Ca^{2+}-activated Cl^- currents in taste cells

We asked whether taste cells have functional Ca^{2+}-activated Cl^- channels and compared whole-cell recordings in dissociated cells dialyzed with intracellular solutions in the presence or in the absence of 1.5 µM free Ca^{2+}.

In a first set of experiments, we evaluated the viability of electrophysiological recordings and the possibility to identify the three types of taste cells using a KCl based intracellular solution in the absence of Ca^{2+}. Indeed, it is difficult to identify the dissociated cell types by their morphology, but their electrophysiological fingerprint can be used to identify them. It has been shown that, in physiological solutions, type I cells are characterized by the presence of only voltage-gated outward K^+ currents, type II cells by the combination of voltage-gated inward Na^+ and non-selective outward currents, and type III cells by both voltage-gated inward Na^+ and outward K^+ currents (Bigiani, 2001; Medler *et al.*, 2003; Noguchi *et al.*, 2003; Romanov & Kolesnikov, 2006; Vandenbeuch *et al.*, 2008). Figure 5*A* shows representative recordings from taste cells displaying three different patterns of currents typical of the different cell types: i) cells with only outward currents (type I, green traces); ii) cells with small inward and large outward currents (type II, blue traces); and iii) cells with large inward and outward currents (type III, orange traces), indicating that all three cell types are viable in our preparation of dissociated taste cells.

In a second set of experiments, we modified the intracellular solution to suppress outward K^+ currents by replacing K^+ ions with $NMDG^+$, a large cation that does not permeate K^+ channels. Figure 5*B* shows that outward currents were eliminated from type I and type III cells, while large voltage-gated outward currents were still present in type II cells as they are due to the activation of CALHM1/CALHM3 channels, which are characterized by a wide pore with very weak ion selectivity and allow the permeation of large ions, including $NMDG^+$ (Bigiani, 2017; Ma *et al.*, 2016, 2018; Taruno *et al.*, 2013). Altogether, we recorded from 709 viable taste cells and electrophysiologically identified 279 type I (39 %), 198 type II (28%) and 232 type III cells (33%).

As our goal was the measurement of Ca^{2+}- activated Cl^- currents in electrophysiologically identified cells, we further replaced the external Ringer with a solution containing only NMDG-Cl and set the resting potential to 0 mV. In these experimental conditions, with $NMDG^+$ as the main intra- and extracellular cation, there is no contribution from inward and outward currents due to voltage-gated Na^+ and K^+ channels (Fig. 5*C*).

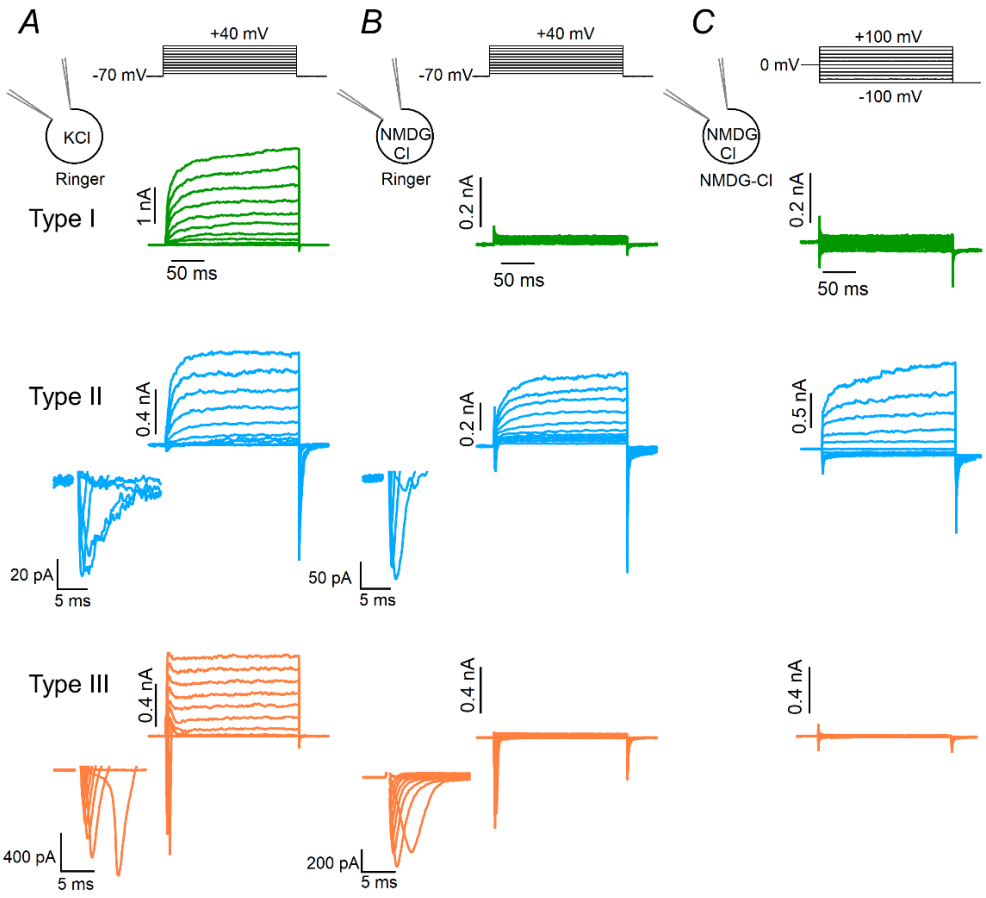

Figure 5. Electrophysiological identification of taste bud cell types.

***A**, representative whole-cell recordings obtained with a pipette solution containing KCl from type I (green), II (blue) or III (orange) taste bud cells bathed in mammalian Ringer's solution. The holding potential was -70 mV and voltage steps from -60 mV to + 40 mV with 10 mV increments were applied as shown at the top of the panel. Enlarged transient inward currents of type II and III cells are shown in the insets. **B**, representative whole-cell recordings using NMDG-Cl in the patch pipette and mammalian Ringer's solution as extracellular solution. The voltage protocol was the same of the recordings shown in A. Voltage-gated outward currents in type I and III cells were abolished by the replacement of K^+ with $NMDG^+$, whereas they were still recorded in type II cells. **C**, the same cells in B were bathed in NMDG-Cl symmetrical solutions. Note that the voltage protocol was different from that used in B, as the holding potential was 0 mV and voltage steps from -100 mV to +100 mV with 20 mV increments were applied followed by a step to -100 mV, as indicated at the top of the panel. In these conditions, type I and III cells did not show voltage-gated inward and outward currents, whereas type II cells still had robust voltage-gated outward currents. Intracellular solutions always contained nominally 0 Ca^{2+}.*

To investigate the presence of Ca^{2+}-activated currents in the three types of taste cells, we compared recordings obtained in symmetrical NMDG-Cl solutions with nominally 0 Ca^{2+} or 1.5 µM free intracellular Ca^{2+}. The cell type was determined in external Ringer by using the voltage protocol shown at the top of Fig. 5*B* and then Ringer was replaced by NMDG-Cl as in Fig. 5*C*.

Type II cells showed voltage-gated outward currents slowly activated by depolarization both in the absence and in the presence of 1.5 µM intracellular free Ca^{2+} (Fig. 6*A*). Average current amplitudes at +100 mV were not significantly different (Fig. 6*B*; p = 0.14 unpaired t-test), indicating that no additional currents were activated by Ca^{2+} in type II cells. To further investigate the presence of Ca^{2+}-activated currents that could be masked by the very large CALHM-mediated outward currents, we blocked these currents by adding 200 µM Gd^{3+}, a non-specific ion channel blocker, and verified that also after the blockage the residual outward currents amplitudes were not significantly different with 0 or 1.5 µM Ca^{2+} (Fig. 6*A*, *B*; p = 0.57 Mann–Whitney U-test). As a control, we also tested if Gd^{3+} blocks TMEM16A or TMEM16B channels, by recording Ca^{2+}-activated Cl^- currents in HEK293T cells transfected with TMEM16A or TMEM16B and did not measure any blocking effect by 200 µM $GdCl_3$ on these channels (not shown).

Type III cells showed negligible currents both in the absence and in the presence of 1.5 µM Ca^{2+} indicating the absence of functional Ca^{2+}-activated currents in symmetrical NMDG-Cl solutions (Fig. 6*C*, *D*; p = 0.33 unpaired t-test).

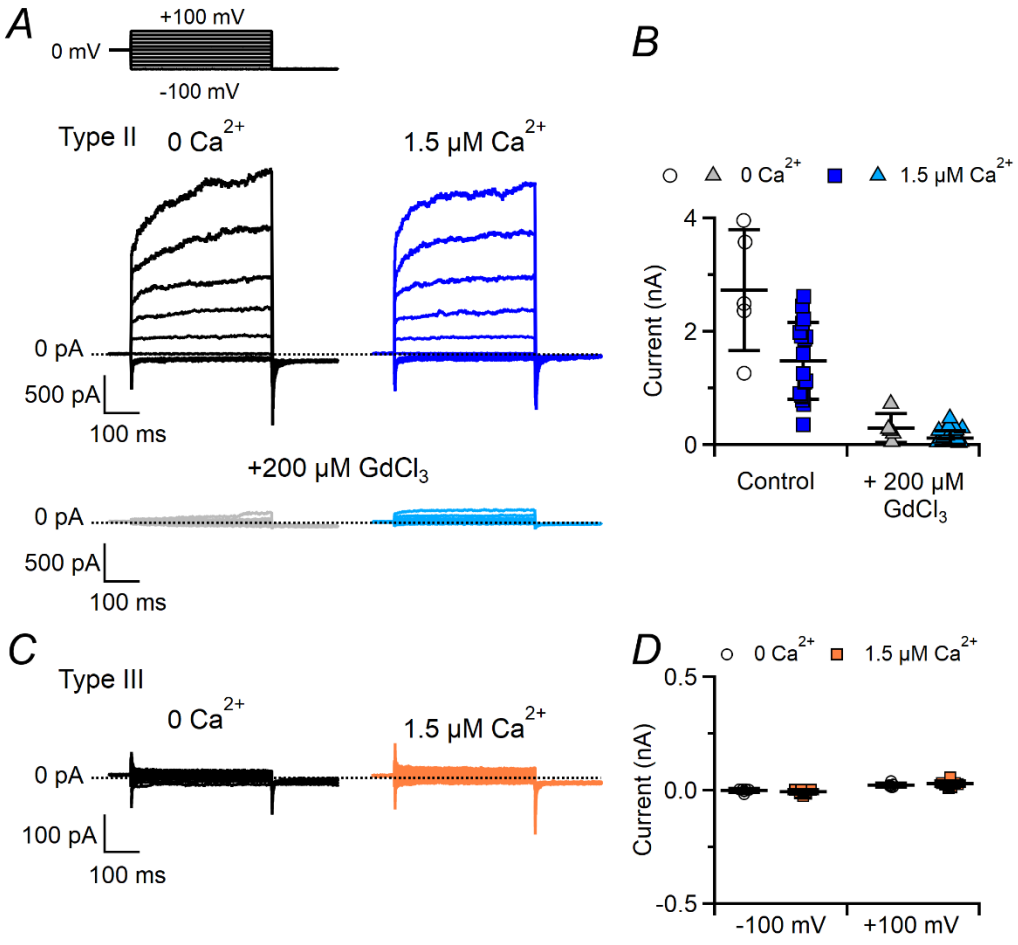

Figure 6. Type II and III taste bud cells do not have Ca^{2+}- activated Cl^- currents. *Representative whole-cell recordings from type II (**A**) and type III (**C**) taste cells obtained in symmetrical NMDG-Cl solutions. The pipette solution contained nominally 0 Ca^{2+} or 1.5 µM Ca^{2+} as indicated. The holding potential was 0 mV and voltage steps from -100 mV to +100 mV with 20 mV increments were applied followed by a step to -100 mV, as indicated at the top of panel (A). 200 µM Gd^{+3} was added to block the large CALHM-mediated outward currents in type II cells. **B** and **D**, scatter dot plots with averages ± SD showing current amplitudes in 0 or 1.5 µM Ca^{2+} in type II (B, currents at +100 mV in the absence or in the presence of 200 µM Gd^{+3}, n = 5-18; p = 0.14 unpaired t-test for control; p = 0.57 Mann–Whitney U-test for Gd^{3+}) or type III taste cells (D, n = 6-13; p = 0.26 unpaired t-test for -100 mV; p=0.33 unpaired t-test for +100 mV).*

In type I cells, 1.5 µM free Ca^{2+} generated large currents while currents in 0 Ca^{2+} were very small (Fig. 7*A*, *B*). Ca^{2+}-activated currents had the typical time-dependent features of Ca^{2+}-activated Cl^- channels, displaying time-dependent deactivation kinetics with hyperpolarizing potentials, activation kinetics with depolarizing potentials, and deactivating inward tail currents when the voltage was stepped

to -100 mV at the end of the protocol (Fig. 7*A*, *D*, *G*). The I-V relation of the steady-state Ca^{2+}-activated current at the end of the voltage steps was outwardly rectifying with an average ratio between currents at +100 mV and -100 mV of 1.6 ± 0.7 (n = 17).

To examine whether the Ca^{2+}- activated current in type I cells was carried by Cl^-, we replaced extracellular Cl^- with MeS^-, a large impermeant anion and found that the reversal potential shifted toward a positive value (+36 ± 8 mV, n = 7), as expected for Cl^- channels, indicating that the Ca^{2+}- activated current in type I cells is mainly carried by Cl^- (Fig. 7*D*, *E*, *F*). We also tested the blockage of Ca^{2+}-activated Cl^- currents by Ani-9, a compound that fully blocks TMEM16A in the sub-micromolar range and has a high selectivity for TMEM16A compared with TMEM16B (Seo *et al.*, 2016). Figure 7*G* and *H* show that 1 μM Ani-9 caused a strong reversible inhibition of the current in WT type I cells, with an average current block of 75 ± 8% at +100 mV and 90 ± 5% at -100 mV (Fig. 7*I*), indicating that the current was mainly carried through TMEM16A channels.

We also performed experiments in type I taste cells from *Tmem16b* KO mice. In agreement with our previous results showing the absence of TMEM16B in taste buds (Figs. 1, 3), we did not find any statistical difference between Ca^{2+}- activated currents in type I taste cells from WT and *Tmem16b* KO (Fig. 7*C*; p=0.42 Mann–Whitney U-test). Moreover, the shift of the reversal potential upon replacement of Cl^- with MeS^- and the blocking effect of Ani-9 were similar in type I taste cells from WT and *Tmem16b* KO (Fig. 7*F*, *I*), in agreement with the previous experiments indicating that TMEM16A is the channel responsible for the measured Ca^{2+}- activated Cl^- currents.

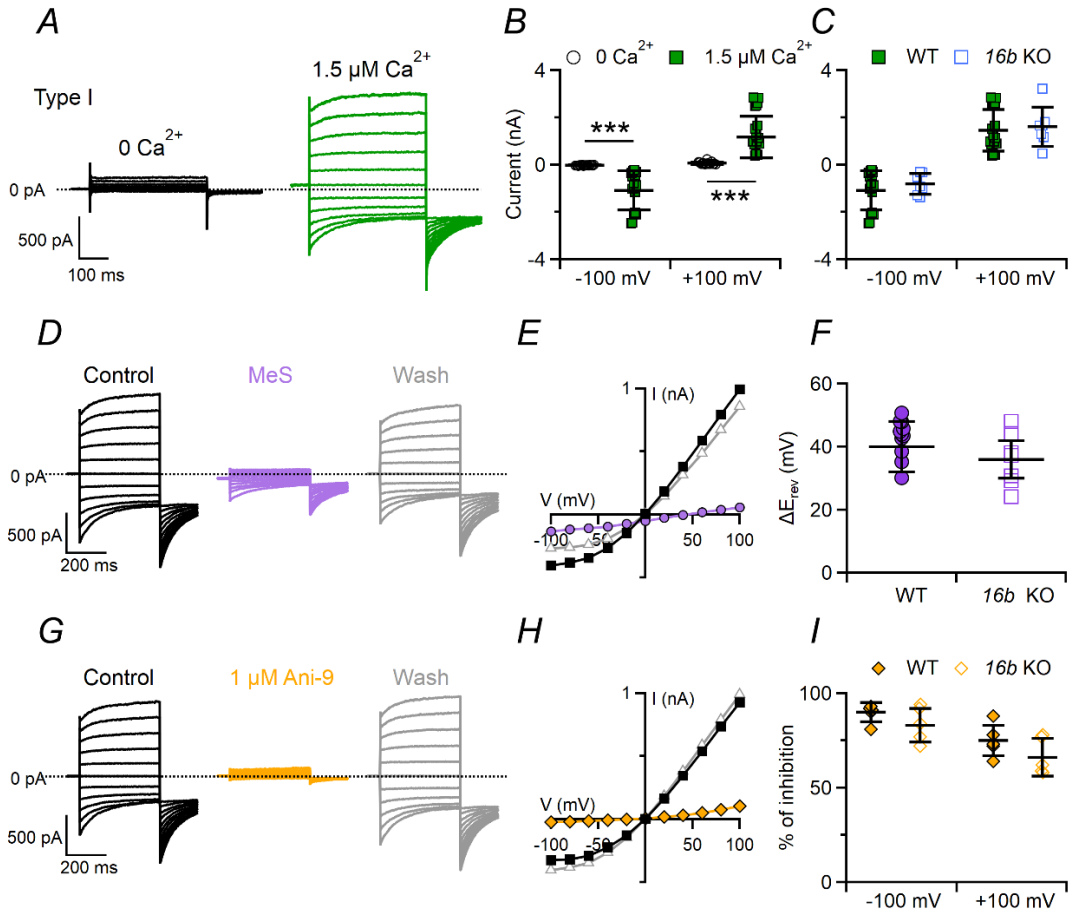

Figure 7. Ca^{2+}- activated Cl^- currents in type I taste bud cells.

***A**, representative whole-cell recordings from type I taste cells measured in symmetrical NMDG-Cl solutions with an intracellular solution containing nominally 0 Ca^{2+} or 1.5 µM Ca^{2+}. The holding potential was 0 mV, and voltage steps from −100 mV to +100 mV with 20 mV increments were applied followed by a step to -100 mV. **B** and **C**, scatter dot plots with averages ± SD showing (B) current amplitudes measured at steady state in 0 or 1.5 µM Ca^{2+} (n = 10-15, ***p = 3.46 x10^{-9} unpaired t-test) and (C) Ca^{2+}-activated currents in cells from WT (n = 15) or Tmem16B KO (n = 9; p = 0.42 unpaired t-test) mice. **D** and **G**, the same cell was exposed to a control solution containing NMDG-Cl (black traces), or NMDG-MeS (purple traces) or NMDG-Cl with 1 µM Ani-9 (yellow traces), followed by washout in NMDG-Cl (gray traces). **E** and **H**, steady-state I-V relations measured at steady state from the recordings shown in D and G in control condition (squares), MeS (E, circles), or 1 µM Ani-9 (H, diamonds) and after washout (triangles). **F** and **I**, scatter dot plots with average ± SD showing (F) ΔE_{rev} (mV) after MeS perfusion in cells from WT (n = 10) and Tmem16b KO (n = 7; p = 0.08 unpaired t-test) mice, and (I) percentage of current inhibition by 1 µM Ani-9 measured at −100 and +100 mV in cells from WT (n = 4) and Tmem16b KO mice (n = 4; p = 0.27 unpaired t-test for -100 mV; p = 0.2 unpaired t-test for +100 mV) mice.*

To further investigate the possibility that a small inward current could be activated by Ca^{2+} in type II or III taste cells, we compared recordings in symmetrical NMDG-Cl solutions from the three cell types obtained by holding the cell at -100 mV for several seconds in the presence of 1.5 µM Ca^{2+} in the pipette. Figure 8 further shows that large currents blocked by 1 µM Ani-9 were activated only in type I cells, while type II and III cells had low amplitude currents that were not blocked by Ani-9 (Fig. 8*A*, *C*, *E*). Average currents amplitudes at -100 mV were -1083 ± 824 pA (n = 17) for type I, -68 ± 95 pA (n = 18) for type II, and -6 ± 8 pA (n = 13) for type III cells. Cell viability was tested after application of the blocker (Fig. 8*B*, *D*, *F*). A significant blockage by Ani-9 in type I was observed within a few seconds from the application of the blocker and was very similar to that measured in HEK-293 transiently transfected with *Tmem16a* (Fig. S1).

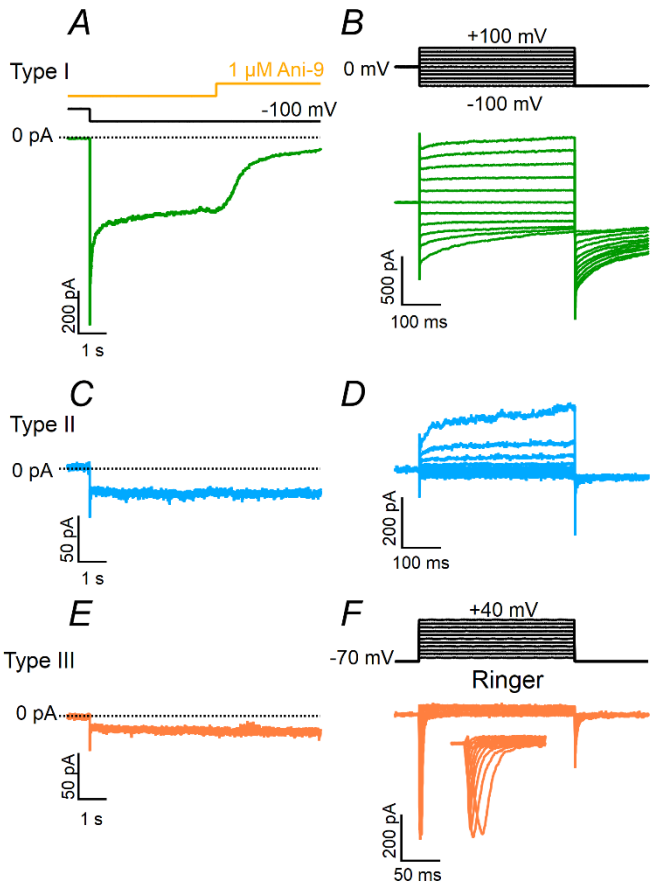

Figure 8. Blockage of inward currents by Ani-9.

A, ***C***, ***E***, Representative whole-cell recordings from type I (green traces), II (blue traces) or III (orange traces) taste cells recorded in symmetrical NMDG-Cl solutions with an intracellular solution containing 1.5 µM Ca^{2+}. The holding potential was 0 mV and was stepped to -100 mV as indicated. 1 µM Ani-9 was applied as indicated in the upper trace. ***B***, ***D***, ***F***, After the application of Ani-9, cell viability was tested with the indicated voltage protocols. The extracellular solution was NMDG-Cl in *B* and *D* or Ringer in *F*.

We could not perform experiments in taste cells from *Tmem16A* KO mice because more than 50% of these mice die within five days of birth (Rock *et al.*, 2008) and, as shown by Bigiani *et al.* (2002),

it is difficult to identify taste buds in very young mice preventing the possibility to obtain a number of dissociated cells sufficient for electrophysiological experiments.

Collectively, these data show that intracellular Ca^{2+} can activate a large Cl^- current in type I (but not in type II or III) taste cells, carried through the TMEM16A channel.

ATP evokes a Cl^- current in type I taste cells

Previous studies by Kim *et al.* (2000) and Cherkashin *et al*. (2016) showed that a subpopulation of taste cells exhibited large Ca^{2+}-activated Cl^- currents when stimulated with P2Y receptor agonists. Perforated patch recordings showed that the subpopulation consisted of type I cells (Cherkashin *et al.*, 2016). Here, we used whole-cell recordings instead of perforated patch to test whether ATP stimulation could activate Ca^{2+}- activated Cl^- currents in type I cells. We found that 50 μM ATP at the holding potential of -70 mV induced large inward currents in 71 % of type I taste cells (89 out of 125) in extracellular Ringer's solution (Fig. 9*A*). ATP-evoked currents were still present when NaCl in the Ringer solution was replaced with NMDG-Cl and 0 K^+ indicating that the inward current was not carried by Na^+ or K^+ (Fig. 9*B*).

To measure the IV-relation and to determine the ionic selectivity of the ATP-induced current, we applied voltage ramps before and during ATP stimulation in various ionic conditions (Fig. 9*C, D*). The I-V relation of the current activated by ATP was calculated by subtracting the current generated by the voltage ramp before stimulation (Fig. 9*E, F*). Rectification properties in Ringer varied in different cells from outward to linear rectification, with an average ratio of the current amplitude at +60 mV and -60 mV of 1.3 ± 0.6 (n = 18, Fig. 9 *G*). Different rectifications are probably due to different intracellular Ca^{2+} concentrations elicited by ATP. The average reversal potential was -6 ± 8 mV (n = 20) in Ringer solution and shifted to +40 ± 9 mV (n = 7) upon reduction of the extracellular Cl^- concentration by replacing NaCl with Na-gluconate, indicating that the current was mainly carried by Cl^- (Fig. 9 *H*). To test whether the ATP-induced Cl^- current was due to activation of TMEM16A, we applied the specific blocker Ani-9. Figure 9*H* shows that Ani-9 caused a sudden reduction of the inward current with a time course similar to that observed in HEK-293 transiently transfected with TMEM16A (Fig. S1) indicating that the Cl^- current was carried through TMEM16A channels. However, we cannot completely exclude the possibility that a prolonged application of Ani-9 could have a non-specific action and perhaps inhibit ATP-induced Ca^{2+} signals as observed in some cell lines (Centeio et al., 2020).

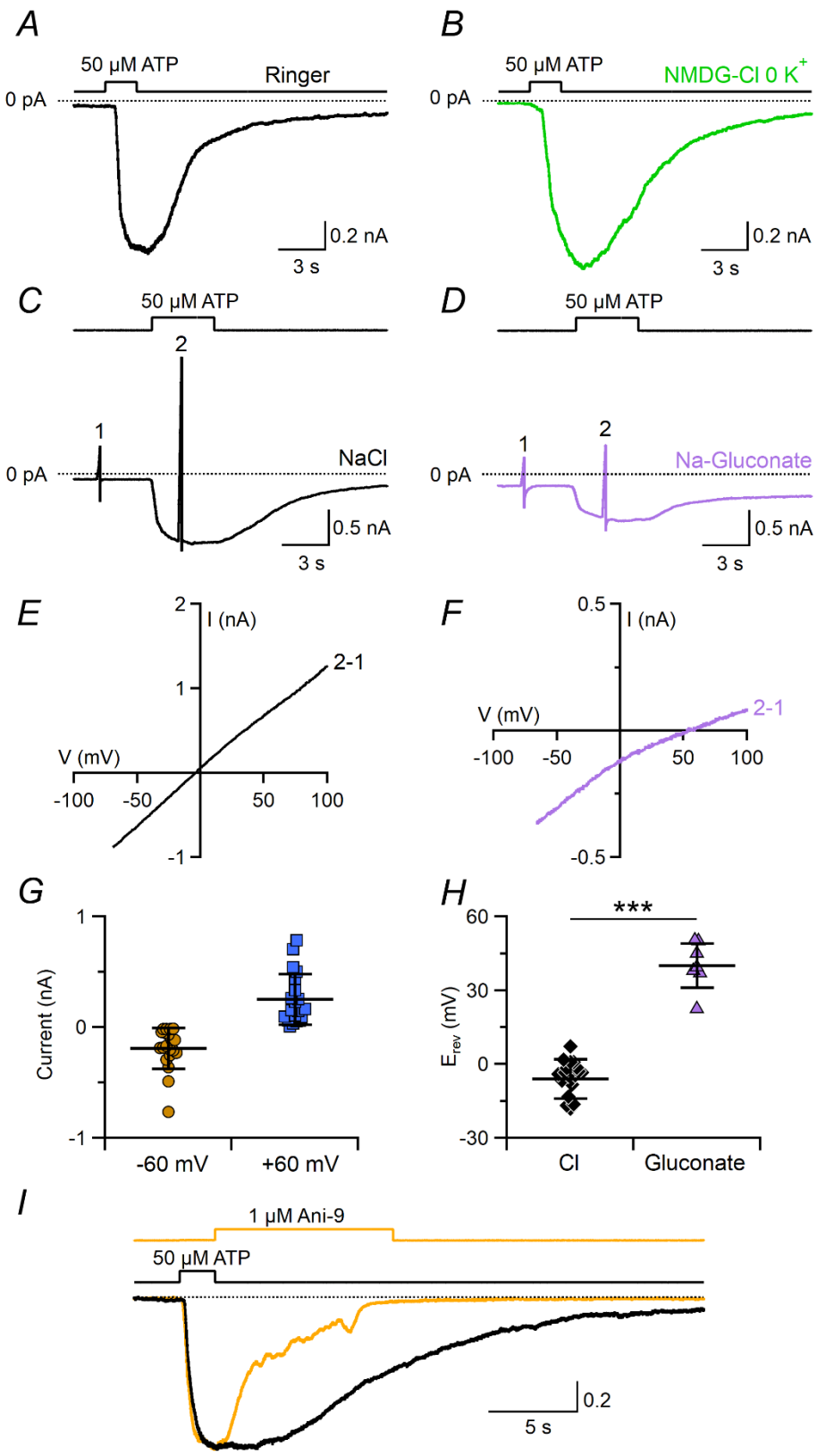
A
50 μM ATP
Ringer
0 pA
0.2 nA
3 s
B
50 μM ATP
NMDG-Cl 0 K+
0 pA
0.2 nA
3 s
C
50 μM ATP
2
1
NaCl
0 pA
0.5 nA
3 s
D
50 μM ATP
1
2
Na-Gluconate
0 pA
0.5 nA
3 s
E
I (nA)
2-1
V (mV)
-100
-50
50
100
2
1
-1
F
0.5
I (nA)
V (mV)
2-1
-100
-50
50
100
-0.5
G
Current (nA)
1
0
-1
-60 mV
+60 mV
H
***
60
30
0
-30
Erev (mV)
Cl
Gluconate
I
1 μM Ani-9
50 μM ATP
0.2
5 s

Figure 9. ATP induces a Cl^- current blocked by Ani-9 in type I taste bud cells.
Representative whole-cell recordings from type I taste cells stimulated with 50 μM ATP in Ringer's solution (***A***) or in a Ringer's solution modified by replacing NaCl with NMDG-Cl and omitting KCl (***B***). The pipette solution contained NMDG-Cl. The holding potential was -70 mV. ATP was applied for the time indicated in the upper trace. ***C*** and ***D****,* voltage ramps from −70 to +100 mV before (1) and during (2) ATP application were used to measure I-V relations in the presence of Ringer with NaCl or Ringer with Na-gluconate (*D*). ***E*** and ***F****,* I-V relations from the cells shown in (*C*) and (*D*) respectively obtained by subtracting the traces (1) from those in the presence of ATP (2). ***G***, scatter dot plots with averages ± SD of current amplitudes at -60 and +60 mV (n = 18). ***H***, scatter dot plots with averages ± SD of E_{rev} recorded in Ringer with NaCl (n = 20, black diamonds) or in Ringer with Na-gluconate (n = 7, purple triangles; p= 1.93×10^{-11} unpaired t-test). ***I***, blockage by 1 μM Ani-9 of the ATP-induced current in Ringer's solution. ATP and Ani-9 were applied as indicated in the upper traces. Currents from the same cell were normalized to the peak amplitude. ATP stimulus duration was 2 s. Ani-9 was applied after ATP for 10 s and completely blocked the current (yellow trace, -756 pA peak current). Control trace recorded after Ani-9 application (black trace, -948 pA peak current).

Thus, our results in the whole-cell configuration confirm previous data obtained with perforated patch recordings (Kim *et al.*, 2000; Cherkashin *et al.*, 2016) showing that ATP evokes large Ca^{2+}-activated Cl^- currents in type I cells and extend those results showing that these currents are blocked by Ani-9, consistent with our data indicating that these currents are due to activation of TMEM16A channels.

DISCUSSION

In this study, we have demonstrated that a large Ca^{2+}-activated Cl^- current can be physiologically activated in type I, but not in type II and III taste bud cells. Moreover, we have shown that the Ca^{2+}-activated Cl^- channel TMEM16A, but not TMEM16B, is expressed mainly at the apical part of type I cells where it largely colocalizes with the inwardly rectifying K^+ channel KCNJ1.

Ca^{2+}-activated Cl^- channels in taste bud cells

Our study confirms some data of the previous pioneering reports showing the presence of Ca^{2+}-activated Cl^- currents in taste cells and significantly extends and revises them (Cherkashin *et al.*, 2016; Kim *et al.*, 2000;). Indeed, Kim *et al*. (2000) used perforated patch-clamp recordings combined with Ca^{2+} imaging and demonstrated that intracellular Ca^{2+} increase, produced by ionomycin or by ATP, activated Cl^- currents in a subpopulation of taste cells, which exhibited no voltage-gated Na^+ and Ca^{2+} currents. The same authors also showed that the cytosolic Ca^{2+} increase produced by ATP was mediated by P2Y receptors, demonstrating that ATP indirectly activated Cl^- channels by causing Ca^{2+} release from intracellular stores. Cherkashin *et al*. (2016) further investigated the distribution of Ca^{2+}-activated Cl^- currents in taste cell types using the perforated patch clamp technique. They found clear evidence that type I cells have functional Ca^{2+}-activated Cl^- channels that can be activated by ionomycin or purinergic agonists. By measuring the effect of available blockers for TMEM16A, they found that channels in type I cells were blocked by CaCCinh-A01 but not by T16Ainh-A01. The authors also recorded a very small inward current in type II cells activated by ionomycin or by photorelease of caged Ca^{2+} that could be blocked by T16Ainh-A01. Type III cells exhibited no ion current induced by ionomycin or photorelease of caged Ca. In addition, the same authors found transcripts of *Tmem16a* and *Tmem16b* in vallate papillae and confirmed their expression by using immunohistochemistry. They also identified *Tmem16a* transcripts in type II cells, and *Tmem16b* transcripts in both type I and type II cells. On the basis of their results, Cherkashin *et al*. (2016) concluded that type I cells express only TMEM16B, while type II express both TMEM16A and TMEM16B channels.

In our study, we used a more recently discovered selective blocker of TMEM16A, Ani-9 (Seo *et al.*, 2016) and had the possibility to use KO mice for *Tmem16a* and *Tmem16b* as a control for the specificity of antibodies. This allowed us to confirm, revise and extend some of the previous discoveries. By using specific antibodies for TMEM16A and TMEM16B validated on tissues from KO mice, we

confirmed the expression of TMEM16A in taste buds whereas we did not find expression of TMEM16B. We further investigated the expression of TMEM16B by using the *Tmem16b* KO mice line engineered by Zhang *et al*. (2017) to express mCherry under the *Tmem16b* promoter. We confirmed that mCherry was not expressed in taste buds, whereas it was expressed by olfactory sensory neurons in the olfactory epithelium, further showing that TMEM16B is not expressed in taste buds.

From a functional point of view, we performed patch-clamp experiments in the whole-cell configuration and compared recordings obtained with nominally 0 or 1.5 μM intracellular Ca^{2+} and measured large Ca^{2+} activated Cl^- current in type I cells blocked by Ani-9, a selective blocker of TMEM16A, whereas we could not measure any Ca^{2+}-activated Cl^- current in type II and type III cells. Moreover, in type I cells, extracellular ATP produced activation of a large Cl^- current that was inhibited by Ani-9, further demonstrating the functional expression of TMEM16A in type I cells.

Recently, Ávalos Padro *et al.* (2021) reported that the interaction of TMEM16A with KCNE1 switches the gating mode of TMEM16A from Ca^{2+}-dependent to voltage-dependent, showing that TMEM16A could also be activated in the absence of Ca^{2+} if it is associated with KCNE1. However, our data show that type II and type III cells lack voltage-gated Cl^- currents also in nominally 0 intracellular Ca^{2+} (Fig. 6), further excluding the possibility that TMEM16A could be active in these cell types.

As type II cells are very heterogeneous (Chandrashekar *et al.*, 2006), we cannot exclude the possibility that some rare type II cells could exhibit Ca^{2+} activated Cl^- currents.

Physiological activators and role of Ca^{2+}-activated Cl^- currents in type I taste bud cells

Type I cells are about 50% of the cells in each taste bud and are considered to have mainly glial-like functions. Not much is known about their physiological roles that still need to be extensively investigated. It is well established that ATP is released from type II taste cells and is degraded by NTPDase2 on the surface of type I cells (Bartel *et al.*, 2006; Vandenbeuch *et al.*, 2013). However, type I cells also express P2Y receptors that have been shown to increase cytosolic Ca^{2+} when activated by ATP (Bystrova *et al.*, 2006; Kim *et al.*, 2000). Immunohistochemical data showed that $P2Y_1$ receptors (Kataoka *et al.*, 2004) and $P2Y_2$ receptors (Bystrova *et al.*, 2006) are expressed in the basolateral membrane of a subset of taste bud cells. Thus, we speculate that ATP released through CALHM1/CALHM3 channels of type II cells reaching the surface of type I cells, where it is degraded by NTPDase2, can also bind to P2Y receptors, and indirectly activate TMEM16A channels causing a flux of Cl^- according to its electrochemical gradient.

In addition to P2Y receptors, type I cells also express other receptors that, upon activation by their agonists, produce an increase in intracellular Ca^{2+} and can therefore activate TMEM16A channels. Sinclair *et al.* (2010) have shown that a subset of type I cells expresses the oxytocin receptor that upon stimulation by oxytocin causes an intracellular Ca^{2+} increase similar to that induced by ATP. In another study, Huang and Wu (2018) have measured Ca^{2+} release from intracellular stores in type I cells in response to substance P.

What is, then, the physiological role of Ca^{2+}-activated Cl^- channels in type I taste cells? Depending on the Cl^- equilibrium potential and on the membrane potential, these channels may allow influx or efflux of Cl^-, increasing or decreasing the cytoplasmic Cl^- concentration and contributing to cell hyperpolarization or depolarization. At present, estimates of the Cl^- concentration inside taste cells are not available and may differ between the basolateral and apical side. The extracellular Cl^- concentration varies depending on apical or basolateral parts of the cell. Indeed, the apical part of taste cells is likely to be immersed in saliva, while the cell body is surrounded by interstitial fluid. Saliva has a naturally low Cl^- concentration, being composed by 15 mM NaCl, 22 mM KCl, 3 mM $CaCl_2$, and 0.6 mM $MgCl_2$, corresponding to a Cl^- concentration of about 44 mM (Breza *et al.*, 2010; Matsuo, 2000), while the interstitial fluid contains about 100-110 mM Cl^- (Yunos *et al.*, 2010). However, when salty tastants enter the taste pore, the concentration of Cl^- can greatly increase, modifying the Cl^- equilibrium potential. We have shown that TMEM16A largely colocalized with the inwardly rectifying K^+ channel KCNJ1 at the apical part of type I cells. KCNJ1 has been proposed to be involved in buffering of basolateral extracellular K^+ by mediating the K^+ efflux through the apical pore (Dvoryanchikov *et al.*, 2009). As stimulation by tastants of type II cells produces both the local increase of extracellular K^+ and release of ATP, we speculate that the activation of TMEM16A by ATP could mediate an influx of Cl^- allowing a sustained apical extrusion of K^+.

Interestingly, it has been shown that TMEM16A can be activated in the absence of intracellular Ca^{2+} by low extracellular pH through the titration of glutamic acid 623 (Cruz-Rangel *et al.*, 2017). We speculate that this modulation could be relevant during sour stimulation of type III cells. Indeed, the activation of TMEM16A by low pH could contribute, together with KCNJ1, to buffer the increase of extracellular K^+ due to action potential firing of type III cells. However, Cruz-Rangel *et al.* (2017) also showed that an increase in intracellular Ca^{2+} to about 1 μM abolished the pH-dependent gating of TMEM16A. Moreover, since TMEM16A has different permeabilities for anions, it is tempting to

speculate that this channel may contribute to the long known “anion effect” in which responses to sodium salts differ depending on the anion (Beidler, 1953; Breza & Contreras, 2012; Roebber *et al.*, 2019).

Finally, it is of interest to note that Tizzano *et al*. (2015) have shown that human vallate papillae share most of the structural, morphological, and molecular features observed in rodents, and therefore future work should also investigate the expression of TMEM16A and verify a possible physiological role of this channel in human taste buds.

In summary, our data provide a definitive demonstration that TMEM16A-mediated currents are functional in type I taste cells of mouse vallate papillae and provide a foundation for future studies investigating additional physiological roles for type I cells, often neglected with respect to studies on the type II and III taste cells.

ACKNOWLEDGMENTS:

We thank Michele Dibattista (University of Bari) and Paul A. Heppenstall (SISSA) for helpful discussions. We thank Elettra Grdina, Angel Pascual Camerota, Cristina Degrassi, Lorenzo Maschietto, and Giovanni Tamburin for mice handling, Helena Krmac and Christina Vlachouli for mice genotyping. We thank Lily Jan (UCSF), Jason R. Rock (Boston University School of Medicine) and Brain D. Harfe (University of Florida) for providing us KO mice.

REFERENCES

Ávalos Padro P, Häfner S, Comoglio Y, Wdziekonski B, Duranton C, Attali B, Barhanin J & Sandoz G (2021). KCNE1 is an auxiliary subunit of two distinct ion channel superfamilies.*Cell* **184,** 534-544.

Barry PH (1994). JPCalc, a software package for calculating liquid junction potential corrections in patch-clamp, intracellular, epithelial and bilayer measurements and for correcting junction potential measurements. *J Neurosci Methods* **51,** 107–116.

Bartel DL, Sullivan SL, Lavoie EG, Sévigny J & Finger TE (2006). Nucleoside triphosphate diphosphohydrolase-2 is the ecto-ATPase of type I cells in taste buds. *J Comp Neurol* **497,** 1–12.

Baumer-Harrison C, Raymond MA, Myers TA, Sussman KM, Rynberg ST, Ugartechea AP, Lauterbach D, Mast TG & Breza JM (2020). Optogenetic Stimulation of Type I GAD65+ Cells in Taste Buds Activates Gustatory Neurons and Drives Appetitive Licking Behavior in Sodium-Depleted Mice. *J Neurosci* **40,** 7795–7810.

Béhé P, DeSimone JA, Avenet P & Lindemann B (1990). Membrane currents in taste cells of the rat fungiform papilla. Evidence for two types of Ca currents and inhibition of K currents by saccharin. *J Gen Physiol* **96,** 1061–1084.

Beidler LM (1953). Properties of chemoreceptors of tongue of rat. *J Neurophysiol* **16,** 595–607.

Bigiani A (2001). Mouse taste cells with glialike membrane properties. *J Neurophysiol* **85,** 1552–1560.

Bigiani A (2017). Calcium Homeostasis Modulator 1-Like Currents in Rat Fungiform Taste Cells Expressing Amiloride-Sensitive Sodium Currents. *Chem Senses* **42,** 343–359.

Bigiani A, Cristiani R, Fieni F, Ghiaroni V, Bagnoli P & Pietra P (2002). Postnatal development of membrane excitability in taste cells of the mouse vallate papilla. *J Neurosci* **22,** 493–504.

Breza JM & Contreras RJ (2012). Anion size modulates salt taste in rats. *J Neurophysiol* **107,** 1632–1648.

Breza JM, Nikonov AA & Contreras RJ (2010). Response latency to lingual taste stimulation distinguishes neuron types within the geniculate ganglion. *J Neurophysiol* **103,** 1771–1784.

Bystrova MF, Yatzenko YE, Fedorov IV, Rogachevskaja OA & Kolesnikov SS (2006). P2Y isoforms operative in mouse taste cells. *Cell Tissue Res* **323,** 377–382.

Caputo A, Caci E, Ferrera L, Pedemonte N, Barsanti C, Sondo E, Pfeffer U, Ravazzolo R, Zegarra-Moran O & Galietta LJV (2008). TMEM16A, a membrane protein associated with calcium-dependent chloride channel activity. *Science* **322,** 590–594.

Centeio R, Cabrita I, Benedetto R, Talbi K, Ousingsawat J, Schreiber R, Sullivan JK & Kunzelmann K (2020). Pharmacological Inhibition and Activation of the Ca2+ Activated Cl- Channel TMEM16A. *Int J Mol Sci* **21,** 2557.

Chandrashekar J, Hoon MA, Ryba NJP & Zuker CS (2006). The receptors and cells for mammalian taste. *Nature* **444,** 288–294.

Cherkashin AP, Kolesnikova AS, Tarasov MV, Romanov RA, Rogachevskaja OA, Bystrova MF & Kolesnikov SS (2016). Expression of calcium-activated chloride channels Ano1 and Ano2 in mouse taste cells. *Pflugers Arch* **468,** 305–319.

Clapp TR, Medler KF, Damak S, Margolskee RF & Kinnamon SC (2006). Mouse taste cells with G protein-coupled taste receptors lack voltage-gated calcium channels and SNAP-25. *BMC Biol* **4,** 7.

Cruz-Rangel S, De Jesús-Pérez JJ, Aréchiga-Figueroa IA, A Rodríguez-Menchaca AA, Pérez-Cornejo P , Hartzell HC & , Arreola J (2017). Extracellular protons enable activation of the calcium-dependent chloride channel TMEM16A. *J Physiol* **595**, 1515-1531.

Dauner K, Lissmann J, Jeridi S, Frings S & Möhrlen F (2012). Expression patterns of anoctamin 1 and anoctamin 2 chloride channels in the mammalian nose. *Cell Tissue Res* **347,** 327–341.

DeFazio RA, Dvoryanchikov G, Maruyama Y, Kim JW, Pereira E, Roper SD & Chaudhari N (2006). Separate populations of receptor cells and presynaptic cells in mouse taste buds. *J Neurosci* **26,** 3971–3980.

Dibattista M, Pifferi S, Boccaccio A, Menini A & Reisert J (2017). The long tale of the calcium activated Cl- channels in olfactory transduction. *Channels (Austin)* **11,** 399–414.

Dutta Banik D, Martin LE, Freichel M, Torregrossa A-M & Medler KF (2018). TRPM4 and TRPM5 are both required for normal signaling in taste receptor cells. *Proc Natl Acad Sci USA* **115,** E772–E781.

Dvoryanchikov G, Sinclair MS, Perea-Martinez I, Wang T & Chaudhari N (2009). Inward rectifier channel, ROMK, is localized to the apical tips of glial-like cells in mouse taste buds. *J Comp Neurol* **517,** 1–14.

Henriques T, Agostinelli E, Hernandez-Clavijo A, Maurya DK, Rock JR, Harfe BD, Menini A & Pifferi S (2019). TMEM16A calcium-activated chloride currents in supporting cells of the mouse olfactory epithelium. *J Gen Physiol* **151,** 954–966.

Herness MS & Sun XD (1999). Characterization of chloride currents and their noradrenergic modulation in rat taste receptor cells. *J Neurophysiol* **82,** 260–271.

Hisatsune C, Yasumatsu K, Takahashi-Iwanaga H, Ogawa N, Kuroda Y, Yoshida R, Ninomiya Y & Mikoshiba K (2007). Abnormal taste perception in mice lacking the type 3 inositol 1,4,5-trisphosphate receptor. *J Biol Chem* **282,** 37225–37231.

Huang AY & Wu SY (2018). Substance P as a putative efferent transmitter mediates GABAergic inhibition in mouse taste buds. *Br J Pharmacol* **175,** 1039–1053.

Huang YA, Maruyama Y & Roper SD (2008). Norepinephrine is coreleased with serotonin in mouse taste buds. *J Neurosci* **28,** 13088–13093.

Kataoka S, ToyonoT, Seta Y, Ogura T & Toyoshima (2004). Expression of P2Y1 receptors in rat taste buds. *Histochem Cell Biol* **121**, 419-426.

Kim YV, Bobkov YV & Kolesnikov SS (2000). Adenosine triphosphate mobilizes cytosolic calcium and modulates ionic currents in mouse taste receptor cells. *Neurosci Lett* **290,** 165–168.

Kinnamon SC & Finger TE (2019). Recent advances in taste transduction and signaling. *F1000Res*; DOI: 10.12688/f1000research.21099.1.

Lawton DM, Furness DN, Lindemann B & Hackney CM (2000). Localization of the glutamate-aspartate transporter, GLAST, in rat taste buds. *Eur J Neurosci* **12,** 3163–3171.

Liman ER, Zhang YV & Montell C (2014). Peripheral coding of taste. *Neuron* **81,** 984–1000.

Ma Z, Tanis JE, Taruno A & Foskett JK (2016). Calcium homeostasis modulator (CALHM) ion channels. *Pflugers Arch* **468,** 395–403.

Ma Z, Taruno A, Ohmoto M, Jyotaki M, Lim JC, Miyazaki H, Niisato N, Marunaka Y, Lee RJ, Hoff H, Payne R, Demuro A, Parker I, Mitchell CH, Henao-Mejia J, Tanis JE, Matsumoto I, Tordoff MG & Foskett JK (2018). CALHM3 Is Essential for Rapid Ion Channel-Mediated Purinergic Neurotransmission of GPCR-Mediated Tastes. *Neuron* **98,** 547-561.e10.

Matsuo R (2000). Role of saliva in the maintenance of taste sensitivity. *Crit Rev Oral Biol Med* **11,** 216–229.

Maurya DK, Henriques T, Marini M, Pedemonte N, Galietta LJV, Rock JR, Harfe BD & Menini A (2015). Development of the Olfactory Epithelium and Nasal Glands in TMEM16A-/- and TMEM16A+/+ Mice. *PLoS ONE* **10,** e0129171.

Maurya DK & Menini A (2014). Developmental expression of the calcium-activated chloride channels TMEM16A and TMEM16B in the mouse olfactory epithelium. *Dev Neurobiol* **74,** 657–675.

McBride DW & Roper SD (1991). Ca(2+)-dependent chloride conductance in Necturus taste cells. *J Membr Biol* **124,** 85–93.

Medler KF, Margolskee RF & Kinnamon SC (2003). Electrophysiological characterization of voltage-gated currents in defined taste cell types of mice. *J Neurosci* **23,** 2608–2617.

Noguchi T, Ikeda Y, Miyajima M & Yoshii K (2003). Voltage-gated channels involved in taste responses and characterizing taste bud cells in mouse soft palates. *Brain Res* **982,** 241–259.

Nomura K, Nakanishi M, Ishidate F, Iwata K & Taruno A (2020). All-Electrical Ca^{2+}-Independent Signal Transduction Mediates Attractive Sodium Taste in Taste Buds. *Neuron* **106,** 816-829.

O'Driscoll KE, Pipe RA & Britton FC (2011). Increased complexity of Tmem16a/Anoctamin 1 transcript alternative splicing. *BMC Mol Biol* **12,** 35.

Oliva AA, Jiang M, Lam T, Smith KL & Swann JW (2000). Novel hippocampal interneuronal subtypes identified using transgenic mice that express green fluorescent protein in GABAergic interneurons. *J Neurosci* **20,** 3354–3368.

Patton C, Thompson S & Epel D (2004). Some precautions in using chelators to buffer metals in biological solutions. *Cell Calcium* **35,** 427–431.

Pedemonte N & Galietta LJV (2014). Structure and function of TMEM16 proteins (anoctamins). *Physiol Rev* **94,** 419–459.

Pifferi S, Dibattista M & Menini A (2009*a*). TMEM16B induces chloride currents activated by calcium in mammalian cells. *Pflugers Arch* **458,** 1023–1038.

Pifferi S, Dibattista M, Sagheddu C, Boccaccio A, Al Qteishat A, Ghirardi F, Tirindelli R & Menini A (2009*b*). Calcium-activated chloride currents in olfactory sensory neurons from mice lacking bestrophin-2. *J Physiol* **587,** 4265–4279.

Pifferi S, Pascarella G, Boccaccio A, Mazzatenta A, Gustincich S, Menini A & Zucchelli S (2006). Bestrophin-2 is a candidate calcium-activated chloride channel involved in olfactory transduction. *Proc Natl Acad Sci U S A* **103,** 12929–12934.

Ponissery Saidu S, Stephan AB, Talaga AK, Zhao H & Reisert J (2013). Channel properties of the splicing isoforms of the olfactory calcium-activated chloride channel Anoctamin 2. *J Gen Physiol* **141,** 691–703.

Rock JR, Futtner CR & Harfe BD (2008). The transmembrane protein TMEM16A is required for normal development of the murine trachea. *Dev Biol* **321,** 141–149.

Roebber JK, Roper SD & Chaudhari N (2019). The Role of the Anion in Salt (NaCl) Detection by Mouse Taste Buds. *J Neurosci* **39,** 6224–6232.

Romanov RA & Kolesnikov SS (2006). Electrophysiologically identified subpopulations of taste bud cells. *Neurosci Lett* **395,** 249–254.

Romanov RA, Rogachevskaja OA, Bystrova MF, Jiang P, Margolskee RF & Kolesnikov SS (2007). Afferent neurotransmission mediated by hemichannels in mammalian taste cells. *EMBO J* **26,** 657–667.

Roper SD & Chaudhari N (2017). Taste buds: cells, signals and synapses. *Nat Rev Neurosci* **18,** 485–497.

Sagheddu C, Boccaccio A, Dibattista M, Montani G, Tirindelli R & Menini A (2010). Calcium concentration jumps reveal dynamic ion selectivity of calcium-activated chloride currents in mouse olfactory sensory neurons and TMEM16b-transfected HEK 293T cells. *J Physiol (Lond)* **588,** 4189–4204.

Schroeder BC, Cheng T, Jan YN & Jan LY (2008). Expression cloning of TMEM16A as a calcium-activated chloride channel subunit. *Cell* **134,** 1019–1029.

Scudieri P, Caci E, Bruno S, Ferrera L, Schiavon M, Sondo E, Tomati V, Gianotti A, Zegarra-Moran O, Pedemonte N, Rea F, Ravazzolo R & Galietta LJV (2012). Association of TMEM16A chloride channel overexpression with airway goblet cell metaplasia. *J Physiol (Lond)* **590,** 6141–6155.

Seo Y, Lee HK, Park J, Jeon D-K, Jo S, Jo M & Namkung W (2016). Ani9, A Novel Potent Small-Molecule ANO1 Inhibitor with Negligible Effect on ANO2. *PLoS ONE* **11,** e0155771.

Sinclair MS, Perea-Martinez I, Dvoryanchikov G, Yoshida M, Nishimori K, Roper SD & Chaudhari N (2010). Oxytocin signaling in mouse taste buds. *PLoS One* **5,** e11980.

Stephan AB, Shum EY, Hirsh S, Cygnar KD, Reisert J & Zhao H (2009). ANO2 is the cilial calcium-activated chloride channel that may mediate olfactory amplification. *Proc Natl Acad Sci USA* **106,** 11776–11781.

Stöhr H, Heisig JB, Benz PM, Schöberl S, Milenkovic VM, Strauss O, Aartsen WM, Wijnholds J, Weber BHF & Schulz HL (2009). TMEM16B, a novel protein with calcium-dependent chloride channel activity, associates with a presynaptic protein complex in photoreceptor terminals. *J Neurosci* **29,** 6809–6818.

Taruno A, Vingtdeux V, Ohmoto M, Ma Z, Dvoryanchikov G, Li A, Adrien L, Zhao H, Leung S, Abernethy M, Koppel J, Davies P, Civan MM, Chaudhari N, Matsumoto I, Hellekant G, Tordoff MG, Marambaud P & Foskett JK (2013). CALHM1 ion channel mediates purinergic neurotransmission of sweet, bitter and umami tastes. *Nature* **495,** 223–226.

Taylor R & Roper S (1994). Ca(2+)-dependent Cl- conductance in taste cells from Necturus. *J Neurophysiol* **72,** 475–478.

Teng B, Wilson CE, Tu Y-H, Joshi NR, Kinnamon SC & Liman ER (2019). Cellular and Neural Responses to Sour Stimuli Require the Proton Channel Otop1. *Curr Biol* **29,** 3647-3656.e5.

Tizzano M, Grigereit L, Shultz N, Clary MS & Finger TE (2015). Immunohistochemical Analysis of Human Vallate Taste Buds. *Chem Senses* **40,** 655–660.

Tomchik SM, Berg S, Kim JW, Chaudhari N & Roper SD (2007). Breadth of tuning and taste coding in mammalian taste buds. *J Neurosci* **27,** 10840–10848.

Tu Y-H, Cooper AJ, Teng B, Chang RB, Artiga DJ, Turner HN, Mulhall EM, Ye W, Smith AD & Liman ER (2018). An evolutionarily conserved gene family encodes proton-selective ion channels. *Science* **359,** 1047–1050.

Vandenbeuch A, Anderson CB, Parnes J, Enjyoji K, Robson SC, Finger TE & Kinnamon SC (2013). Role of the ectonucleotidase NTPDase2 in taste bud function. *Proc Natl Acad Sci U S A* **110,** 14789–14794.

Vandenbeuch A, Clapp TR & Kinnamon SC (2008). Amiloride-sensitive channels in type I fungiform taste cells in mouse. *BMC Neurosci* **9,** 1.

Vandenbeuch A, Zorec R & Kinnamon SC (2010). Capacitance measurements of regulated exocytosis in mouse taste cells. *J Neurosci* **30,** 14695–14701.

Wladkowski SL, Lin W, McPheeters M, Kinnamon SC & Mierson S (1998). A basolateral chloride conductance in rat lingual epithelium. *J Membr Biol* **164,** 91–101.

Yang R, Crowley HH, Rock ME & Kinnamon JC (2000). Taste cells with synapses in rat circumvallate papillae display SNAP-25-like immunoreactivity. *J Comp Neurol* **424,** 205–215.

Yang R, Dzowo YK, Wilson CE, Russell RL, Kidd GJ, Salcedo E, Lasher RS, Kinnamon JC & Finger TE (2020). Three-dimensional reconstructions of mouse circumvallate taste buds using serial blockface scanning electron microscopy: I. Cell types and the apical region of the taste bud. *J Comp Neurol* **528,** 756–771.

Yang YD, Cho H, Koo JY, Tak MH, Cho Y, Shim W-S, Park SP, Lee J, Lee B, Kim B-M, Raouf R, Shin YK & Oh U (2008). TMEM16A confers receptor-activated calcium-dependent chloride conductance. *Nature* **455,** 1210–1215.

Ye W, Chang RB, Bushman JD, Tu Y-H, Mulhall EM, Wilson CE, Cooper AJ, Chick WS, Hill-Eubanks DC, Nelson MT, Kinnamon SC & Liman ER (2016). The K+ channel KIR2.1 functions in tandem with proton influx to mediate sour taste transduction. *Proc Natl Acad Sci U S A* **113,** E229-238.

Yunos NM, Bellomo R, Story D & Kellum J (2010). Bench-to-bedside review: Chloride in critical illness. *Critical Care* **14,** 226.

Zhang Y, Hoon MA, Chandrashekar J, Mueller KL, Cook B, Wu D, Zuker CS & Ryba NJP (2003). Coding of sweet, bitter, and umami tastes: different receptor cells sharing similar signaling pathways. *Cell* **112,** 293–301.

Zhang Y, Zhang Z, Xiao S, Tien J, Le S, Le T, Jan LY & Yang H (2017). Inferior Olivary TMEM16B Mediates Cerebellar Motor Learning. *Neuron* **95,** 1103-1111.e4.

Supplementary materials

Methods

Cell culture and transfection

HEK-293 cells were grown in medium composed of DMEM (Gibco, Italy) supplemented with 10% fetal bovine serum (Sigma, Italy), 100 IU/ml penicillin and 100 µg/ml streptomycin (Sigma, Italy) at 37°C in a humidified atmosphere of 5% CO_2.

pEGFP-N1 plasmid containing the cDNA of mouse TMEM16A (version ac, as in Ferrera *et al.*, 2009) was provided by Professor Criss Hartzell (Emory University, USA). HEK-293 cells were transfected with 2 µg of plasmid using the transfection reagent XtremeGENE (Roche Diagnostic, USA). 24h after transfection, the cells were subcultured in 35-mm petri dishes at a lower density. Electrophysiological recordings were performed between 48 and 72 h after transfection as previously described (Pifferi et al., 2009).

Electrophysiological recording from HEK-293 cells

TMEM16A-transfected HEK-293 cells were identified by EGFP fluorescence using an Olympus IX70 microscope (Olympus, Japan) equipped with the appropriate filter. TMEM16A currents were recorded in whole-cell configurations in voltage-clamp mode using an Multiclamp 700B amplifier controlled by Clampex 9.2 via Digidata 1322A (Axon Instruments, USA). The data were acquired at a rate of 10 kHz, and the signals were low-pass filtered at 5 kHz. Patch electrodes were made of borosilicate glass (WPI, USA) and pulled with a PP-830 micropipette puller (Narishige, Japan). Pulled patch electrodes had a resistance of 2-3 MΩ f when filled with pipette solution.

Cells were kept in mammalian Ringer's solution composed of (in mM) 140 NaCl, 5 KCl, 2 $CaCl_2$, 1 $MgCl_2$, 10 glucose and 10 Hepes, pH 7.4 with NaOH. The pipette solution contained (in mM): 140 NMDG-Cl, 10 HEDTA, 10 HEPES, 1.242 $CaCl_2$ adjusted to pH 7.3 with NMDG to obtain the final concentration of 0.5 µM free Ca^{2+}. The extracellular solution contained (in mM): 140 NMDG-Cl, 2 $CaCl_2$, 1 $MgCl_2$, 10 HEPES, adjusted to pH 7.4 with NMDG. Ani-9 was prepared in DMSO at 10 mM as a stock solution and diluted in the extracellular solution to the final concentration of 1 µM.

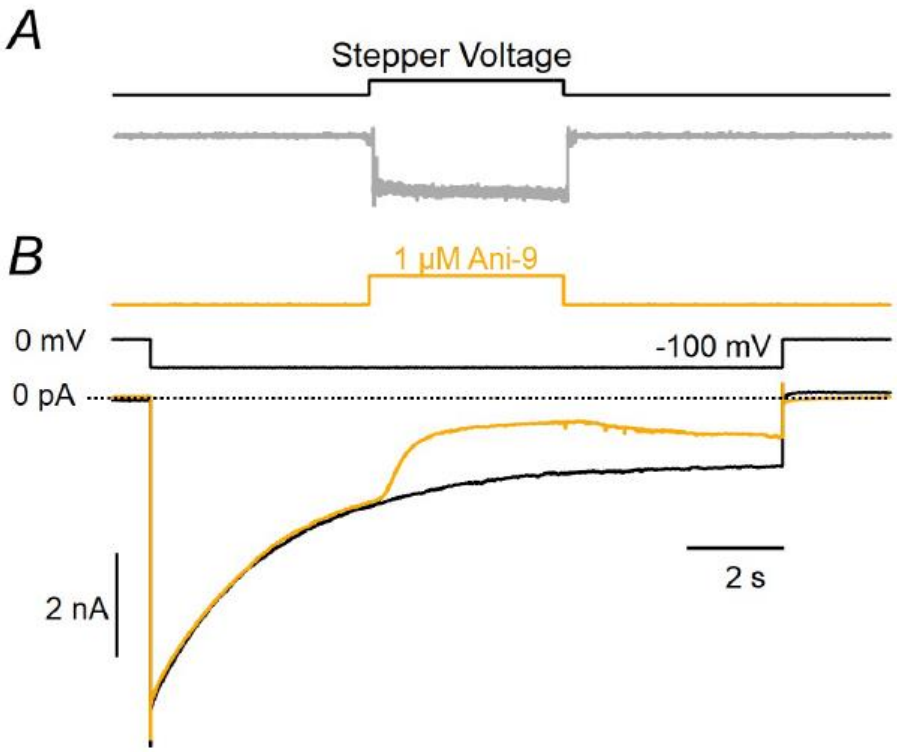

Supplementary Figure 1. Blockage of TMEM16A-mediated current by Ani-9.

(***A***) The upper trace shows the voltage command of the stepper motor moving glass pipes in which different solutions were flowing. The bottom trace shows the time course of the solution exchange from Ringer to 1 M KCl moving the pipes in front of a patch electrode. The change of solution was obtained in less than 50 ms. (***B***) Representative whole-cell recording from HEK-293 cells expressing TMEM16A recorded in symmetrical NMDG-Cl solutions with an intracellular solution containing 0.5 µM Ca^{2+}. The holding potential was 0 mV and was stepped to -100 mV as indicated. 1 µM Ani-9 was applied as indicated in the upper trace. A significant reduction of the currents was observed within a few seconds from the application of the blocker.

Supplementary references

Ferrera L, Caputo A, Ubby I, Bussani E, Zegarra-Moran O, Ravazzolo R, Pagani F & Galietta LJV (2009). Regulation of TMEM16A chloride channel properties by alternative splicing. *J Biol Chem* **284,** 33360–33368.

Pifferi S, Dibattista M & Menini A (2009). TMEM16B induces chloride currents activated by calcium in mammalian cells. *Pflugers Arch* **458,** 1023–1038.

CONCLUSIONS

This work shows the functional expression of TMEM16A, but not TMEM16B, in taste buds of mouse vallate papillae. Moreover, TMEM16A is expressed only in type I TBCs.

We performed RT-PCR analysis on whole mRNA extracts from the whole vallate papilla revealing the expression of Tmem16a, but not Tmem16b. Immunohistochemistry experiments confirmed the expression of TMEM16A, but not TMEM16B, in TBCs. For these experiments, we used specific antibodies against TMEM16A and TMEM16B, validated on tissues from KO mice. Further, we investigated the expression of TMEM16B, by using the Tmem16b KO mouse line engineered by Zhang et al. (2017) that expresses mCherry, a red fluorescent protein, in cells that normally express TMEM16B. We did not find any signal from mCherry in taste buds, whereas we found a strong signal in olfactory sensory neurons, where TMEM16B is known to be expressed (Sagheddu et al., 2010; Stephan et al., 2009). Altogether these data show that TMEM16A, but not TMEM16B, is expressed in TBCs. Moreover, we showed that TMEM16A is mainly located to the apical tip of taste cells and it appears largely colocalized with the inwardly rectifying K^+ channel KCNJ1.

We performed electrophysiological experiments in the whole-cell voltage-clamp configuration and compared recordings obtained using nominally 0 or 1.5 µM intracellular Ca^{2+} in the three types of TBCs. Our results showed that type I cells, but not type II and III cells, generated a large Cl^- current when dialyzed with 1.5 µM Ca^{2+} in the intracellular solution. This current was inhibited by Ani9, a specific blocker of TMEM16A (Seo et al., 2016). Moreover, by repeating the same experiments on *Tmem16b* KO mice, we found that type I TBCs still exhibited Ca^{2+}-activated Cl^- currents similar to those measured in WT mice, further indicating that TMEM16B is not involved in mediating the Ca^{2+} -activated Cl^- currents in type I TBCs.

Combining the results from the different experimental approaches, we concluded that only TMEM16A is functional in taste buds, and its expression is confined to type I TBCs.

Type I TBCs are the most abundant cells in each taste bud and are considered to have mainly glial-like functions (Roper and Chaudhari, 2017; Bigiani, 2001). We also showed that extracellular ATP produced a large Cl^- current in type I TBCs, confirming previous results. The ATP-evoked current was strongly inhibited by Ani9 further demonstrating the functional expression of TMEM16A in type I TBCs. ATP, released by type II TBCs is one of the most important neurotransmitters linking responses in taste buds to nerve fibers. Indeed, P2X KO mice completely lost taste nerve responses, although nerves

still responded to touch and temperature (Finger, et al., 2005). ATP is degraded by NTPDase2 on the surface of type I cells (Bartel et al., 2006; Vandenbeuch et al., 2013). The same cells also express P2Y receptors and their activation triggers an increase in cytosolic Ca^{2+} (Kim et al., 2000; Bystrova et al., 2010) that can activate the TMEM16A channel causing a flux of Cl^- according to its electrochemical gradient. In addition to ATP, it is important to note that also other substances can cause an increase intracellular Ca^{2+} in type I cells. Indeed, Sinclair et al. (2010) showed that oxytocin, a hormone found also in taste buds, can generate a cytosolic Ca^{2+} increase, while Huang and Wu (2018) measured Ca^{2+} release from intracellular stores in response to substance P. Thus, both oxytocin and substance P could also cause activation of TMEM16A in type I cells.

To conclude, our data show that type I taste cells of mouse vallate papillae express functional TMEM16A channels that could be activated by intracellular Ca^{2+} release. The use of conditional KO mice for TMEM16A could be useful to further understand the physiological role of TMEM16A.

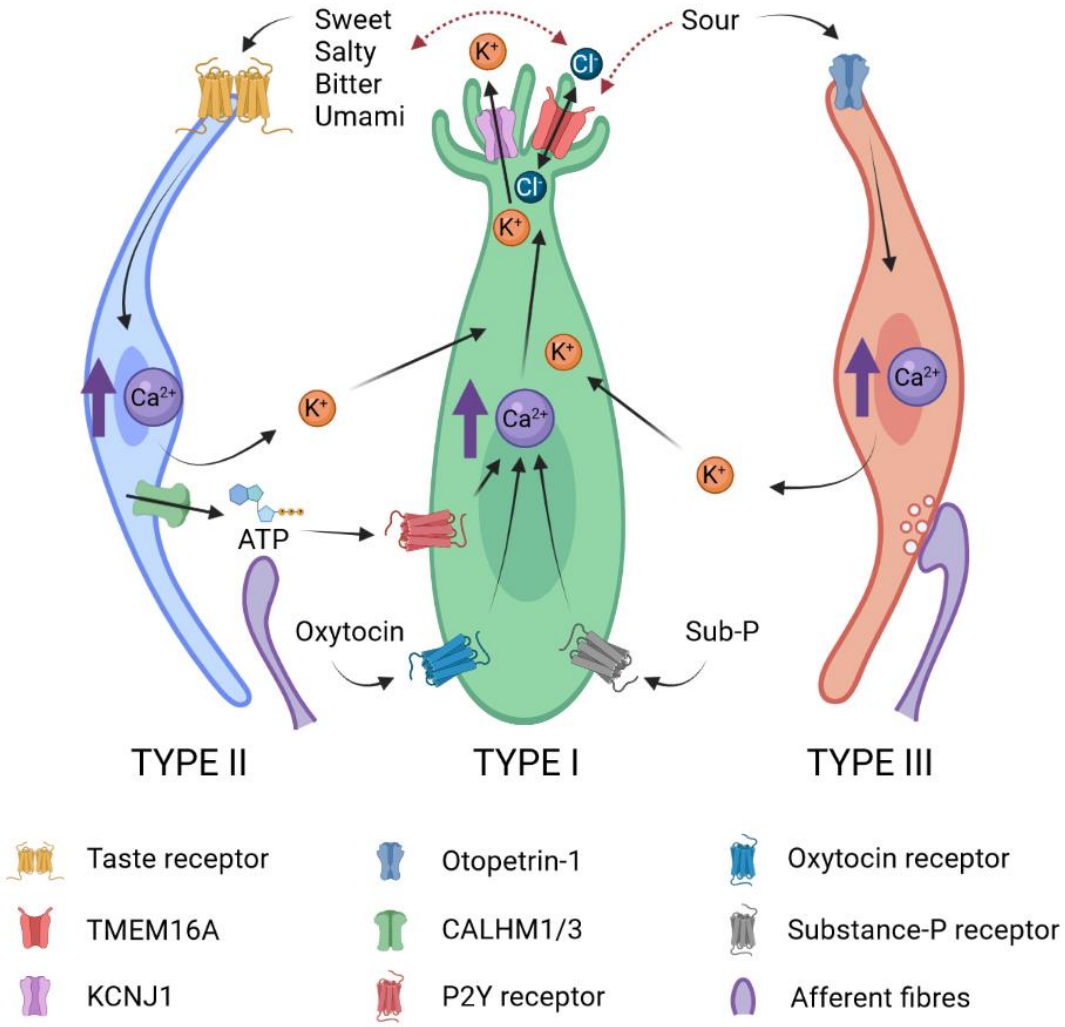

Figure 33. ***Hypothetical roles of TMEM16A in taste transduction cascade.***

During taste perception type II and type III TBCs generate action potentials resulting in realizing K^+ in the extracellular matrix. Accumulation of K^+ in the extracellular space can disrupt the membrane excitability of the cells. For this reason, is important to remove K^+. Type I TBCs taking the advantage of the chemical gradient between the extracellular matrix and mouth lumen can first accumulate the K^+ in the cytosol through leak channels, expressed on the basolateral membrane, and then shunt the K^+ in the mouth lumen through the KCNJ1 from the apical side. Moreover, ATP released by type II TBCs can bind P2Y receptors expressed on type I TBCs producing an increase of cytosolic Ca^{2+}. Cytosolic Ca^{2+} can open TMEM16A channel expressed in the microvilli of type I. TMEM16A is strictly related to the equilibrium potential of Cl^-. Indeed, based on its concentration in the mouth lumen and the extracellular matrix around TBCs, TMEM16A could cause influx or efflux of Cl^-. During salt consumption, type II and Type III TBCs increase their firing activity. At the same time the concentration of Cl^- strongly increases in the mouth lumen. In this condition, It is conceivable that TMEM16A favorite influx of Cl^- allowing a sustained apical extrusion of K^+. Moreover, also Substance P and Oxytocin can increase cytosolic Ca^{2+} in type I TBC, however, the role of TMEM16A in this condition needs to be investigated.

Figure 33. ***Hypotetical roles of TMEM16A in taste transduction cascade.*** *During taste perception type II and type III TBCs generate action potentials resulting in realsing K^+ in the extracellular matrix. Accumulation of K^+ in the extracellular space can disrupt membrane excitability of the cells. For this reason is important remove K^+. Type I TBCs taking the advantage of the chemical gradient between extracellular matrix and mouth lumen can first accumulate the K^+ in the cytosol throught leak channels, expressed on the basolateral membrane, and than shunt the K^+ in the mouth lumen thrught the KCNJ1 from the apical side. Moreover, ATP released by type II TBCs can bind P2Y receptors expressed on type I TBCs producing an increase of cytosolic Ca^{2+}. Cytosolic Ca^{2+} can open TMEM16A channel expressed in the microvilli of type I. TMEM16A is strictly related with the equilibrium potential of Cl^-. Indeed, based on its concentration in the mouth lumen and the extracellular matrix around TBCs, TMEM16A could couses influx or efflux of Cl^-. During salt consumption, type II and Type III TBCs increase their firing activity. In the same time the concentration of Cl^- strongly increase in mouth lumen. In this condition It is conceivable that TMEM16A favorite influx of Cl^- allowing a sustained apical extrusion of K^+.*

GENERAL REFERENCES

Adachi, K., S. Fujita, A. Yoshida, H. Sakagami, N. Koshikawa, and M. Kobayashi. **2013**. Anatomical and electrophysiological mechanisms for asymmetrical excitatory propagation in the rat insular cortex: In vivo optical imaging and whole-cell patch-clamp studies. J. Comp. Neurol. 521:1598–1613. doi:10.1002/cne.23246.

Adler, E., M.A. Hoon, K.L. Mueller, J. Chandrashekar, N.J.P. Ryba, and C.S. Zuker. **2000**. A Novel Family of Mammalian Taste Receptors. Cell. 100:693–702. doi:10.1016/S0092-8674(00)80705-9.

Adomaviciene, A., K.J. Smith, H. Garnett, and P. Tammaro. **2013**. Putative pore-loops of TMEM16/anoctamin channels affect channel density in cell membranes: Structural determinants of surface expression in TMEM16 channels. The Journal of Physiology. 591:3487–3505. doi:10.1113/jphysiol.2013.251660.

Allen, G.V., C.B. Saper, K.M. Hurley, and D.F. Cechetto. **1991**. Organization of visceral and limbic connections in the insular cortex of the rat. J. Comp. Neurol. 311:1–16. doi:10.1002/cne.903110102.

Amjad, A., A. Hernandez-Clavijo, S. Pifferi, D.K. Maurya, A. Boccaccio, J. Franzot, J. Rock, and A. Menini. **2015**. Conditional knockout of TMEM16A/anoctamin1 abolishes the calcium-activated chloride current in mouse vomeronasal sensory neurons. Journal of General Physiology. 145:285–301. doi:10.1085/jgp.201411348.

Arreola, J., J.E. Melvin, and T. Begenisich. **1996**. Activation of calcium-dependent chloride channels in rat parotid acinar cells. Journal of General Physiology. 108:35–47. doi:10.1085/jgp.108.1.35.

Banik D, Martin LE, Freichel M, Torregrossa AM, Medler KF. **2018**. TRPM4 and TRPM5 are both required for normal signaling in taste receptor cells. Proc Natl Acad Sci U S A. 115(4): E772-E781. doi: 10.1073/pnas.1718802115. Epub 2018 Jan 8.

Barlow, L.A. **2015**. Progress and renewal in gustation: new insights into taste bud development. Development. 142:3620–3629. doi:10.1242/dev.120394.

Barnes, S., and M.C. Deschenes. **1992**. Contribution of Ca and Ca-activated Cl channels to regenerative depolarization and membrane bistability of cone photoreceptors. Journal of Neurophysiology. 68:745–755. doi:10.1152/jn.1992.68.3.745.

Bartel DL, Sullivan SL, Lavoie EG, Sévigny J, Finger TE. **2006**.Nucleoside triphosphate diphosphohydrolase-2 is the ecto-ATPase of type I cells in taste buds. J Comp Neurol. 497(1):1-12. doi: 10.1002/cne.20954.

Baylis, L.L., E.T. Rolls, and G.C. Baylis. **1995**. Afferent connections of the caudolateral orbitofrontal cortex taste area of the primate. Neuroscience. 64:801–812. doi:10.1016/0306-4522(94)00449-F.

Beckstead, R.M., J.R. Morse, and R. Norgren. **1980**. The nucleus of the solitary tract in the monkey: Projections to the thalamus and brain stem nuclei. J. Comp. Neurol. 190:259–282. doi:10.1002/cne.901900205.

Behrens M, Meyerhof W. **2009**. Results Probl Cell Differ. Mammalian bitter taste perception. 47:203-20. doi: 10.1007/400_2008_5.

Behrens, M., and W. Meyerhof. **2013**. Bitter taste receptor research comes of age: From characterization to modulation of TAS2Rs. Seminars in Cell & Developmental Biology. 24:215–221. doi:10.1016/j.semcdb.2012.08.006.

Beidler, L.M., and R.L. Smallman. **1965**. Renewal of cells within taste buds. Journal of Cell Biology. 27:263–272. doi:10.1083/jcb.27.2.263.

Benjamin, R.M., and H. Burton. **1968**. Projection of taste nerve afferents to anterior opercular- insular cortex in squirrel monkey (Saimiri sciureus). Brain Research. 7:221–231. doi:10.1016/0006-8993(68)90100-5.

Berglund E, Akcakaya P, Berglund D, Karlsson F, Vukojević V, Lee L, Bogdanović D, Lui WO, Larsson C, Zedenius J, Fröbom R, Bränström R. **2014**. Functional role of the Ca2+-activated Cl-

channel DOG1/TMEM16A in gastrointestinal stromal tumor cells.Exp Cell Res. 2014 Aug 15;326(2):315-25. doi: 10.1016/j.yexcr.2014.05.003.

Besnard, P., P. Passilly-Degrace, and N.A. Khan. **2016**. Taste of Fat: A Sixth Taste Modality? Physiological Reviews. 96:151–176. doi:10.1152/physrev.00002.2015.

Bianchi, R., G. Corsetti, L. Rodella, G. Tredici, and M. Gioia. **1998**. Supraspinal connections and termination patterns of the parabrachial complex determined by the biocytin anterograde tract-tracing technique in the rat. J Anatomy. 193:417–430. doi:10.1046/j.1469-7580.1998.19330417.x.

Bigiani, A. **2001**. Mouse Taste Cells With Glialike Membrane Properties. Journal of Neurophysiology. 85:1552–1560. doi:10.1152/jn.2001.85.4.1552.

Bigiani, A., R. Cristiani, F. Fieni, V. Ghiaroni, P. Bagnoli, and P. Pietra. **2002**. Postnatal Development of Membrane Excitability in Taste Cells of the Mouse Vallate Papilla. J. Neurosci. 22:493–504. doi:10.1523/JNEUROSCI.22-02-00493.2002.

Bigiani, A., and V. Cuoghi. **2007**. Localization of Amiloride-Sensitive Sodium Current and Voltage-Gated Calcium Currents in Rat Fungiform Taste Cells. Journal of Neurophysiology. 98:2483–2487. doi:10.1152/jn.00716.2007.

Boccaccio, A., and A. Menini. **2007**. Temporal Development of Cyclic Nucleotide-Gated and Ca 2+ -Activated Cl − Currents in Isolated Mouse Olfactory Sensory Neurons. Journal of Neurophysiology. 98:153–160. doi:10.1152/jn.00270.2007.

Britschgi, A., A. Bill, H. Brinkhaus, C. Rothwell, I. Clay, S. Duss, M. Rebhan, P. Raman, C.T. Guy, K. Wetzel, E. George, M.O. Popa, S. Lilley, H. Choudhury, M. Gosling, L. Wang, S. Fitzgerald, J. Borawski, J. Baffoe, M. Labow, L.A. Gaither, and M. Bentires-Alj. **2013**. Calcium-activated chloride channel ANO1 promotes breast cancer progression by activating EGFR and CAMK signaling. Proc Natl Acad Sci USA. 110:E1026–E1034. doi:10.1073/pnas.1217072110.

Brunner, J.D., N.K. Lim, S. Schenck, A. Duerst, and R. Dutzler. **2014**. X-ray structure of a calcium-activated TMEM16 lipid scramblase. Nature. 516:207–212. doi:10.1038/nature13984.

Bushman, J.D., W. Ye, and E.R. Liman. **2015**. A proton current associated with sour taste: distribution and functional properties. FASEB j. 29:3014–3026. doi:10.1096/fj.14-265694.

Calvo SS, Egan JM. **2015**. The endocrinology of taste receptors. Nat Rev Endocrinol. 11(4):213-27. doi: 10.1038/nrendo.2015.7. Epub 2015 Feb 24.

Canessa CM, Schild L, Buell G, Thorens B, Gautschi I, Horisberger JD, Rossier BC. 1994. Amiloride-sensitive epithelial Na+ channel is made of three homologous subunits. Nature. 367(6462):463-7. doi: 10.1038/367463a0.

Caputo, A., E. Caci, L. Ferrera, N. Pedemonte, C. Barsanti, E. Sondo, U. Pfeffer, R. Ravazzolo, O. Zegarra-Moran, and L.J.V. Galietta. **2008**. TMEM16A, A Membrane Protein Associated with Calcium-Dependent Chloride Channel Activity. Science. 322:590–594. doi:10.1126/science.1163518.

Carpenter, G.H. **2013**. The Secretion, Components, and Properties of Saliva. Annu. Rev. Food Sci. Technol. 4:267–276. doi:10.1146/annurev-food-030212-182700.

Cavada, C. **2000**. The Anatomical Connections of the Macaque Monkey Orbitofrontal Cortex. A Review. Cerebral Cortex. 10:220–242. doi:10.1093/cercor/10.3.220.

Chandrashekar, J., C. Kuhn, Y. Oka, D.A. Yarmolinsky, E. Hummler, N.J.P. Ryba, and C.S. Zuker. **2010**. The cells and peripheral representation of sodium taste in mice. Nature. 464:297–301. doi:10.1038/nature08783.

Chang, R.B., H. Waters, and E.R. Liman. **2010**. A proton current drives action potentials in genetically identified sour taste cells. Proceedings of the National Academy of Sciences. 107:22320–22325. doi:10.1073/pnas.1013664107.

Chaudhari, N., A.M. Landin, and S.D. Roper. **2000**. A metabotropic glutamate receptor variant functions as a taste receptor. Nat Neurosci. 3:113–119. doi:10.1038/72053.

Chaudhari, N., E. Pereira, and S.D. Roper. **2009**. Taste receptors for umami: the case for multiple receptors. The American Journal of Clinical Nutrition. 90:738S-742S. doi:10.3945/ajcn.2009.27462H.

Chaudhari, N., and S.D. Roper. **2010**. The cell biology of taste. The Journal of Cell Biology. 190:285–296. doi:10.1083/jcb.201003144.

Chaudhary, F.A., K.P. Lehre, M. van Lookeren Campagne, O.P. Ottersen, N.C. Danbolt, and J. Storm-Mathisen. **1995**. Glutamate transporters in glial plasma membranes: Highly differentiated localizations revealed by quantitative ultrastructural immunocytochemistry. Neuron. 15:711–720. doi:10.1016/0896-6273(95)90158-2.

Chen, Y., X.D. Sun, and S. Herness. **1996**. Characteristics of action potentials and their underlying outward currents in rat taste receptor cells. Journal of Neurophysiology. 75:820–831. doi:10.1152/jn.1996.75.2.820.

Cherkashin AP, Kolesnikova AS, Tarasov MV, Romanov RA, Rogachevskaja OA, Bystrova MF & Kolesnikov SS. **2016**. Expression of calcium-activated chloride channels Ano1 and Ano2 in mouse taste cells. Pflugers Arch 468, 305–319.

Collier, M.L., P.C. Levesque, J.L. Kenyon, and J.R. Hume. **1996**. Unitary Cl − Channels Activated by Cytoplasmic Ca 2+ in Canine Ventricular Myocytes. Circulation Research. 78:936–944. doi:10.1161/01.RES.78.5.936.

Contreras, R.J., R.M. Beckstead, and R. Norgren. **1982**. The central projections of the trigeminal, facial, glossopharyngeal and vagus nerves: an autoradiographic study in the rat. Journal of the Autonomic Nervous System. 6:303–322. doi:10.1016/0165-1838(82)90003-0.

Corson, J., A. Aldridge, K. Wilmoth, and A. Erisir. **2012**. A survey of oral cavity afferents to the rat nucleus tractus solitarii. J. Comp. Neurol. 520:495–527. doi:10.1002/cne.22715.

Cui, M., P. Jiang, E. Maillet, M. Max, R. Margolskee, and R. Osman. **2006**. The Heterodimeric Sweet Taste Receptor has Multiple Potential Ligand Binding Sites. CPD. 12:4591–4600. doi:10.2174/138161206779010350.

Cuthbert, A. **2011**. New horizons in the treatment of cystic fibrosis: Drugs and CF. British Journal of Pharmacology. 163:173–183. doi:10.1111/j.1476-5381.2010.01137.x.

Damak S, Rong M, Yasumatsu K, Kokrashvili Z, Varadarajan V, Zou S, Jiang P, Ninomiya Y, Margolskee RF. Detection of sweet and umami taste in the absence of taste receptor T1r3. Science. **2003** Aug 8;301(5634):850-3. doi: 10.1126/science.1087155. Epub 2003 Jul 17.

Dando, R., and S.D. Roper. **2012**. Acetylcholine is released from taste cells, enhancing taste signalling: Acetylcholine release from taste cells. The Journal of Physiology. 590:3009–3017. doi:10.1113/jphysiol.2012.232009.

Davis, A.J., A.S. Forrest, T.A. Jepps, M.L. Valencik, M. Wiwchar, C.A. Singer, W.R. Sones, I.A. Greenwood, and N. Leblanc. **2010**. Expression profile and protein translation of TMEM16A in murine smooth muscle. American Journal of Physiology-Cell Physiology. 299:C948–C959. doi:10.1152/ajpcell.00018.2010.

De Castro, F., E. Geijo-Barrientos, and R. Gallego. **1997**. Calcium-activated chloride current in normal mouse sympathetic ganglion cells. The Journal of Physiology. 498:397–408. doi:10.1113/jphysiol.1997.sp021866.

DeFazio, R.A. **2006**. Separate Populations of Receptor Cells and Presynaptic Cells in Mouse Taste Buds. Journal of Neuroscience. 26:3971–3980. doi:10.1523/JNEUROSCI.0515-06.2006.

Delay, E.R., N.P. Hernandez, K. Bromley, and R.F. Margolskee. **2006**. Sucrose and Monosodium Glutamate Taste Thresholds and Discrimination Ability of T1R3 Knockout Mice. Chemical Senses. 31:351–357. doi:10.1093/chemse/bjj039.

Di Zanni, E., A. Gradogna, C. Picco, J. Scholz-Starke, and A. Boccaccio. **2020**. TMEM16E/ANO5 mutations related to bone dysplasia or muscular dystrophy cause opposite effects on lipid scrambling. Human Mutation. 41:1157–1170. doi:10.1002/humu.24006.

Dibattista, M., S. Pifferi, A. Boccaccio, A. Menini, and J. Reisert. **2017**. The long tale of the calcium activated Cl − channels in olfactory transduction. Channels. 11:399–414. doi:10.1080/19336950.2017.1307489.

Di Lorenzo PM, Monroe S.J Neurophysiol. **1995**. Corticofugal influence on taste responses in the nucleus of the solitary tract in the rat. 74(1):258-72. doi: 10.1152/jn.1995.74.1.258.

Doolin, R.E., and T.A. Gilbertson. **1996**. Distribution and characterization of functional amiloride-sensitive sodium channels in rat tongue. The Journal of General Physiology. 107:545–554. doi:10.1085/jgp.107.4.545.

Duran, C., Z. Qu, A.O. Osunkoya, Y. Cui, and H.C. Hartzell. **2012**. ANOs 3–7 in the anoctamin/Tmem16 Cl − channel family are intracellular proteins. American Journal of Physiology-Cell Physiology. 302:C482–C493. doi:10.1152/ajpcell.00140.2011.

Duvvuri, U., D.J. Shiwarski, D. Xiao, C. Bertrand, X. Huang, R.S. Edinger, J.R. Rock, B.D. Harfe, B.J. Henson, K. Kunzelmann, R. Schreiber, R.S. Seethala, A.M. Egloff, X. Chen, V.W. Lui, J.R. Grandis, and S.M. Gollin. **2012**. TMEM16A Induces MAPK and Contributes Directly to Tumorigenesis and Cancer Progression. Cancer Res. 72:3270–3281. doi:10.1158/0008-5472.CAN-12-0475-T.

Dvoryanchikov, G., Y.A. Huang, R. Barro-Soria, N. Chaudhari, and S.D. Roper. **2011**. GABA, Its Receptors, and GABAergic Inhibition in Mouse Taste Buds. Journal of Neuroscience. 31:5782–5791. doi:10.1523/JNEUROSCI.5559-10.2011.

Dvoryanchikov, G., M.S. Sinclair, I. Perea-Martinez, T. Wang, and N. Chaudhari. **2009**. Inward rectifier channel, ROMK, is localized to the apical tips of glial-like cells in mouse taste buds. J. Comp. Neurol. 517:1–14. doi:10.1002/cne.22152.

Elliott, E.J., and S.A. Simon. **1990**. The anion in salt taste: a possible role for paracellular pathways. Brain Research. 535:9–17. doi:10.1016/0006-8993(90)91817-Z.

Ferrera, L., A. Caputo, I. Ubby, E. Bussani, O. Zegarra-Moran, R. Ravazzolo, F. Pagani, and L.J.V. Galietta. **2009**. Regulation of TMEM16A Chloride Channel Properties by Alternative Splicing. Journal of Biological Chemistry. 284:33360–33368. doi:10.1074/jbc.M109.046607.

Finger, T.E. **2005**. ATP Signaling Is Crucial for Communication from Taste Buds to Gustatory Nerves. Science. 310:1495–1499. doi:10.1126/science.1118435.

Frank, M. **1973**. An Analysis of Hamster Afferent Taste Nerve Response Functions. Journal of General Physiology. 61:588–618. doi:10.1085/jgp.61.5.588.

Fu, W., T. Sugai, H. Yoshimura, and N. Onoda. **2004**. Convergence of olfactory and gustatory connections onto the endopiriform nucleus in the rat. Neuroscience. 126:1033–1041. doi:10.1016/j.neuroscience.2004.03.041.

Fujita, S., K. Adachi, N. Koshikawa, and M. Kobayashi. **2010**. Spatiotemporal dynamics of excitation in rat insular cortex: intrinsic corticocortical circuit regulates caudal-rostro excitatory propagation from the insular to frontal cortex. Neuroscience. 165:278–292. doi:10.1016/j.neuroscience.2009.09.073.

Furness, D.N., and K.P. Lehre. **1997**. Immunocytochemical Localization of a High-affinity Glutamate-Aspartate Transporter, GLAST, in the Rat and Guinea-pig Cochlea. European Journal of Neuroscience. 9:1961–1969. doi:10.1111/j.1460-9568.1997.tb00763.x.

Gabbott, P.L.A., T.A. Warner, P.R.L. Jays, and S.J. Bacon. **2003**. Areal and synaptic interconnectivity of prelimbic (area 32), infralimbic (area 25) and insular cortices in the rat. Brain Research. 993:59–71. doi:10.1016/j.brainres.2003.08.056.

Gao, N., M. Lu, F. Echeverri, B. Laita, D. Kalabat, M.E. Williams, P. Hevezi, A. Zlotnik, and B.D. Moyer. **2009**. Voltage-gated sodium channels in taste bud cells. BMC Neurosci. 10:20. doi:10.1186/1471-2202-10-20.

Gardner, A., and G.H. Carpenter. **2019**. Anatomical stability of human fungiform papillae and relationship with oral perception measured by salivary response and intensity rating. Sci Rep. 9:9759. doi:10.1038/s41598-019-46093-z.

Ghiaroni V, Fieni F, Pietra P, Bigiani A. **2003**. Electrophysiological heterogeneity in a functional subset of mouse taste cells during postnatal development. Chem Senses. 28(9):827-33. doi: 10.1093/chemse/bjg076.

Gomez-Pinilla, P.J., S.J. Gibbons, M.R. Bardsley, A. Lorincz, M.J. Pozo, P.J. Pasricha, M.V. de Rijn, R.B. West, M.G. Sarr, M.L. Kendrick, R.R. Cima, E.J. Dozois, D.W. Larson, T. Ordog, and G. Farrugia. **2009**. Ano1 is a selective marker of interstitial cells of Cajal in the human and mouse gastrointestinal tract. American Journal of Physiology-Gastrointestinal and Liver Physiology. 296:G1370–G1381. doi:10.1152/ajpgi.00074.2009.

Gray, M.A., J.P. Winpenny, B. Verdon, H. McAlroy, and B.E. Argent. **1995**. Chloride channels and cystic fibrosis of the pancreas. Bioscience Reports. 15:531–541. doi:10.1007/BF01204355.

Halpern, B.P. **1998**. Amiloride and vertebrate gustatory responses to NaCl. Neuroscience & Biobehavioral Reviews. 23:5–47. doi:10.1016/S0149-7634(97)00063-8.

Hamilton, R.B., and R. Norgren. **1984**. Central projections of gustatory nerves in the rat. J. Comp. Neurol. 222:560–577. doi:10.1002/cne.902220408.

Hartzell, C., I. Putzier, and J. Arreola. **2005**. CALCIUM-ACTIVATED CHLORIDE CHANNELS. Annu. Rev. Physiol. 67:719–758. doi:10.1146/annurev.physiol.67.032003.154341.

Hartzell, H.C., K. Yu, Q. Xiao, L.-T. Chien, and Z. Qu. **2009**. Anoctamin/TMEM16 family members are Ca 2+ -activated Cl − channels: Anoctamin/TMEM16 family members are Ca 2+ -activated Cl − channels. The Journal of Physiology. 587:2127–2139. doi:10.1113/jphysiol.2008.163709.

Heck, G., S. Mierson, and J. DeSimone. **1984**. Salt taste transduction occurs through an amiloride-sensitive sodium transport pathway. Science. 223:403–405. doi:10.1126/science.6691151.

Helm, J.F., W.J. Dodds, W.J. Hogan, K.H. Soergel, M.S. Egide, and C.M. Wood. **1982**. Acid Neutralizing Capacity of Human Saliva. Gastroenterology. 83:69–74. doi:10.1016/S0016-5085(82)80286-2.

Henriques, T., E. Agostinelli, A. Hernandez-Clavijo, D.K. Maurya, J.R. Rock, B.D. Harfe, A. Menini, and S. Pifferi. **2019**. TMEM16A calcium-activated chloride currents in supporting cells of the mouse olfactory epithelium. Journal of General Physiology. 151:954–966. doi:10.1085/jgp.201812310.

Herness, M.S., and X.-D. Sun. **1999**. Characterization of Chloride Currents and Their Noradrenergic Modulation in Rat Taste Receptor Cells. Journal of Neurophysiology. 82:260–271. doi:10.1152/jn.1999.82.1.260.

Holtz, S.L., A. Fu, W. Loflin, J.A. Corson, and A. Erisir. **2015**. Morphology and connectivity of parabrachial and cortical inputs to gustatory thalamus in rats: Gustatory thalamic circuitry. J. Comp. Neurol. 523:139–161. doi:10.1002/cne.23673.

Horio N, Yoshida R, Yasumatsu K, Yanagawa Y, Ishimaru Y, Matsunami H, Ninomiya Y. **2011**. Sour taste responses in mice lacking PKD channels. PLoS One.; 6(5):e20007. doi: 10.1371/journal.pone.0020007.

Huang, A.L., X. Chen, M.A. Hoon, J. Chandrashekar, W. Guo, D. Tränkner, N.J.P. Ryba, and C.S. Zuker. **2006a**. The cells and logic for mammalian sour taste detection. Nature. 442:934–938. doi:10.1038/nature05084.

Huang, F., J.R. Rock, B.D. Harfe, T. Cheng, X. Huang, Y.N. Jan, and L.Y. Jan. **2009a**. Studies on expression and function of the TMEM16A calcium-activated chloride channel. PNAS. 106:21413–21418. doi:10.1073/pnas.0911935106.

Huang, F., X. Wang, E.M. Ostertag, T. Nuwal, B. Huang, Y.-N. Jan, A.I. Basbaum, and L.Y. Jan. **2013**. TMEM16C facilitates Na+-activated K+ currents in rat sensory neurons and regulates pain processing. nature NEUROSCIENCE. 16:9.

Huang, F., X. Wong, and L.Y. Jan. **2012a**. International Union of Basic and Clinical Pharmacology. LXXXV: Calcium-Activated Chloride Channels. Pharmacol Rev. 64:1–15. doi:10.1124/pr.111.005009.

Huang, W.C., S. Xiao, F. Huang, B.D. Harfe, Y.N. Jan, and L.Y. Jan. **2012b**. Calcium-Activated Chloride Channels (CaCCs) Regulate Action Potential and Synaptic Response in Hippocampal Neurons. Neuron. 74:179–192. doi:10.1016/j.neuron.2012.01.033.

Huang X, Godfrey TE, Gooding WE, McCarty KS Jr, Gollin SM. **2006b**. Comprehensive genome and transcriptome analysis of the 11q13 amplicon in human oral cancer and synteny to the 7F5 amplicon in murine oral carcinoma. Genes Chromosomes Cancer. 45(11):1058-69. doi: 10.1002/gcc.20371.

Huang, Y.A., R. Dando, and S.D. Roper. **2009b**. Autocrine and Paracrine Roles for ATP and Serotonin in Mouse Taste Buds. Journal of Neuroscience. 29:13909–13918. doi:10.1523/JNEUROSCI.2351-09.2009.

Huang, Y.A., Y. Maruyama, and S.D. Roper. **2008a**. Norepinephrine Is Coreleased with Serotonin in Mouse Taste Buds. Journal of Neuroscience. 28:13088–13093. doi:10.1523/JNEUROSCI.4187-08.2008.

Huang, Y.A., Y. Maruyama, R. Stimac, and S.D. Roper. **2008b**. Presynaptic (Type III) cells in mouse taste buds sense sour (acid) taste: Sour taste mechanisms in mouse taste buds. The Journal of Physiology. 586:2903–2912. doi:10.1113/jphysiol.2008.151233.

Huang, Y.A., E. Pereira, and S.D. Roper. **2011a**. Acid Stimulation (Sour Taste) Elicits GABA and Serotonin Release from Mouse Taste Cells. PLoS ONE. 6:e25471. doi:10.1371/journal.pone.0025471.

Huang, Y.A., L.M. Stone, E. Pereira, R. Yang, J.C. Kinnamon, G. Dvoryanchikov, N. Chaudhari, T.E. Finger, S.C. Kinnamon, and S.D. Roper. **2011b**. Knocking Out P2X Receptors Reduces Transmitter Secretion in Taste Buds. Journal of Neuroscience. 31:13654–13661. doi:10.1523/JNEUROSCI.3356-11.2011.

Huang, Y.-J. **2005**. Mouse Taste Buds Use Serotonin as a Neurotransmitter. Journal of Neuroscience. 25:843–847. doi:10.1523/JNEUROSCI.4446-04.2005.

Humphrey, S.P., and R.T. Williamson. **2001**. A review of saliva: Normal composition, flow, and function. The Journal of Prosthetic Dentistry. 85:162–169. doi:10.1067/mpr.2001.113778.

Hwang, D.G., X. Qian, and J.L. Hornick. **2011**. DOG1 Antibody Is a Highly Sensitive and Specific Marker for Gastrointestinal Stromal Tumors in Cytology Cell Blocks. American Journal of Clinical Pathology. 135:448–453. doi:10.1309/AJCP0PPKOBNDT9LB.

Ikeda, K. **1909**. College of Science, Imperial University of Tokyo, Tokyo, Japan. 3.

Ishimaru Y, Matsunami H. J Dent Res. **2009**. Transient receptor potential (TRP) channels and taste sensation. 88(3):212-8. doi: 10.1177/0022034508330212.

Jaffe LA, Cross NL. **1986**. Electrical regulation of sperm-egg fusion. Annu Rev Physiol. 48:191-200. doi: 10.1146/annurev.ph.48.030186.001203.

Jung, H.-S., K. Akita, and J.-Y. Kim. **2004**. Spacing patterns on tongue surface-gustatory papilla. Int. J. Dev. Biol. 48:157–161. doi:10.1387/ijdb.15272380.

Kataoka S, Yang R, Ishimaru Y, Matsunami H, Sévigny J, Kinnamon JC, Finger TE. **2008**. The candidate sour taste receptor, PKD2L1, is expressed by type III taste cells in the mouse. Chem Senses. 33(3):243-54. doi: 10.1093/chemse/bjm083.

Katoh M, Katoh M. **2003**. FLJ10261 gene, located within the CCND1-EMS1 locus on human chromosome 11q13, encodes the eight-transmembrane protein homologous to C12orf3, C11orf25 and FLJ34272 gene products. Int J Oncol. 22(6):1375-81.

Kawano, S., Y. Hirayama, and M. Hiraoka. **1995**. Activation mechanism of Ca(2+)-sensitive transient outward current in rabbit ventricular myocytes. The Journal of Physiology. 486:593–604. doi:10.1113/jphysiol.1995.sp020837.

Kawasaki, K., T. Porntaveetus, S. Oommen, S. Ghafoor, M. Kawasaki, Y. Otsuka-Tanaka, J. Blackburn, J.A. Kessler, P.T. Sharpe, and A. Ohazama. **2012**. Bmp signalling in filiform tongue papillae development. Archives of Oral Biology. 57:805–813. doi:10.1016/j.archoralbio.2011.11.014.

Kim YV, Bobkov YV & Kolesnikov SS. **2000**. Adenosine triphosphate mobilizes cytosolic calcium and modulates ionic currents in mouse taste receptor cells. Neurosci Lett 290, 165–168.

Kinnamon, S.C., and T.E. Finger. **2019**. Recent advances in taste transduction and signaling. F1000Res. 8:2117. doi:10.12688/f1000research.21099.1.

Kosar, E., H.J. Grill, and R. Norgren. **1986**. Gustatory cortex in the rat. II. Thalamocortical projections. Brain Research. 379:342–352. doi:10.1016/0006-8993(86)90788-2.

Kumazawa, T., and K. Kurihara. **1990**. Large enhancement of canine taste responses to sugars by salts. The Journal of General Physiology. 95:1007–1018. doi:10.1085/jgp.95.5.1007.

Kurahashi, T., and K.-W. Yau. **1994**. Olfactory Transduction: Tale of an unusual chloride current. Current Biology. 4:256–258. doi:10.1016/S0960-9822(00)00058-0.

Kuruma, A., and H.C. Hartzell. **1999**. Dynamics of calcium regulation of chloride currents in Xenopus oocytes. American Journal of Physiology-Cell Physiology. 276:C161–C175. doi:10.1152/ajpcell.1999.276.1.C161.

Kusuhara, Y., R. Yoshida, T. Ohkuri, K. Yasumatsu, A. Voigt, S. Hübner, K. Maeda, U. Boehm, W. Meyerhof, and Y. Ninomiya. **2013**. Taste responses in mice lacking taste receptor subunit T1R1: Role of taste receptor subunit T1R1 in taste detection. The Journal of Physiology. 591:1967–1985. doi:10.1113/jphysiol.2012.236604.

Larson, E.D., A. Vandenbeuch, C.B. Anderson, and S.C. Kinnamon. **2020**. Function, Innervation, and Neurotransmitter Signaling in Mice Lacking Type-II Taste Cells. eNeuro. 7:ENEURO.0339-19.2020. doi:10.1523/ENEURO.0339-19.2020.

Larson ED, Vandenbeuch A, Voigt A, Meyerhof W, Kinnamon SC, Finger TE. **2015**. The Role of 5-HT3 Receptors in Signaling from Taste Buds to Nerves. J Neurosci. 35(48):15984-95. doi: 10.1523/JNEUROSCI.1868-15.2015.

Le, S.C., Z. Jia, J. Chen, and H. Yang. **2019**. Molecular basis of PIP2-dependent regulation of the Ca2+-activated chloride channel TMEM16A. Nat Commun. 10:3769. doi:10.1038/s41467-019-11784-8.

Lehre, K.P., S. Davanger, and N.C. Danbolt. **1997**. Localization of the glutamate transporter protein GLAST in rat retina. Brain Research. 744:129–137. doi:10.1016/S0006-8993(96)01022-0.

Lewandowski, B.C., S.K. Sukumaran, R.F. Margolskee, and A.A. Bachmanov. **2016**. Amiloride-Insensitive Salt Taste Is Mediated by Two Populations of Type III Taste Cells with Distinct Transduction Mechanisms. J. Neurosci. 36:1942–1953. doi:10.1523/JNEUROSCI.2947-15.2016.

Liman, E.R., Y.V. Zhang, and C. Montell. **2014**. Peripheral Coding of Taste. Neuron. 81:984–1000. doi:10.1016/j.neuron.2014.02.022.

Lindemann, B. **2001**. Receptors and transduction in taste. Nature. 413:219–225. doi:10.1038/35093032.

Linster, C., and A. Fontanini. **2014**. Functional neuromodulation of chemosensation in vertebrates. Current Opinion in Neurobiology. 29:82–87. doi:10.1016/j.conb.2014.05.010.

Liu, D., and E.R. Liman. **2003**. Intracellular Ca2+ and the phospholipid PIP2 regulate the taste transduction ion channel TRPM5. Proceedings of the National Academy of Sciences. 100:15160–15165. doi:10.1073/pnas.2334159100.

Liu, H.C., and J.C. Lee. **1982**. Scanning Electron Microscopic and Histochemical Studies of Foliate Papillae in the Rabbit, Rat and Mouse. Acta Anatomica. 112:310–320. doi:10.1159/000145524.

Liu Y, Zhang H, Huang D, Qi J, Xu J, Gao H, Du X, Gamper N, Zhang H. **2015**. Characterization of the effects of Cl- channel modulators on TMEM16A and bestrophin-1 Ca2+ activated Cl- channels. Pflugers Arch. 467(7):1417-1430. doi: 10.1007/s00424-014-1572-5. Epub 2014 Aug 1.

Lossow K, Hermans-Borgmeyer I, Meyerhof W, Behrens M. **2020**. Segregated Expression of ENaC Subunits in Taste Cells. Chem Senses. 45(4):235-248. doi: 10.1093/chemse/bjaa004.

Lundy, R.F., and R. Norgren. **2004**. Activity in the Hypothalamus, Amygdala, and Cortex Generates Bilateral and Convergent Modulation of Pontine Gustatory Neurons. Journal of Neurophysiology. 91:1143–1157. doi:10.1152/jn.00840.2003.

Ma, Z., A. Taruno, M. Ohmoto, M. Jyotaki, J.C. Lim, H. Miyazaki, N. Niisato, Y. Marunaka, R.J. Lee, H. Hoff, R. Payne, A. Demuro, I. Parker, C.H. Mitchell, J. Henao-Mejia, J.E. Tanis, I. Matsumoto, M.G. Tordoff, and J.K. Foskett. **2018**. CALHM3 Is Essential for Rapid Ion Channel-Mediated Purinergic Neurotransmission of GPCR-Mediated Tastes. Neuron. 98:547-561.e10. doi:10.1016/j.neuron.2018.03.043.

Maffei, A., M. Haley, and A. Fontanini. **2012**. Neural processing of gustatory information in insular circuits. Current Opinion in Neurobiology. 22:709–716. doi:10.1016/j.conb.2012.04.001.

Margolskee, R.F., J. Dyer, Z. Kokrashvili, K.S.H. Salmon, E. Ilegems, K. Daly, E.L. Maillet, Y. Ninomiya, B. Mosinger, and S.P. Shirazi-Beechey. **2007**. T1R3 and gustducin in gut sense sugars to regulate expression of Na+-glucose cotransporter 1. Proceedings of the National Academy of Sciences. 104:15075–15080. doi:10.1073/pnas.0706678104.

Matsuo, R. **2000**. Role of Saliva in the Maintenance of Taste Sensitivity. Critical Reviews in Oral Biology & Medicine. 11:216–229. doi:10.1177/10454411000110020501.

Maurya, D.K., T. Henriques, M. Marini, N. Pedemonte, L.J.V. Galietta, J.R. Rock, B.D. Harfe, and A. Menini. **2015**. Development of the Olfactory Epithelium and Nasal Glands in TMEM16A-/- and TMEM16A+/+ Mice. PLoS ONE. 10:e0129171. doi:10.1371/journal.pone.0129171.

McBride DW Jr, Roper SD. **1991**. Ca(2+)-dependent chloride conductance in Necturus taste cells. J Membr Biol. 124(1):85-93. doi: 10.1007/BF01871367.

McBurney, D.H., and C. Pfaffmann. **1963**. Gustatory adaptation to saliva and sodium chloride. Journal of Experimental Psychology. 65:523–529. doi:10.1037/h0047573.

Medler, K.F., R.F. Margolskee, and S.C. Kinnamon. **2003**. Electrophysiological Characterization of Voltage-Gated Currents in Defined Taste Cell Types of Mice. J. Neurosci. 23:2608–2617. doi:10.1523/JNEUROSCI.23-07-02608.2003.

Mehansho H, Butler LG, Carlson DM. **1987**. Dietary tannins and salivary proline-rich proteins: interactions, induction, and defense mechanisms. Annu Rev Nutr. 7:423-40. doi: 10.1146/annurev.nu.07.070187.002231.

Merigo, F., D. Benati, M. Cristofoletti, F. Osculati, and A. Sbarbati. **2011**. Glucose transporters are expressed in taste receptor cells: Glucose transporters are expressed in TRCs. Journal of Anatomy. 219:243–252. doi:10.1111/j.1469-7580.2011.01385.x.

Meyerhof, W., C. Batram, C. Kuhn, A. Brockhoff, E. Chudoba, B. Bufe, G. Appendino, and M. Behrens. **2010**. The Molecular Receptive Ranges of Human TAS2R Bitter Taste Receptors. Chemical Senses. 35:157–170. doi:10.1093/chemse/bjp092.

Michlig, S., S. Damak, and J. Le Coutre. **2007**. Claudin-based permeability barriers in taste buds. J. Comp. Neurol. 502:1003–1011. doi:10.1002/cne.21354.

Milenkovic, V.M., M. Brockmann, H. Stöhr, B.H. Weber, and O. Strauss. **2010**. Evolution and functional divergence of the anoctamin family of membrane proteins. BMC Evol Biol. 10:319. doi:10.1186/1471-2148-10-319.

Mizuta, K., S. Tsutsumi, H. Inoue, Y. Sakamoto, K. Miyatake, K. Miyawaki, S. Noji, N. Kamata, and M. Itakura. **2007**. Molecular characterization of GDD1/TMEM16E, the gene product responsible for autosomal dominant gnathodiaphyseal dysplasia. Biochemical and Biophysical Research Communications. 357:126–132. doi:10.1016/j.bbrc.2007.03.108.

Mufson, E.J., and M.-M. Mesulam. **1982**. Insula of the old world monkey. II: Afferent cortical input and comments on the claustrum. J. Comp. Neurol. 212:23–37. doi:10.1002/cne.902120103.

Murray, N.J., M.P. Williamson, T.H. Lilley, and E. Haslam. **1994**. Study of the interaction between salivary proline-rich proteins and a polyphenol by 1H-NMR spectroscopy. Eur J Biochem. 219:923–935. doi:10.1111/j.1432-1033.1994.tb18574.x.

Murray, R.G. **1993**. Cellular relations in mouse circumvallate taste buds. Microsc. Res. Tech. 26:209–224. doi:10.1002/jemt.1070260304.

Nelson, G., J. Chandrashekar, M.A. Hoon, L. Feng, G. Zhao, N.J.P. Ryba, and C.S. Zuker. **2002**. An amino-acid taste receptor. Nature. 416:199–202. doi:10.1038/nature726.

Nelson, G., M.A. Hoon, J. Chandrashekar, Y. Zhang, N.J.P. Ryba, and C.S. Zuker. **2001**. Mammalian Sweet Taste Receptors. Cell. 106:381–390. doi:10.1016/S0092-8674(01)00451-2.

Nelson, M.T., M.A. Conway, H.J. Knot, and J.E. Brayden. **1997**. Chloride channel blockers inhibit myogenic tone in rat cerebral arteries. The Journal of Physiology. 502:259–264. doi:10.1111/j.1469-7793.1997.259bk.x.

Nilius, B., J. Prenen, G. Szücs, L. Wei, F. Tanzi, T. Voets, and G. Droogmans. **1997**. Calcium-activated chloride channels in bovine pulmonary artery endothelial cells. The Journal of Physiology. 498:381–396. doi:10.1113/jphysiol.1997.sp021865.

Ninomiya, Y. **1998**. Reinnervation of cross-regenerated gustatory nerve fibers into amiloride-sensitive and amiloride-insensitive taste receptor cells. Proceedings of the National Academy of Sciences. 95:5347–5350. doi:10.1073/pnas.95.9.5347.

Noguchi, T., Y. Ikeda, M. Miyajima, and K. Yoshii. **2003**. Voltage-gated channels involved in taste responses and characterizing taste bud cells in mouse soft palates. Brain Research. 982:241–259. doi:10.1016/S0006-8993(03)03013-0.

Nomura, K., M. Nakanishi, F. Ishidate, K. Iwata, and A. Taruno. **2020**. All-Electrical Ca2+-Independent Signal Transduction Mediates Attractive Sodium Taste in Taste Buds. Neuron. S0896627320301926. doi:10.1016/j.neuron.2020.03.006.

Norris, M.B., A.C. Noble, and R.M. Pangborn. **1984**. Human saliva and taste responses to acids varying in anions, titratable acidity, and pH. Physiology & Behavior. 32:237–244. doi:10.1016/0031-9384(84)90136-7.

Oh, U., and J. Jung. **2016**. Cellular functions of TMEM16/anoctamin. Pflugers Arch - Eur J Physiol. 468:443–453. doi:10.1007/s00424-016-1790-0.

Oka, Y., M. Butnaru, L. von Buchholtz, N.J.P. Ryba, and C.S. Zuker. **2013**. High salt recruits aversive taste pathways. Nature. 494:472–475. doi:10.1038/nature11905.

Ossebaard CA, Smith DV. **1996**. Amiloride suppresses the sourness of NaCl and LiCl. Physiol Behav. Nov;60(5):1317-22. doi: 10.1016/s0031-9384(96)00258-2.

Paran, N., and C.F.T. Mattern. **1975**. The distribution of acetylcholinesterase in buds of the rat vallate papilla as determined by electron microscope histochemistry. J. Comp. Neurol. 159:29–43. doi:10.1002/cne.901590104.

Paulino, C., V. Kalienkova, A.K.M. Lam, Y. Neldner, and R. Dutzler. **2017**. Activation mechanism of the calcium-activated chloride channel TMEM16A revealed by cryo-EM. Nature. 552:421–425. doi:10.1038/nature24652.

Pedemonte, N., and L.J.V. Galietta. **2014**. Structure and Function of TMEM16 Proteins (Anoctamins). Physiological Reviews. 94:419–459. doi:10.1152/physrev.00039.2011.

Pietra, G., M. Dibattista, A. Menini, J. Reisert, and A. Boccaccio. **2016**. The Ca2+-activated Cl− channel TMEM16B regulates action potential firing and axonal targeting in olfactory sensory neurons. Journal of General Physiology. 148:293–311. doi:10.1085/jgp.201611622.

Pifferi, S., M. Dibattista, and A. Menini. **2009**. TMEM16B induces chloride currents activated by calcium in mammalian cells. Pflugers Arch - Eur J Physiol. 458:1023–1038. doi:10.1007/s00424-009-0684-9.

Pin, J.-P., T. Galvez, and L. Prézeau. **2003**. Evolution, structure, and activation mechanism of family 3/C G-protein-coupled receptors. Pharmacology & Therapeutics. 98:325–354. doi:10.1016/S0163-7258(03)00038-X.

Pumplin DW, Yu C, Smith DV. **1997.** Light and dark cells of rat vallate taste buds are morphologically distinct cell types. J Comp Neurol. 378(3):389-410. doi: 10.1002/(sici)1096-9861(19970217)378:3<389::aid-cne7>3.0.co;2-#.

Richter, T.A., A. Caicedo, and S.D. Roper. **2003**. Sour Taste Stimuli Evoke Ca 2+ and pH Responses in Mouse Taste Cells. The Journal of Physiology. 547:475–483. doi:10.1113/jphysiol.2002.033811.

Rock, J.R., C.R. Futtner, and B.D. Harfe. **2008**. The transmembrane protein TMEM16A is required for normal development of the murine trachea. Developmental Biology. 321:141–149. doi:10.1016/j.ydbio.2008.06.009.

Rock, J.R., W.K. O'Neal, S.E. Gabriel, S.H. Randell, B.D. Harfe, R.C. Boucher, and B.R. Grubb. **2009**. Transmembrane Protein 16A (TMEM16A) Is a Ca2+-regulated Cl– Secretory Channel in Mouse Airways. Journal of Biological Chemistry. 284:14875–14880. doi:10.1074/jbc.C109.000869.

Roebber, J.K., S.D. Roper, and N. Chaudhari. **2019**. The Role of the Anion in Salt (NaCl) Detection by Mouse Taste Buds. J. Neurosci. 39:6224–6232. doi:10.1523/JNEUROSCI.2367-18.2019.

Rolls ET. **1989**. Information processing in the taste system of primates. J Exp Biol. 146:141-64.

Romanenko, V.G., M.A. Catalán, D.A. Brown, I. Putzier, H.C. Hartzell, A.D. Marmorstein, M. Gonzalez-Begne, J.R. Rock, B.D. Harfe, and J.E. Melvin. **2010**. Tmem16A Encodes the Ca2+-activated Cl− Channel in Mouse Submandibular Salivary Gland Acinar Cells. Journal of Biological Chemistry. 285:12990–13001. doi:10.1074/jbc.M109.068544.

Romanov, R.A., and S.S. Kolesnikov. **2006**. Electrophysiologically identified subpopulations of taste bud cells. Neuroscience Letters. 395:249–254. doi:10.1016/j.neulet.2005.10.085.

Romanov, R.A., R.S. Lasher, B. High, L.E. Savidge, A. Lawson, O.A. Rogachevskaja, H. Zhao, V.V. Rogachevsky, M.F. Bystrova, G.D. Churbanov, I. Adameyko, T. Harkany, R. Yang, G.J. Kidd, P. Marambaud, J.C. Kinnamon, S.S. Kolesnikov, and T.E. Finger. **2018**. Chemical synapses without synaptic vesicles: Purinergic neurotransmission through a CALHM1 channel-mitochondrial signaling complex. Sci. Signal. 11:eaao1815. doi:10.1126/scisignal.aao1815.

Roper, S.D. **2007**. Signal transduction and information processing in mammalian taste buds. Pflugers Arch - Eur J Physiol. 454:759–776. doi:10.1007/s00424-007-0247-x.

Roper, S.D., and N. Chaudhari. **2017**. Taste buds: cells, signals and synapses. Nat Rev Neurosci. 18:485–497. doi:10.1038/nrn.2017.68.

Rössler, P., C. Kroner, J. Freitag, J. Noè, and H. Breer. **1998**. Identification of a phospholipase C β subtype in rat taste cells. European Journal of Cell Biology. 77:253–261. doi:10.1016/S0171-9335(98)80114-3.

Sainz, E., M.M. Cavenagh, J. Gutierrez, J.F. Battey, J.K. Northup, and S.L. Sullivan. **2007**. Functional characterization of human bitter taste receptors. Biochemical Journal. 403:537–543. doi:10.1042/BJ20061744.

Saleh, S.N., and I.A. Greenwood. **2005**. Activation of chloride currents in murine portal vein smooth muscle cells by membrane depolarization involves intracellular calcium release. American Journal of Physiology-Cell Physiology. 288:C122–C131. doi:10.1152/ajpcell.00384.2004.

Salzer, I., and S. Boehm. **2019**. Calcium-activated chloride channels: Potential targets for antinociceptive therapy. The International Journal of Biochemistry & Cell Biology. 111:37–41. doi:10.1016/j.biocel.2019.04.006.

San Gabriel, A., T. Maekawa, H. Uneyama, and K. Torii. **2009**. Metabotropic glutamate receptor type 1 in taste tissue. The American Journal of Clinical Nutrition. 90:743S-746S. doi:10.3945/ajcn.2009.27462I.

Saotome, K., B. Teng, C.C. Tsui, W.-H. Lee, Y.-H. Tu, J.P. Kaplan, M.S.P. Sansom, E.R. Liman, and A.B. Ward. **2019**. Structures of the otopetrin proton channels Otop1 and Otop3. Nat Struct Mol Biol. 26:518–525. doi:10.1038/s41594-019-0235-9.

Saper, C.B. **1982**. Convergence of autonomic and limbic connections in the insular cortex of the rat. J. Comp. Neurol. 210:163–173. doi:10.1002/cne.902100207.

Shepherd, G.M. **2006**. Smell images and the flavour system in the human brain. Nature. 444:316–321. doi:10.1038/nature05405.

Schreiber, R., I. Uliyakina, P. Kongsuphol, R. Warth, M. Mirza, J.R. Martins, and K. Kunzelmann. **2010**. Expression and Function of Epithelial Anoctamins. Journal of Biological Chemistry. 285:7838–7845. doi:10.1074/jbc.M109.065367.

Schroeder, B.C., T. Cheng, Y.N. Jan, and L.Y. Jan. **2008**. Expression Cloning of TMEM16A as a Calcium-Activated Chloride Channel Subunit. Cell. 134:1019–1029. doi:10.1016/j.cell.2008.09.003.

Seo, Y., H.K. Lee, J. Park, D. Jeon, S. Jo, M. Jo, and W. Namkung. **2016**. Ani9, A Novel Potent Small-Molecule ANO1 Inhibitor with Negligible Effect on ANO2. PLoS ONE. 11:e0155771. doi:10.1371/journal.pone.0155771.

Shi CJ, Cassell MD. **1998**. Cortical, thalamic, and amygdaloid connections of the anterior and posterior insular cortices. J Comp Neurol. 399(4):440-68. doi: 10.1002/(sici)1096-9861(19981005)399:4<440::aid-cne2>3.0.co;2-1.

Shipley, M.T. **1982**. Insular cortex projection to the nucleus of the solitary tract and brainstem visceromotor regions in the mouse. Brain Research Bulletin. 8:139–148. doi:10.1016/0361-9230(82)90040-5.

Shipley MT, Geinisman Y. Brain Res Bull. **1984** Mar; Anatomical evidence for convergence of olfactory, gustatory, and visceral afferent pathways in mouse cerebral cortex. 12(3):221-6. doi: 10.1016/0361-9230(84)90049-2.

Simon, S., F. Grabellus, L. Ferrera, L. Galietta, B. Schwindenhammer, T. Mühlenberg, G. Taeger, G. Eilers, J. Treckmann, F. Breitenbuecher, M. Schuler, T. Taguchi, J.A. Fletcher, and S. Bauer. **2013**. DOG1 Regulates Growth and IGFBP5 in Gastrointestinal Stromal Tumors. Cancer Res. 73:3661–3670. doi:10.1158/0008-5472.CAN-12-3839.

Stephan, A.B., E.Y. Shum, S. Hirsh, K.D. Cygnar, J. Reisert, and H. Zhao. **2009**. ANO2 is the cilial calcium-activated chloride channel that may mediate olfactory amplification. PNAS. 106:11776–11781. doi:10.1073/pnas.0903304106.

Stohr, H., J.B. Heisig, P.M. Benz, S. Schoberl, V.M. Milenkovic, O. Strauss, W.M. Aartsen, J. Wijnholds, B.H.F. Weber, and H.L. Schulz. **2009**. TMEM16B, A Novel Protein with Calcium-Dependent Chloride Channel Activity, Associates with a Presynaptic Protein Complex in Photoreceptor Terminals. Journal of Neuroscience. 29:6809–6818. doi:10.1523/JNEUROSCI.5546-08.2009.

Storck, T., S. Schulte, K. Hofmann, and W. Stoffel. **1992**. Structure, expression, and functional analysis of a Na(+)-dependent glutamate/aspartate transporter from rat brain. Proceedings of the National Academy of Sciences. 89:10955–10959. doi:10.1073/pnas.89.22.10955.

Suzuki, J., T. Fujii, T. Imao, K. Ishihara, H. Kuba, and S. Nagata. **2013**. Calcium-dependent Phospholipid Scramblase Activity of TMEM16 Protein Family Members. Journal of Biological Chemistry. 288:13305–13316. doi:10.1074/jbc.M113.457937.

Takumi, Y., A. Matsubara, N.C. Danbolt, J.H. Laake, J. Storm-Mathisen, S. Usami, H. Shinkawa, and O.P. Ottersen. **1997**. Discrete cellular and subcellular localization of glutamine synthetase and the glutamate transporter GLAST in the rat vestibular end organ. Neuroscience. 79:1137–1144. doi:10.1016/S0306-4522(97)00025-0.

Tarran, R., M.E. Loewen, A.M. Paradiso, J.C. Olsen, M.A. Gray, B.E. Argent, R.C. Boucher, and S.E. Gabriel. **2002**. Regulation of Murine Airway Surface Liquid Volume by CFTR and Ca2+-activated Cl− Conductances. Journal of General Physiology. 120:407–418. doi:10.1085/jgp.20028599.

Taruno, A., V. Vingtdeux, M. Ohmoto, Z. Ma, G. Dvoryanchikov, A. Li, L. Adrien, H. Zhao, S. Leung, M. Abernethy, J. Koppel, P. Davies, M.M. Civan, N. Chaudhari, I. Matsumoto, G. Hellekant, M.G. Tordoff, P. Marambaud, and J.K. Foskett. **2013**. CALHM1 ion channel mediates purinergic neurotransmission of sweet, bitter and umami tastes. Nature. 495:223–226. doi:10.1038/nature11906.

Taylor, R., and S. Roper. **1994**. Ca(2+)-dependent Cl- conductance in taste cells from Necturus. Journal of Neurophysiology. 72:475–478. doi:10.1152/jn.1994.72.1.475.

Teng, B., C.E. Wilson, Y.-H. Tu, N.R. Joshi, S.C. Kinnamon, and E.R. Liman. **2019**. Cellular and Neural Responses to Sour Stimuli Require the Proton Channel Otop1. Current Biology. 29:3647-3656.e5. doi:10.1016/j.cub.2019.08.077.

Thoreson, W.B., R. Nitzan, and R.F. Miller. **2000**. Chloride efflux inhibits single calcium channel open probability in vertebrate photoreceptors: Chloride imaging and cell-attached patch-clamp recordings. Vis Neurosci. 17:197–206. doi:10.1017/S0952523800172025.

Tomchik, S.M., S. Berg, J.W. Kim, N. Chaudhari, and S.D. Roper. **2007**. Breadth of Tuning and Taste Coding in Mammalian Taste Buds. Journal of Neuroscience. 27:10840–10848. doi:10.1523/JNEUROSCI.1863-07.2007.

Wong GT, Gannon KS, Margolskee RF. **1996**. Transduction of bitter and sweet taste by gustducin. Nature. 381(6585):796-800. doi: 10.1038/381796a0.

Turner, B.H., and M. Herkenham. **1991**. Thalamoamygdaloid projections in the rat: A test of the amygdala's role in sensory processing. J. Comp. Neurol. 313:295–325. doi:10.1002/cne.903130208.

Vandenbeuch, A., C.B. Anderson, J. Parnes, K. Enjyoji, S.C. Robson, T.E. Finger, and S.C. Kinnamon. **2013**. Role of the ectonucleotidase NTPDase2 in taste bud function. Proc Natl Acad Sci USA. 110:14789–14794. doi:10.1073/pnas.1309468110.

Vandenbeuch, A., T.R. Clapp, and S.C. Kinnamon. **2008**. Amiloride-sensitive channels in type I fungiform taste cells in mouse. BMC Neurosci. 9:1. doi:10.1186/1471-2202-9-1.

Vandenbeuch, A., R. Zorec, and S.C. Kinnamon. **2010**. Capacitance Measurements of Regulated Exocytosis in Mouse Taste Cells. Journal of Neuroscience. 30:14695–14701. doi:10.1523/JNEUROSCI.1570-10.2010.

Vocke, K., K. Dauner, A. Hahn, A. Ulbrich, J. Broecker, S. Keller, S. Frings, and F. Möhrlen. **2013**. Calmodulin-dependent activation and inactivation of anoctamin calcium-gated chloride channels. Journal of General Physiology. 142:381–404. doi:10.1085/jgp.201311015.

Wagner, J.A., A.L. Cozens, H. Schulman, D.C. Gruenert, L. Stryer, and P. Gardner. **1991**. Activation of chloride channels in normal and cystic fibrosis airway epithelial cells by multifunctional calcium/calmodulin-dependent protein kinase. Nature. 349:793–796. doi:10.1038/349793a0.

Wang, H., N. Iguchi, Q. Rong, M. Zhou, M. Ogunkorode, M. Inoue, E.A. Pribitkin, A.A. Bachmanov, R.F. Margolskee, K. Pfeifer, and L. Huang. **2009**. Expression of the voltage-gated potassium channel KCNQ1 in mammalian taste bud cells and the effect of its null-mutation on taste preferences. J. Comp. Neurol. 512:384–398. doi:10.1002/cne.21899.

Wang, Z., B. Fermini, J. Feng, and S. Nattel. **1995**. Role of chloride currents in repolarizing rabbit atrial myocytes. American Journal of Physiology-Heart and Circulatory Physiology. 268:H1992–H2002. doi:10.1152/ajpheart.1995.268.5.H1992.

Whitehead, M.C., and M.E. Frank. **1983**. Anatomy of the gustatory system in the hamster: Central projections of the chorda tympani and the lingual neirve. J. Comp. Neurol. 220:378–395. doi:10.1002/cne.902200403.

Wladkowski, S.L., and W. Lin † , ‡ , M. McPheeters. **1998**. A Basolateral Chloride Conductance in Rat Lingual Epithelium. Journal of Membrane Biology. 164:91–101. doi:10.1007/s002329900396.

Wright, C.I., and H.J. Groenewegen. **1996**. Patterns of overlap and segregation between insular cortical, intermediodorsal thalamic and basal amygdaloid afferents in the nucleus accumbens of the rat. Neuroscience. 73:359–373. doi:10.1016/0306-4522(95)00592-7.

Xiao, Q., K. Yu, P. Perez-Cornejo, Y. Cui, J. Arreola, and H.C. Hartzell. **2011**. Voltage- and calcium-dependent gating of TMEM16A/Ano1 chloride channels are physically coupled by the first intracellular loop. Proceedings of the National Academy of Sciences. 108:8891–8896. doi:10.1073/pnas.1102147108.

Yamaguchi, S. **1991**. Basic properties of umami and effects on humans. Physiology & Behavior. 49:833–841. doi:10.1016/0031-9384(91)90192-Q.

Yamamoto, T., R. Matsuo, and Y. Kawamura. **1980**. Localization of cortical gustatory area in rats and its role in taste discrimination. Journal of Neurophysiology. 44:440–455. doi:10.1152/jn.1980.44.3.440.

Yang, H., A. Kim, T. David, D. Palmer, T. Jin, J. Tien, F. Huang, T. Cheng, S.R. Coughlin, Y.N. Jan, and L.Y. Jan. **2012**. TMEM16F Forms a Ca2+-Activated Cation Channel Required for Lipid Scrambling in Platelets during Blood Coagulation. Cell. 151:111–122. doi:10.1016/j.cell.2012.07.036.

Yang, R., Y.K. Dzowo, C.E. Wilson, R.L. Russell, G.J. Kidd, E. Salcedo, R.S. Lasher, J.C. Kinnamon, and T.E. Finger. **2020**. Three-dimensional reconstructions of mouse circumvallate taste buds using serial blockface scanning electron microscopy: I. Cell types and the apical region of the taste bud. J Comp Neurol. 528:756–771. doi:10.1002/cne.24779.

Yang, Y.D., H. Cho, J.Y. Koo, M.H. Tak, Y. Cho, W.-S. Shim, S.P. Park, J. Lee, B. Lee, B.-M. Kim, R. Raouf, Y.K. Shin, and U. Oh. **2008**. TMEM16A confers receptor-activated calcium-dependent chloride conductance. Nature. 455, pages1210–1215, doi: 10.1038/nature07313.

Yarmolinsky, D.A., C.S. Zuker, and N.J.P. Ryba. **2009**. Common Sense about Taste: From Mammals to Insects. Cell. 139:234–244. doi:10.1016/j.cell.2009.10.001.

Yasumatsu, K., T. Manabe, R. Yoshida, K. Iwatsuki, H. Uneyama, I. Takahashi, and Y. Ninomiya. **2015**. Involvement of multiple taste receptors in umami taste: analysis of gustatory nerve responses in metabotropic glutamate receptor 4 knockout mice: Umami receptors in the tongue. J Physiol. 593:1021–1034. doi:10.1113/jphysiol.2014.284703.

Ye, Q., G. Heck, and J. DeSimone. **1991**. The anion paradox in sodium taste reception: resolution by voltage-clamp studies. Science. 254:724–726. doi:10.1126/science.1948054.

Yee, K.K., S.K. Sukumaran, R. Kotha, T.A. Gilbertson, and R.F. Margolskee. **2011**. Glucose transporters and ATP-gated K+ (KATP) metabolic sensors are present in type 1 taste receptor 3 (T1r3)-expressing taste cells. Proceedings of the National Academy of Sciences. 108:5431–5436. doi:10.1073/pnas.1100495108.

Yoshida, R., A. Miyauchi, T. Yasuo, M. Jyotaki, Y. Murata, K. Yasumatsu, N. Shigemura, Y. Yanagawa, K. Obata, H. Ueno, R.F. Margolskee, and Y. Ninomiya. **2009**. Discrimination of taste qualities among mouse fungiform taste bud cells: Discrimination of taste qualities among taste cells. The Journal of Physiology. 587:4425–4439. doi:10.1113/jphysiol.2009.175075.

Yoshida, R., N. Shigemura, K. Sanematsu, K. Yasumatsu, S. Ishizuka, and Y. Ninomiya. **2006**. Taste Responsiveness of Fungiform Taste Cells With Action Potentials. Journal of Neurophysiology. 96:3088–3095. doi:10.1152/jn.00409.2006.

Yuan, H., C. Gao, Y. Chen, M. Jia, J. Geng, H. Zhang, Y. Zhan, L.M. Boland, and H. An. **2013**. Divalent Cations Modulate TMEM16A Calcium-Activated Chloride Channels by a Common Mechanism. J Membrane Biol. 246:893–902. doi:10.1007/s00232-013-9589-9.

Zhang, C., Y. Kang, and R.F. Lundy. **2011**. Terminal field specificity of forebrain efferent axons to the pontine parabrachial nucleus and medullary reticular formation. Brain Research. 1368:108–118. doi:10.1016/j.brainres.2010.10.086.

Zhang, Z., Z. Zhao, R. Margolskee, and E. Liman. **2007**. The Transduction Channel TRPM5 Is Gated by Intracellular Calcium in Taste Cells. Journal of Neuroscience. 27:5777–5786. doi:10.1523/JNEUROSCI.4973-06.2007.

Zhao, G.Q., Y. Zhang, M.A. Hoon, J. Chandrashekar, I. Erlenbach, N.J.P. Ryba, and C.S. Zuker. **2003**. The Receptors for Mammalian Sweet and Umami Taste. Cell. 115:255–266. doi:10.1016/S0092-8674(03)00844-4.

Zygmunt, A.C., and W.R. Gibbons. **1991**. Calcium-activated chloride current in rabbit ventricular myocytes. Circ Res. 68:424–437. doi:10.1161/01.RES.68.2.424.